UNIVERSIDAD DE SEVILLA

Escuela Técnica Superior de Ingeniería Informática
Programa de Doctorado en Ingeniería Informática

Sistema asistencial inteligente basado en tecnologías IoT para la mejora de la movilidad de peatones con discapacidad visual en ciudades inteligentes

TESIS DOCTORAL

Autor:
Aleksandro Montanha

Directora:
Dra. María del Carmen Romero Ternero
Dpto. Tecnología Electrónica

Sevilla, julio de 2023

Agradecimientos

Estoy seguro de que no puedo mencionar a todos los que me han ayudado de alguna manera a cumplir esta importante etapa de mi vida, pero hago de los que menciono aquí los representantes de los que me han acompañado de alguna manera en este camino. Para ello, mi agradecimiento en primer lugar a Dios, a mi supervisora del trabajo de doctorado, la Dra. María del Carmen Romero Ternero, su competencia y atención fueron de importancia fundamental a indispensable para el cumplimiento de esta etapa tan importante de mi vida. Al Doctor Airton Polidório, que precedió a todo el trabajo presentado en este programa, cuya profesionalidad y colaboración fueron más allá de las aulas y alcanzaron una profunda amistad. A la Dra. María José Escalona que me presentó a la Universidad de Sevilla e hizo posible todo esto. A mis amigos y compañeros Dr Elias César Carvalho, Andreea Madalina Oprescu, Rodrigo Salazar Gamarra y Francisco José Domínguez Mayo.

A mi esposa Ana Paula Hungria Montanha, por ser el pilar de mi vida, participando y apoyando en todo momento. A mis hermanos, inspiradores hasta el punto de empujarme como profesional y persona constantemente. A mi tía Zília, por ser el guía de nuestra familia. A mi hijo Gabriel, que tanto me enorgullece y da energía para continuar en este camino de búsqueda del conocimiento y, por último, hago homenaje a mi madre, Maria Aparecida Montanha, que renunció a mucho en su vida para invertir en los estudios de su hijo.

Gracias

Resumen

Las personas realizamos diariamente multitud de actividades sin darnos cuenta de la complejidad de algunas de ellas, tal como puede ser cruzar una vía con mucho tráfico. Cuando se trata de personas con discapacidad visual, esta complejidad aumenta enormemente. La tecnología actual abre camino y facilita el desarrollo de recursos que ayuden a estas personas a realizar con éxito esta tarea. La literatura científica ya presenta estudios dirigidos a mejorar la movilidad de personas con discapacidad visual haciendo uso de la tecnología, que generalmente cuentan con dispositivos físicos que monitorizan el entorno y generan información detallada sobre el mismo. Los denominadores comunes de estos estudios suelen ser los conceptos de Internet de las Cosas (IoT, *Internet of Things*) y de Ciudades Inteligentes (*Smart Cities*). Esto es porque uno de los principales objetivos de las Ciudades Inteligentes es garantizar la movilidad de cualquier persona, independientemente de su condición física o sensorial. Sin embargo, el estudio del arte que hemos realizado ha mostrado que existe un vacío en cuanto al objetivo de brindar asistencia electrónica a la percepción espacial de una manera fácil, económicamente accesible y aceptable para las personas con discapacidad visual. En este sentido, la primera parte de esta tesis ha consistido en la integración de inteligencia en un semáforo digital, previamente diseñado y desarrollado por el doctorando y denominado Agente Seebot. Esta solución innovadora dota de inteligencia al semáforo, a través del procesamiento de imágenes guiado por trilateración de señales WiFi y utilizando señales de geolocalización (GPS) que se integran en una aplicación móvil dirigida a personas con discapacidad visual. Esta integración se lleva a cabo a través de una serie de dispositivos y su correspondiente software, que permiten crear puntos de acceso a Internet y gestionar el control de acceso de los usuarios de la plataforma. Una vez finalizado este primer estudio, que ha sido probado en un piloto en las ciudades de Maringá y Campina Grande (Brasil), se ha llevado a cabo una segunda parte de la investigación con el objetivo de mejorar la localización de los peatones. En este segundo estudio se ha propuesto un nuevo enfoque para ampliar las técnicas y métodos existentes para localizar la posición 2D de una fuente de señal enviada por un dispositivo emisor. En este contexto, hemos presentado cinco modelos geométricos: PPC-Modelo Centroide de Puntos Polares, CHC-Modelo Centroide de Casco Convexo, PLI-Modelo de Intersecciones de Líneas Polares, TLI-Modelo de Intersecciones de Líneas Tangentes y MAI-Modelo de Líneas Tangentes con Ángulos Mínimos, para resolver el problema de ubicación de puntos, que fueron comparados con las soluciones tradicionales: NRm - Método de Newton-Rapson, LSm -

Método de los mínimos cuadrados, WLSm - Método de los mínimos cuadrados ponderados. Los métodos propuestos han reducido el número de operaciones aritméticas requeridas por los métodos convencionales y han generado mejores estimaciones. Seguidamente, en un tercer estudio, se ha propuesto un nuevo método de ubicación de la señal, que hemos denominado centroide polo-polar ponderado, basado en la geometría polo-polar ponderada con el fin de mejorar la precisión de la estimación de la ubicación de la señal, evitar el aumento de costos en la capacidad computacional y evitar el aumento del número de nodos en la composición de la red local. Nuestro planteamiento ha sido capaz de producir resultados más precisos cuando se procesan datos con errores, ayudando a resolver el problema de aplicar la ubicación de puntos 2D en una relación geométrica, reduciendo la cantidad de operaciones aritméticas requeridas por los métodos convencionales actuales y reduciendo la propagación de errores inherentes a la adquisición de datos. Además, este nuevo método se ha beneficiado de la interacción inalámbrica entre teléfonos móviles para el rastreo de contactos de proximidad, lo que permite mejorar la precisión de la estimación de las ubicaciones de las señales. Finalmente, en un cuarto estudio se han realizado nuevas mejoras en el semáforo inteligente inspiradas en el paradigma del Diseño Centrado en el Usuario (U*ser-Centered Design*, UCD). En un principio el sistema no estaba diseñado para brindar orientación personalizada, de manera que fuera capaz de distinguir a las personas con discapacidad visual de los peatones comunes, ayudándolos a cruzar la calle de una manera más adecuada a sus necesidades particulares. Para ello, se ha iterado el diseño y desarrollo del sistema y se han realizado pruebas de campo con usuarios con discapacidad visual para probar la aplicación en la ciudad de Maringá, Paraná (Brasil). Como resultado de este estudio, el semáforo inteligente ha sido capaz de adaptar su propio comportamiento, transcribiendo la situación de las vías e identificando al peatón con discapacidad visual para, a través de una aplicación móvil, llevar a cabo la asistencia personalizada para el cruce de la vía.

En conjunto, como resultado del desarrollo de estos cuatro estudios, esta investigación contribuye al avance científico-tecnológico con un primer sistema asistencial inteligente basado en tecnologías IoT para peatones con discapacidad visual en ciudades inteligentes.

Índice general

Índice de figuras

Índice de tablas

PARTE I:

MEMORIA

Capítulo 1

Introducción

Según la OMS, al menos 2200 millones de personas en todo el mundo tienen problemas de visión de cerca o de lejos. Al menos 1000 millones incluyen personas con discapacidad visual de lejos moderada o grave o ceguera debido a errores de refracción no resueltos (88,4 millones), cataratas (94 millones), degeneración macular relacionada con la edad (8 millones), glaucoma (7,7 millones), diabetes retinopatía (3,9 millones) [1]. La movilidad, definida por la capacidad de desplazarse con seguridad, comodidad, elegancia y, principalmente, de forma autónoma, se ha convertido en un factor esencial en la vida de las personas con discapacidad visual. La persona con esta discapacidad que adquiere esta autonomía de movilidad tiene un estilo de vida no dependiente gracias a la planificación y ejecución de sus quehaceres diarios. Sin embargo, la persona que no logra desarrollar esta habilidad acaba teniendo una vida completamente dependiente de los demás. Además, esta persona dependiente, al moverse a pie por zonas públicas al aire libre, se enfrenta a muchas dificultades y corre un gran peligro [2].

En este contexto, se observa que hasta hace pocos años parecía que este problema de movilidad no podía resolverse de una manera general para este público. En su revisión sistemática, El-taher et al. [3] realizó un análisis exploratorio sobre los sistemas de navegación al aire libre para personas ciegas y con discapacidad visual existentes e identificó un total de 72 estudios. Una comparación de los hallazgos de este estudio muestra que, según la literatura, en 2014 sólo había tres estudios sobre el tema mientras que en 2020 había diez. Esto muestra que la necesidad de los discapacitados visuales ha abierto un espacio para la investigación científica y tecnológica, que se ha traducido en avances en las áreas de adaptación social, rehabilitación, comunicación y habilidades de aprendizaje. En concreto, la investigación en el ámbito de la visión por computador ha supuesto importantes avances en los estudios sobre la segmentación de objetos y la creación de otros tantos métodos de orientación en entornos tanto abiertos como cerrados. En este escenario, la posibilidad de proporcionar un desplazamiento o una mejor movilidad urbana a una persona con discapacidad visual de forma más asistida y guiada por sistemas inteligentes se ha convertido en una realidad.

Los peatones ciegos tienen menos oportunidades de cruzar y, basándose en sus propios juicios, realizan cruces más arriesgados [2]. Normalmente, estos peatones deben esperar en la acera, deben evaluar el tráfico que se mueve frente a ellos y luego lidiar con una cantidad significativa de tráfico de fondo observando el ruido presente en la

intersección principal. Sin embargo, la naturaleza geométrica de las instalaciones de los carriles y la deficiencia en el control de las señales de tráfico en los pasos de cebra influyen negativamente en el retraso y la seguridad de estos peatones [4,5]. Por otro lado, cada vez son más comunes los vehículos eléctricos o híbridos, que emiten poco o ningún ruido durante su recorrido. Esto se está convirtiendo en un problema para la mayoría de las personas, ya que el ruido que tradicionalmente emiten los propios vehículos en movimiento sirve para ponerlos en alerta al cruzar las carreteras. Un estudio en 12 estados en los Estados Unidos reveló que los vehículos híbridos eléctricos, llamados HEV (*Hybrid Electric Vehicles*), tenían una mayor tasa de incidentes en colisiones de peatones o ciclistas que los vehículos de combustión, conocidos como ICEV (*Internal Combustion Engine Vehicles*) [6]. Otro estudio ligeramente más reciente demostró que la posibilidad de que un peatón o bicicleta participe en un accidente de ICF es un 35% más alta que la de un ICEV [7]. Debido a la preocupación por la seguridad de los vehículos eléctricos, se realizó un estudio de simulación en los Estados Unidos y concluyó que los HEV tienen una colisión 25% más alta para los peatones que los ICEV [8]. Cuando se trata de personas con discapacidades visuales, este problema resulta aún más grave.

Por ser una parte común de nuestra vida cotidiana, se da poca importancia a la movilidad de los peatones. Sin embargo, hay que reconocer que esta actividad es compleja. Cuando se trata de personas con discapacidad visual, esta complejidad aumenta significativamente. Por lo tanto, los especialistas en factores humanos deben realizar un análisis exhaustivo de esta actividad. Como afirmaban Shingledecker y Foulke [9], es primordial generar información que contribuya positivamente al desarrollo de proyectos de ayuda a la movilidad y al desarrollo de la formación de personas con discapacidad visual, así como a la evaluación de ambos.

Una revisión sistemática [3] mostró que existen estudios cuyo objetivo principal es generar recursos que capten las estructuras del entorno, proporcionen una descripción de este, y permitan mejorar su comprensión por parte de los discapacitados visuales. En este contexto, encontramos el concepto de ciudades inteligentes que contempla como uno de sus principales objetivos garantizar la movilidad de cualquier persona, independientemente de su condición física o sensorial. Si tenemos en cuenta a las personas con discapacidad visual, este objetivo se convierte en un reto aún mayor al que hay que enfrentarse.

En diversos estudios [10-12] se ha evaluado la creación de varios dispositivos capaces de recoger información para ayudar al desplazamiento de personas con discapacidad visual. Sin embargo, estos estudios demuestran que hasta el momento no ha sido posible alcanzar el objetivo de proporcionar una ayuda en formato digital a la percepción espacial de forma fácil, económicamente accesible y aceptable para las personas con discapacidad visual. Aunque existen diferentes propuestas de estudios para ayudar a la movilidad de los discapacitados visuales, todos tienen en común el proceso de transformar los datos ambientales brutos en una forma adecuada para facilitar la percepción no visual del usuario discapacitado. En este caso, cuando este proceso no implica la comprensión directa o la interpretación compleja de los datos por parte del dispositivo transformador, la persona con discapacidad visual necesita percibir los datos de alguna forma analógica y seguir extrayendo la estructura compleja a través de señales de bajo nivel [13]. Kanwal et al. [14] realizaron un estudio en el que crearon un dispositivo, que utilizaba un sistema de visión por ordenador en tiempo real, cuyo objetivo era mantener a los peatones con discapacidad visual en una trayectoria segura diseñada en el pavimento y alertarles de la presencia de obstáculos cercanos. Por otro lado, Shchekotov [15] mejoró las técnicas de ese estudio utilizando un sistema de visión por ordenador y la fusión de sensores de profundidad. Otros investigadores, Cheng et al. [16], han desarrollado un sistema portátil, para personas con discapacidad visual, que genera imágenes de profundidad RGB y proporciona navegación asistida para peatones con discapacidad visual en las intersecciones urbanas. Li et al. [17] también invirtieron esfuerzos en un dispositivo portátil inteligente basado en la técnica de visión por computadora llamado *Cross-Safe*, que proporcionaba una guía precisa, mediante guía vocal, suministrando información crítica en tiempo real cuando una persona con discapacidad visual atraviesa cruces de carreteras. Además, Bai et al. [18] han desarrollado un sistema de visión y navegación basado en la nube para personas ciegas. Dicho sistema pretende ir más allá de la navegación, proporcionando información a los discapacitados visuales para que puedan percibir el mundo que les rodea. El sistema incluye un casco equipado con cámaras estéreo en el frente, teléfono inteligente con sistema Android, aplicación web y plataforma de computación en la nube. En otro estudio de Y'iariello y Carrella [19] se han utilizado técnicas de redes neuronales en la construcción de una aplicación que utiliza el modelo convolucional de aprendizaje profundo para producir dos piezas de información más importantes para los peatones con discapacidad visual: el color y la dirección del semáforo para peatones, durante el cruce del camino en tiempo real. Esta información se transmite a través de señales auditivas y

vibraciones. Asimismo, Ash et al. [20] utilizaron una técnica similar que utiliza redes convolucionales profundas y un módulo de decisión para detectar semáforos y su estado a partir de un video tomado con la cámara de un teléfono celular. Más recientemente, Ghilardi et al. [21] han desarrollado una aplicación de detección y ubicación de cruces peatonales para dispositivos móviles, basada en imágenes satelitales capturadas de Google Maps, para ayudar a las personas con discapacidad visual. Este sistema detecta el paso de peatones mediante un clasificador y la técnica Support Vector Machine (SVM), en combinación con Google Road Map y alerta al usuario a través de audio.

En este contexto, las investigaciones de la presente tesis doctoral han generado una serie de contribuciones, que han sido publicadas en un congreso y en tres revistas internacionales de reconocido prestigio:

1. **Contribución 1**: Montanha, A., Escalona, M. J., Domínguez-Mayo, F. J., & Polidorio, A. M. (2016, August). ***A technological innovation to safely aid in the spatial orientation of blind people in a complex urban environment***. In *2016 IEEE International Conference on Image, Vision and Computing (ICIVC)* (pp. 102-107). IEEE. h-Index: 14 [22]
2. **Contribución 2**: Montanha, A., Polidorio, A. M., Domínguez-Mayo, F. J., & Escalona, M. J. (2019). **2D triangulation of signals source by pole-polar geometric models**. *Sensors*, *19*(5), 1020. Factor de impacto JCR 3.847, SJR 0.636 y Q1 [23].
3. **Contribución 3**: Montanha, A., Polidorio, A. M., & Romero-Ternero, M.C. (2021). **New signal location method based on signal-range data for proximity tracing tools**. *Journal of Network and Computer Applications*, *180*, 103006. Factor de impacto JCR 7.574, SJR 1.145 y Q1 [24].
4. **Contribución 4**: Montanha, A., Oprescu, A. M., & Romero-Ternero, M.C. (2022). **A Context-Aware Artificial Intelligence-based System to Support Street Crossings For Pedestrians with Visual Impairments**. *Applied Artificial Intelligence*, *36*(1), 2062818. Factor de impacto JCR 2.777, SJR 0.336 y Q3 [25].

Asimismo, en el contexto de los resultados de esta investigación se han logrado otros méritos y reconocimiento de diversa índole y ámbito:

- Patente industrial del agente Seebot, la cual se encuentra protegida bajo registro con descripción de “Cámara Inteligente Multiprocesado de Análisis de Comportamiento Georreferenciado (PI)”, publicado por el INPI (Instituto Nacional de la Propiedad Industrial) número 2620 del 23/03/2021 (Brasil).
- Los productos y servicios de Seebot han pasado la evaluación de Intel y actualmente están disponibles en la cartera internacional de soluciones de Intel a través del programa MRS (Marketing Ready Solutions) [26].
- Finalista de los premios Intel Connect Partner 2018.
- Finalista de los premios Intel Connect Partner 2019.
- Finalista en la categoría de soluciones innovadoras en el IOT World Congress 2019, realizado en Barcelona – España [27].
- Finalista del premio a la innovación social, en la categoría de movilidad de la Fundación Mapfre en 2023 [28].

Capítulo 2

Objetivos

Tal y como se ha introducido en el capítulo anterior, esta tesis doctoral se compone de cuatro estudios científico-tecnológicos principales que se complementan entre sí: el primero de ellos propone el uso de un semáforo inteligente que sea capaz de ayudar a las personas con discapacidad visual a cruzar las carreteras de forma autónoma y segura, el segundo estudio explora una nueva metodología para mejorar los resultados de los métodos de localización de posición 2D a partir de una fuente de señal enviada por un transmisor, generando un menor coste computacional. El tercer estudio tiene como propuesta mejorar la precisión de los resultados del segundo estudio sin aumentar el coste computacional. En el cuarto estudio se propusieron y ejecutaron las mejoras del primer estudio con el objetivo de proporcionar una guía personalizada para distinguir a las personas con discapacidad visual de los peatones ordinarios y ayudarles mejor a cruzar la carretera, también se implementaron mejoras en la aplicación, se realizaron pruebas de campo y se implementaron mejoras en el semáforo inteligente.

A continuación, para cada estudio se formalizan los objetivos que se han cubierto.

Contribución 1: Una innovación tecnológica para ayudar de forma segura en la orientación espacial de personas ciegas en un entorno urbano complejo.

Montanha, A., Escalona, M. J., Domínguez-Mayo, F. J., & Polidorio, A. M. (2016, August). A technological innovation to safely aid in the spatial orientation of blind people in a complex urban environment. In 2016 IEEE International Conference on Image, Vision and Computing (ICIVC), Portsmouth, UK, 2016, pp. 102-107, https://10.1109/ICIVC.2016.7571281 [22]

1. Construir un sistema con capacidad para ayudar a las personas con discapacidad visual a cruzar una calle con mayor seguridad e integrar las funcionalidades de un semáforo inteligente ya existente.
2. Buscar en la literatura e implementar un método de segmentación de imágenes que sea eficiente, pero que requiera un bajo coste computacional, ya que el equipo de semáforos debe tener un tamaño reducido, lo que consecuentemente limita su potencia computacional.
3. Crear e integrar en el semáforo inteligente una aplicación para *smartphones* que ayude a las personas con discapacidad visual en el uso del semáforo inteligente.

4. Crear un centro de *big data* con datos relacionados con el tráfico de vehículos y los pasos de peatones para ayudar a integrar el semáforo inteligente con la aplicación móvil, con el fin de garantizar una mayor eficiencia y seguridad para los discapacitados visuales.

Contribución 2: Modelos geométricos para la mejora de la triangulación de las señales.

Montanha, A., Polidorio, A. M., Domínguez-Mayo, F. J., & Escalona, M. J. (2019). 2D triangulation of signals source by pole-polar geometric models. Sensors, 19(5), 1020, https://doi.org/10.3390/s19051020 [23]

1. Proponer un nuevo enfoque destinado a ampliar las técnicas y métodos existentes para localizar la posición 2D de una fuente de señal enviada por un dispositivo transmisor.
2. Construir este nuevo enfoque basado únicamente en la relación geométrica, sin necesidad de resolver un sistema de ecuaciones no lineales, entre un dispositivo transmisor y un sistema compuesto por $m \geq 2$ dispositivos de recepción de señales, que aprovechan elementos de la geometría polar.
3. Presentar nuevos modelos geométricos para resolver el problema de localización de puntos. En este caso se desarrollaron cinco:
    3.1. PPC-*Polar Points Centroid Model* (Modelo de centróide de punto polar propuesto)
    3.2. CHC-*Convex Hull Centroid Model* (Modelo de casco convexo centróide propuesto)
    3.3. PLI-*Polar Lines Intersections Model* (Propuesta de modelo de intersecciones de líneas polares)
    3.4. TLI-*Tangent Lines Intersections Model* (Propuesta de modelo de intersección de líneas tangentes)
    3.5. MAI-T*angent Lines with Minimal Angles Model* (Modelo propuesto de línea tangente de ángulo mínimo)
4. Realizar un análisis comparativo de los nuevos métodos propuestos frente a métodos numéricos ya consolidados en la literatura. En este caso se seleccionaron tres métodos consolidados existentes:
    4.1. NRm - *Newton–Rapson Method* (Método Newton-Raphson de comparación)

4.2. LSm - *Least Square Method* (Método de mínimos cuadrados para la comparación)

4.3. WLSm - *Weighted Least Square Method* (Método de mínimos cuadrados ponderados para la comparación).

Contribución 3: Nuevo método de ubicación de señales basado en datos de rango de señales para herramientas de rastreo de proximidad

Montanha, A., Polidorio, A. M., & Romero-Ternero, M.C. (2021). New signal location method based on signal-range data for proximity tracing tools, Journal of Network and Computer Applications, Volume 180, 103006, ISSN 1084-8045, https://doi.org/10.1016/j.jnca.2021.103006 [24]

1. Proponer un nuevo método de localización de la señal basado en la geometría polar ponderada que puede mejorar la precisión de la estimación de la localización de la señal.
2. Evitar el aumento del coste computacional $O(m^2)$.
3. Evitar el aumento del número de nodos ($m \geq 2$) en la composición de la red local.

Contribución 4: Un sistema basado en inteligencia artificial consciente del contexto para apoyar los cruces de calles para peatones con discapacidades visuales

Montanha, A., Oprescu, A. M., & Romero-Ternero, M.C. (2022). A Context-Aware Artificial Intelligence-based System to Support Street Crossings For Pedestrians with Visual Impairments, Applied Artificial Intelligence, 36:1, https://doi.org/10.1080/08839514.2022.2062818 [28]

1. Mejorar los resultados del estudio anterior (Montanha et al. 2016) [22], que no proporcionaba una guía personalizada, distinguiendo a las personas con discapacidad visual de los peatones ordinarios, ayudándoles a cruzar la carretera.
2. Utilizar el enfoque *User-Centered Design* (UCD) en el desarrollo de la aplicación.
3. Llevar a cabo pruebas de campo con usuarios con discapacidad visual para probar el sistema asistente.
4. Permitir que el semáforo cambie su comportamiento al transcribir la situación de la carretera e identificar a un peatón con discapacidad visual que comienza a cruzar la carretera para adaptar las indicaciones en función de sus necesidades.

Capítulo 3

Resumen de resultados

Este capítulo presenta los resultados obtenidos durante el desarrollo de esta tesis doctoral, formada por un total de cuatro estudios. En el primer estudio, a partir de un análisis del estado del arte, se ha elaborado la idea principal de diseñar un sistema pensado para Ciudades Inteligentes que integre un semáforo IoT destinado a ayudar a las personas con discapacidad visual a cruzar las carreteras, así como su instalación en dos ciudades para su prueba, recogida de resultados y mejoras durante dos años. Posteriormente, como resultado de la experiencia anterior, donde se contaba con un dispositivo de tamaño reducido y, por lo tanto, con baja potencia computacional, se han estudiado métodos de localización de posición 2D y a partir de ahí se ha implementado un método que generara menor costo computacional. Y en el tercer estudio ha sido posible implementar un nuevo método que puede mejorar aún más la precisión de los resultados manteniendo el mismo coste computacional del estudio anterior. Y finalmente, en el cuarto estudio, se ha desarrollado una solución integral de sistema asistente inteligente basado en tecnología IoT y aplicación móvil para mejorar la movilidad de peatones en ciudades inteligentes, utilizando diseño centrado en el usuario.

En los siguientes apartados se detallan estos resultados para cada publicación.

Contribución 1: Una innovación tecnológica para ayudar de forma segura en la orientación espacial de personas ciegas en un entorno urbano complejo.

Montanha, A., Escalona, M. J., Domínguez-Mayo, F. J., & Polidorio, A. M. (2016, August). A technological innovation to safely aid in the spatial orientation of blind people in a complex urban environment. In 2016 IEEE International Conference on Image, Vision and Computing (ICIVC), Portsmouth, UK, 2016, pp. 102-107, https://10.1109/ICIVC.2016.7571281 [22]

Este estudio analiza el problema que tienen los discapacitados visuales al intentar cruzar las calles y evalúa qué tipo de información puede transmitir el entorno para que puedan desplazarse con mayor seguridad. El estudio contempla el desarrollo de un recurso que permita al entorno avisar a los discapacitados visuales, mediante un dispositivo móvil, de los momentos en los que pueden o no cruzar una vía en el paso de cebra. Este recurso se proporciona dentro de un área geográfica que se ha dotado de semáforos inteligentes, que funcionan junto con una aplicación móvil instalada en el teléfono móvil de la persona con discapacidad visual. Los dispositivos deberían detectar la llegada de la

persona con discapacidad visual, seguir sus movimientos y detectar la dirección en la que se movía, alertándole, a través de la aplicación móvil, de que el lugar estaría controlado por semáforos inteligentes y que debería esperar el momento más seguro para cruzar la calle. A continuación, los dispositivos (semáforos inteligentes) en constante comunicación (envío/recepción y procesamiento de la información) con la aplicación móvil deben, a través de las instrucciones comunicadas por su sistema de audio, garantizar que la persona con discapacidad visual se desplace con seguridad sin salirse del paso de cebra.

En el primer estudio de esta tesis se creó el prototipo inicial integrando un semáforo inteligente desarrollado previamente por el propio doctorando, denominado *Seebot Agent*. Este prototipo tiene la capacidad de supervisar el movimiento de los vehículos en los tramos de carretera donde se instaló, recibir y enviar señales a los vehículos y peatones que se encuentran en el lugar de su instalación. Su composición incluye varios dispositivos (cámara de vídeo, antena *Wi-Fi* y antena *Bluetooth*) interconectados por un sistema informático, además de la estructura básica de un semáforo digital (véase Figura 1). Este conjunto de dispositivos permite captar, procesar, enviar y recibir información de una plataforma (servidor) que gestiona gran volumen de datos (*big data)* sobre la situación de los peatones, los vehículos, el tráfico y los pasos de peatones, con el fin de optimizar el tráfico y la movilidad urbana en las ciudades.

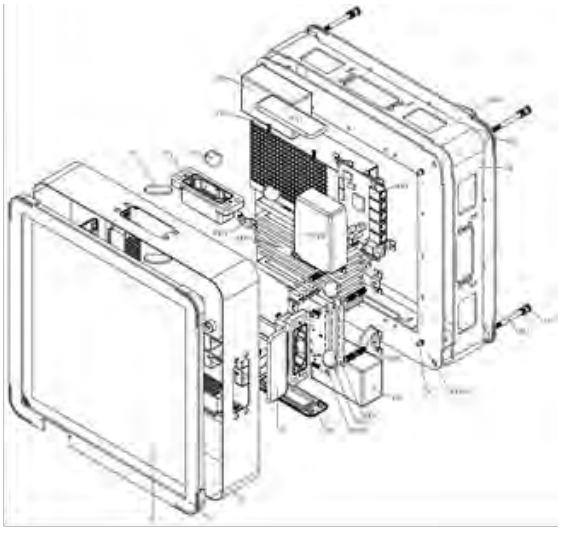

Figura 1. Diagrama esquemático del semáforo inteligente Seebot Agent

Seebot Agent añade innovaciones a la señal de tráfico inteligente mediante el procesamiento de imágenes guiado por la trilateración de señales *wifi* y/o utilizando señales de geolocalización (unidad de Sistema de Posición Global - *GPS*). Además del dispositivo (véase Figura 1), el proyecto también incluye aplicaciones para dispositivos móviles para personas con discapacidad visual (véase Figura 2). Este conjunto de

hardware y software crea recursos para la creación de *hotspots* que permiten el acceso a la red mundial y la autentificación de los miembros en la plataforma. Además, el usuario con discapacidad visual no sólo hará un uso transparente de su geolocalización, sino de muchas más funciones que le ayudarán a cruzar las carreteras con más movilidad y seguridad.

Pensando en crear un dispositivo de semáforo inteligente y eficiente, el proyecto Seebot Agent se desarrolló con la idea de crear métodos que utilizan un bajo coste computacional, ya que el dispositivo tiene un tamaño reducido y, en consecuencia, una potencia computacional reducida. En este sentido, para la ejecución del procesamiento de imágenes, se buscó en la literatura métodos de segmentación de imágenes de bajo coste para actuar en la localización de peatones en áreas delimitadas por coordenadas espaciales generadas por la trilateración de señales WiFi y/o GPS. Preferiblemente, estos métodos deben haber sido utilizados y bien evaluados en este tipo de operaciones, pero en ejecución en tiempo real en entornos no controlados. Entre los métodos estudiados, se eligió la Imagen de Historia del Movimiento [29], que fue creada para detectar y distinguir secuencias de movimiento humano mediante la composición de capas sucesivas compuestas por puntos para el movimiento de las imágenes detectadas entre fotogramas. Este método tiene la capacidad de distinguir el movimiento de una persona del movimiento de un vehículo a partir de una secuencia de imágenes realizando comparaciones de imágenes fotograma a fotograma. El proceso consiste en analizar los bordes, los colores, los aspectos geométricos y extraer las características que permiten trazar el movimiento de un individuo, de esta manera, cada objeto en movimiento de la escena tiene su posición espacial calculada. En este contexto, si el individuo con discapacidad visual, que es el objeto principal de este estudio, se encuentra en un lugar inseguro, *Seebot Agent* crea una alerta para él y envía una señal luminosa de advertencia a los conductores del lugar.

Debido a la gran popularidad de los *smartphones* y a sus características actuales, que otorgan cierta potencia de cálculo a estos dispositivos que ya cuentan con *GPS, WiFi, Bluetooth,* y sistema de voz, entre otros recursos, se decidió crear una aplicación móvil que pudiera integrarse con el *Seebot Agent* como herramienta auxiliar para los discapacitados visuales. Esta idea se presentó a un grupo de personas con discapacidad visual, que ayudaron al desarrollo de esta aplicación. Esta aplicación fue validada por tres personas con discapacidad visual, que ya tenían experiencia en el uso de otras aplicaciones desarrolladas para este público. Esta aplicación cuenta con reconocimiento

de voz, activación por vibración y transmisión de mensajes de voz, creando así un canal de comunicación entre la persona con discapacidad visual y el *Seebot Agent*. Durante su funcionamiento, si un usuario con discapacidad visual se acerca a una carretera monitorizada por *Seebot Agent,* su smartphone, que estará integrado en el sistema, le transmitirá la dirección en la que quiere ir. A continuación, el *Seebot Agent* transmitirá al usuario con discapacidad visual, mediante mensajes de voz, sonidos y vibraciones (figura 2), información sobre el entorno local como: la existencia de vehículos, su estado (en movimiento o detenidos), información de los semáforos (abiertos o cerrados). Tras comenzar a cruzar la calle, el *Seebot Agent* guiará al usuario con discapacidad visual por una ruta correcta y segura, alertándole para que corrija la ruta si se equivoca.

Figura 2. Interfaz del primer prototipo de aplicación móvil para usuarios invidentes

El *Seebot Agent* y el usuario con discapacidad visual están integrados por la aplicación móvil, el flujo de datos relacionado con esta operación se puede ver en la Figura 3. A través de la conexión *WiFi* o *bluetooth* detecta la presencia de un individuo con discapacidad visual cerca de una región monitoreada por el semáforo inteligente. Cuando esto ocurre, la aplicación envía una señal de alerta al *Seebot Agent*, que establece un canal de comunicación entre los dos dispositivos y comienza a transmitir y recibir información entre ellos. Tras establecer esta comunicación, el *Seebot Agent* solicita a la aplicación móvil que transmita un historial de datos de coordenadas *GPS* relacionados con el desplazamiento de la persona con discapacidad visual para estimar la posible

trayectoria de este individuo. Este historial se refiere a la trayectoria del individuo con discapacidad visual durante los dos últimos minutos de su desplazamiento, siempre que haya un cambio en su posición geográfica. El sistema comunica entonces todas las acciones necesarias para cruzar el paso de cebra con seguridad. Mientras la persona con discapacidad visual cruza la carretera, el *Seebot Agent* mantiene el semáforo cerrado para los vehículos. Al mismo tiempo, alerta a los conductores y a otros peatones, a través del panel del semáforo, de que una persona con discapacidad visual está cruzando la carretera. Pueden ocurrir posibles fallos de comunicación con el *GPS* y previendo la ocurrencia de este evento, se implementó una forma de complementar la localización espacial a través de la trilateración de señales *wifi* [22] que requiere la instalación de diferentes puntos de acceso *WiFi* en la región monitorizada por *Seebot Agent*.

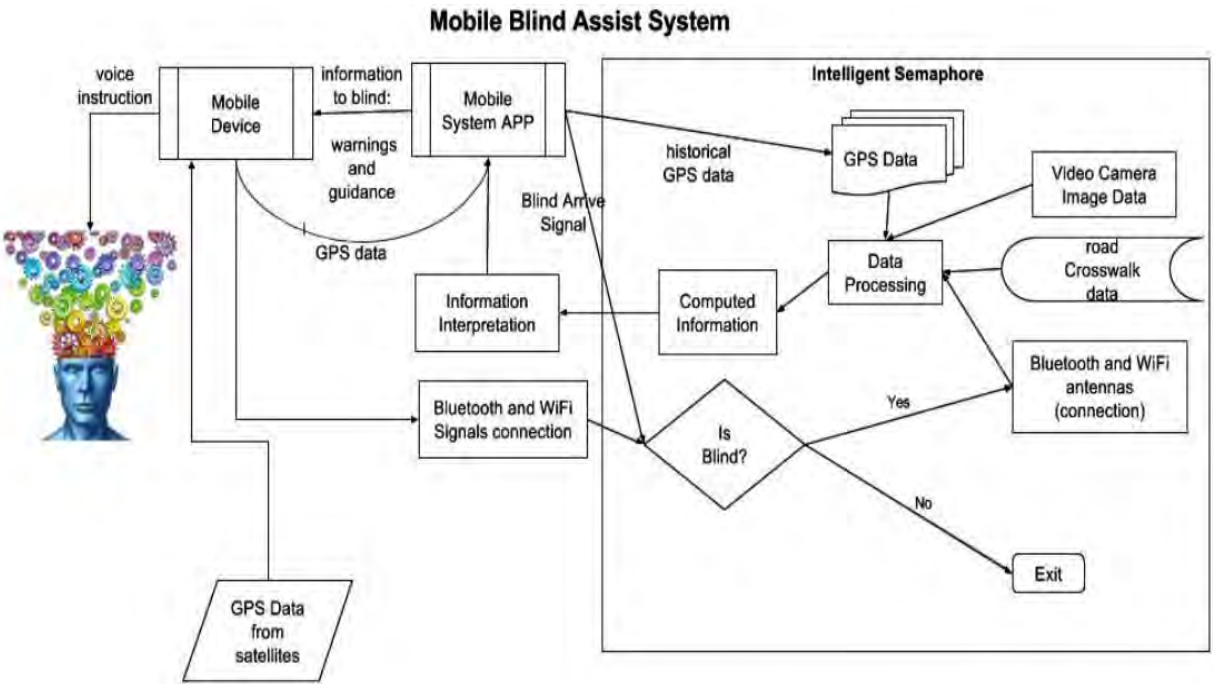

Figura 3. Esquema de integración del sistema en la primera versión del prototipo [22]

Contribución 2: Modelos geométricos para la mejora de la triangulación de las señales.

Montanha, A., Polidorio, A. M., Domínguez-Mayo, F. J., & Escalona, M. J. (2019). 2D triangulation of signals source by pole-polar geometric models. Sensors, 19(5), 1020, https://doi.org/10.3390/s19051020 [23]

La posición de un dispositivo emisor o receptor de señales puede estimarse mediante la triangulación de los datos relativos a las señales enviadas y recibidas por él. Los datos de estas señales comprenden: la naturaleza de la propia señal (luz – energía

electromagnética–, sonido y vibración); los atributos intrínsecos (potencia, frecuencia y amplitud); los atributos extrínsecos (el momento en que la señal llega a cada receptor concreto; la fuerza y el ángulo de propagación de una señal adquirida en cada receptor concreto). La localización de un dispositivo transmisor/receptor puede realizarse mediante métodos deterministas, estadísticos o de aprendizaje automático, denominados en este estudio modelos numéricos. Teniendo en cuenta este contexto, este estudio propone el uso de modelos geométricos que explotan elementos de la geometría polar para realizar la triangulación de los datos.

Entre los modelos propuestos están: (1) basados en el centroide de un conjunto de puntos polares (*centroid of points of pole-polar geometry* - PPC); (2) basado en una región de casco convexo definida por un conjunto de puntos de interés (*convex hull region among pole-points* - CHC); (3) basado en el centroide de un conjunto de puntos de interés obtenidos por la intersección de líneas polares (*centroid of points obtained by polar-lines intersections* - PLI); (4) basado en el centroide de un conjunto de puntos de interés obtenidos por la intersección de líneas tangentes, (*centroid of points obtained by tangent lines intersections* - TLI); (5) basado en el centroide de un conjunto de puntos de interés obtenidos mediante la intersección de líneas tangentes con ángulos mínimos (*centroid of points obtained by tangent lines intersections with minimal angles* - MAI). El primer método (PPC) tiene un coste computacional $O(n)$, mientras que los otros cuestan $O(n \log n)$, donde el valor de n representa el número de puntos de interés. Un sistema compuesto por m los receptores tendrán un máximo de puntos de interés polares generados por: $p = \left(\frac{m}{2}\right) = m!\,(2(m-2)!)$. Para los modelos PPC, CHC e PLI $n=p$; modelos TLI e MAI $n=2p$. Para los métodos propuestos, el coste será $O(m^2)$ en función del coste de realización de (m^2) combinaciones. En este estudio, se han utilizado datos brutos (sin procesar) para evaluar la precisión de los métodos con la presencia de errores. Estos errores son el resultado de la multitrayectoria de la señal, la presencia de obstáculos y la co-presencia de varias fuentes electromagnéticas. Los resultados de los métodos propuestos se compararon con los métodos numéricos ya consolidados en la literatura como *Newton–Rapson* (NRm), Mínimos cuadrados (*Least-Square* - LSm) e *Mínimos Quadrados Ponderados* (*Weighted Least Squares* - WLSm) que tienen costo computacional ~$O(m^3)$. Asegurar la precisión de una localización requiere de datos de alta calidad, sin embargo, esto no siempre es posible, por lo que la propuesta de este trabajo es utilizar métodos geométricos para minimizar los errores y maximizar la precisión para localizar la posición de un dispositivo emisor/receptor de señales.

Se seleccionaron tres situaciones para evaluar los resultados generados por el modelo geométrico propuesto con respecto a la precisión alcanzada: peor resultado, resultado intermedio y resultado más preciso. Esta precisión se refiere únicamente a la calidad de los datos adquiridos. En este caso, como se muestra más adelante en la Figura 4, las métricas: (1) error en la medición de la distancia entre la ubicación estimada del emisor $E_{xy}(E_x,E_y)$ y la posición real del emisor $E_p(X_p,Y_p)$; (2) el error a lo largo del eje x dado por $|E_x-x_p|$ e (3) error a lo largo del eje y dado por $|E_y-y_p|$.

Los resultados de esta evaluación se presentan en la Tabla 1 y muestran que algunos modelos geométricos produjeron resultados con errores equivalentes a los producidos por los métodos numéricos. Los modelos MAI y TLI promueven mayores errores en el eje x, pero menores en el eje y y la distancia. Estos métodos también generaron errores menores y errores máximos más pequeños, lo que indica una mayor eficiencia cuando hay inconsistencia en los datos. Los métodos CHC y PLI se equivocaron menos en el eje x, pero generaron resultados más significativos en el eje y y la distancia. Considerando los errores medios generados por el PPC, éstos son equivalentes a los cometidos por los métodos numéricos (*WLSm*, *NRm* e *LSm*). En el contexto general, los modelos geométricos mostraron mejores resultados que los métodos numéricos.

Tabla 1. Magnitud de los errores en los casos experimentales [23]

Methods	Magnitudes Errors (in Meters)								
	Minimum Error			Maximum Error			Mean Error		
	x-axis	*y*-axis	distance	*x*-axis	*y*-axis	distance	*x*-axis	*y*-axis	distance
PPC*	0.4	0.2	2.7	15.5	12.5	15.7	4.2	4.4	6.9
CHC*	0.1	0.1	0.6	11.9	6.0	12.8	2.5	2.4	3.7
PLI*	0.1	0.1	0.7	12.8	15.9	16.3	2.4	3.8	5.0
MAI*	1.6	0.3	1.7	7.9	5.3	8.9	4.2	1.5	4.7
TLI*	2.3	0.3	2.3	8.3	3.9	9.2	4.1	1.3	4.4
NRm	0.1	1.1	1.3	14.7	12.2	15.2	2.8	5.1	6.5
LSm	0.3	1.2	1.8	14.1	22.5	23.7	3.6	6.4	7.9
WLSm	0.1	0.7	1.3	13.6	15.3	17.7	3.5	4.9	6.5

* Geometric Models proposed in this work

PPC-*Polar Points Centroid Model* (Modelo de centroide de punto polar propuesto), CHC-*Convex Hull Centroid Model* (Modelo de casco convexo centroide propuesto), PLI-*Polar Lines Intersections Model* (Propuesta de modelo de intersecciones de líneas polares), TLI-*Tangent Lines Intersections Model* (Modelo propuesto de intersección de líneas tangentes), MAI-*Tangent Lines with Minimal Angles Model* (Modelo propuesto de línea tangente de ángulo mínimo), NRm-*Newton–Rapson Method* (Método Newton-Raphson de comparación), LSm-*Least Square Method* (Método de mínimos cuadrados para la comparación), WLSm-*Weighted Least Square Method* (Método de mínimos cuadrados ponderados para la comparación).

El proceso de resolución del problema de localización de la señal tiene lugar minimizando los errores alcanzados. Estos errores no son cometidos por los métodos, sino que están presentes en los datos. El error medio global generado por los modelos

geométricos y los métodos numéricos durante los experimentos se presenta en la Tabla 2. En esta tabla los modelos geométricos presentan mejores resultados.

Tabla 2. Errores médios globales (Modelos geométricos vs Métodos numéricos) [23]

	Mean Errors (in Meters)		
	x-axis	*y*-axis	Distance
Geometric Models	3.7	2.9	5.3
NRm + LSm+ WLSm	3.5	4.1	6.0

La variabilidad efectiva del error, una medida que permite analizar lo sensible que es un método a la variación de la calidad de los datos, se calcula mediante la media aritmética de la desviación estándar de los errores cometidos en el eje *x*, en el eje *y* y en la distancia. Esta medida muestra lo cerca que está un método de la solución exacta cuando se ejecuta con datos con errores. Los valores de variabilidad efectiva del error más pequeños indican una menor sensibilidad a los errores en los datos y, por tanto, la generación de resultados más precisos. La Tabla 3 presenta esta medida para los modelos geométricos estudiados indicando mejores resultados para los modelos geométricos, con énfasis en el TLI que demostró mayor capacidad para procesar datos con errores.

Tabla 3. Desviación estándar de los errores [23]

Methods	Standard Deviation of the Errors			Effective Variability
	x-Axis	*y*-Axis	Distance	of the Errors
PPC*	4.1	3.8	4.5	4.1
CHC*	3.1	2.1	3.4	2.9
PLI*	3.3	4.1	4.9	4.1
MAI*	2.5	1.6	2.6	2.2
TLI*	2.3	1.0	2.3	1.9
NRm	4.0	4.0	4.9	4.3
LSm	4.3	6.7	7.4	6.1
WLSm	4.2	4.3	5.5	4.7

*Geometric Models proposed in this work.

Los resultados de los experimentos pueden verse en la Figura 4, Figura 5 y Figura 6, donde se presentan, respectivamente, el peor caso, el caso intermedio y el mejor caso. En todas las situaciones, los modelos geométricos presentaron resultados más eficaces en comparación con los métodos numéricos. Las líneas circulares y punteadas azules representan receptores/emisores que sufrieron graves interferencias y generaron datos con errores.

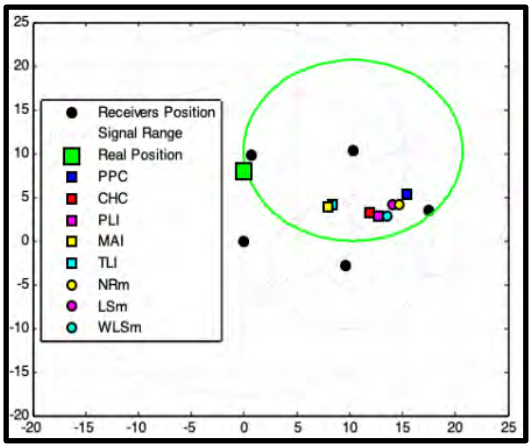

Figura 4. Resultados experimentales para el peor caso [23]

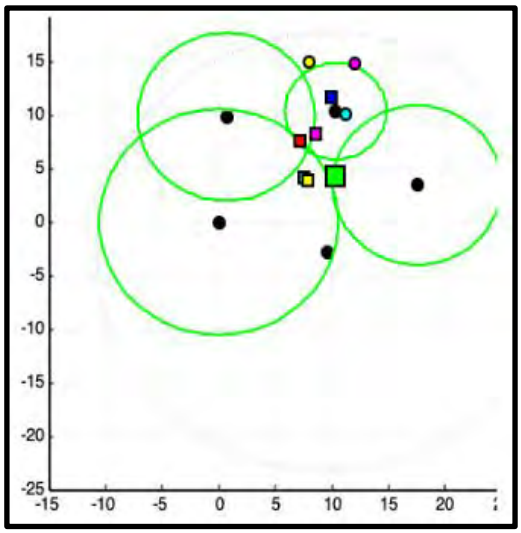

Figura 5. Resultados experimentales para el caso intermedio [23]

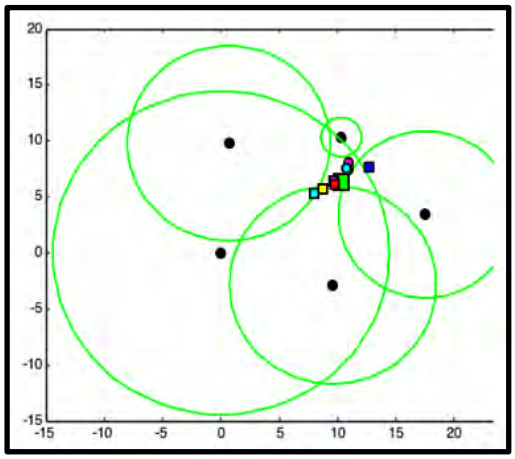

Figura 6. Resultados experimentales para el mejor caso [23]

Se desarrolló un simulador en código *MatLab* para probar las funciones implementadas y construir un prototipo para procesar datos reales. La información y las instrucciones de uso están disponibles en:
git@github.com:aleksmontanha/geometricsmodels.git

Contribución 3: Nuevo método de ubicación de señales basado en datos de rango de señales para herramientas de rastreo de proximidad

Montanha, A., Polidorio, A. M., & Romero-Ternero, M.C. (2021). New signal location method based on signal-range data for proximity tracing tools, Journal of Network and Computer Applications, Volume 180, 103006, ISSN 1084-8045, https://doi.org/10.1016/j.jnca.2021.103006 [24]

Las personas con discapacidad tienen la posibilidad de vivir su vida de forma más independiente y con mayor calidad gracias a las intervenciones de las tecnologías de la información y la comunicación (*Information and Communication Technology*-ICT) [30]. La Inteligencia Artificial (IA) y las tecnologías móviles han contribuido a que las personas con discapacidades aumenten su participación en la sociedad, ayudándoles a comunicarse, aprender, comprar, viajar, moverse por la ciudad, entre otras muchas [31-34]. Entre las personas con discapacidad, las que tienen problemas de visión son el centro de este estudio. En este contexto, la IA, mediante las tecnologías de asistencia, ha destacado en el proceso de mejora de la calidad de vida de estas personas. La Organización Mundial de la Salud (OMS) calcula que 2.200 millones de personas viven con discapacidad visual de cerca o de lejos en todo el mundo (Organización Mundial da Saúde 2021). Entre ellos, una de las actividades más difíciles de su vida diaria es la movilidad, más concretamente, cruzar las calles [35]. Como solución a este problema, las ciudades han implantado dispositivos de accesibilidad para cruzar las carreteras, en su mayoría basados en alertas sonoras emitidas por los semáforos. Sin embargo, este tipo de solución presenta deficiencias en cuanto a su capacidad para transcribir el entorno. Entre otras, hay dos situaciones más críticas para este tipo de solución, la primera es la contaminación acústica de las grandes ciudades y la segunda cuando hay intersecciones muy cercanas entre sí varias emisiones sonoras generarán confusión y aumentarán la dificultad de los discapacitados visuales para cruzar la carretera. La combinación de la informática ubicua, las tecnologías de detección, los protocolos de comunicación en Internet y los dispositivos integrados son los frutos del advenimiento llamado Internet de los objetos (IoT) [36]. El IoT contribuye en la actualidad a la creación de un escenario

con numerosas soluciones para las llamadas "ciudades inteligentes" en las que el uso de los *smartphones*, ampliamente disponibles hoy en día para el público en general, se han convertido en importantes herramientas. En el contexto abordado en este estudio, las personas con discapacidad visual están incluidas en este público, ya que utilizan ampliamente los teléfonos inteligentes como tecnología asistiva [30].

En este estudio presentamos un sistema sensible al contexto que guía a las personas con discapacidad visual para cruzar las carreteras. Este sistema consiste en la instalación de semáforos inteligentes (*Seebot Agent*) [22] emparejados con *WiFi* en una intersección. Este hardware funciona junto con un marco de software que detecta automáticamente los movimientos de los vehículos y los peatones y guía a las personas con discapacidad visual por la carretera. El semáforo calcula la ubicación del usuario y la situación del tráfico mediante la trilateración de señales hacia y desde un modelo de visión por ordenador previamente entrenado. Una aplicación móvil en el smartphone del peatón con discapacidad visual se comunica con el semáforo y le ayuda a cruzar la calle con seguridad**.**

En este estudio se realizaron los mismos experimentos que en el estudio anterior (Montanha et al., 2019) [23], comparando los resultados generados por el nuevo método propuesto (wPPC) con los métodos anteriores (PPC, Centroide de Punto Polar, CHC, Centroide de Casco Convexo, PLI, Centroide de Intersección de Línea Polar, TLI, Centroide de Intersección de Línea Tangente, y MAI, Centroide de Intersección de Línea Tangente de Ángulo Mínimo) y con los métodos numéricos tradicionales TLI. NRm, LSm y WLSm. La Figura 7 muestra los resultados de WPPC y PPC ejecutados con datos de alta calidad y la Figura 8 muestra esta misma ejecución con datos de baja calidad. En ambos experimentos, WPPC produjo las estimaciones de localización con mayor precisión en comparación con PPC. Todos los experimentos presentan errores en los datos de la señal adquirida.

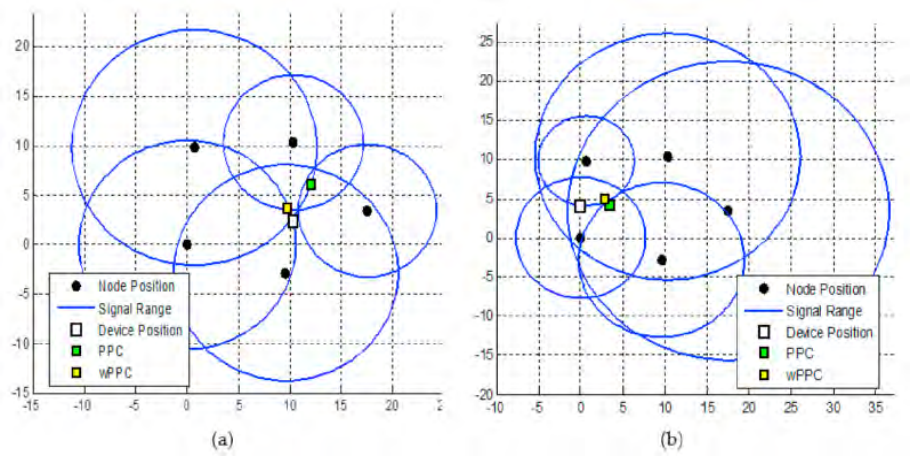

Figura 7. PPC vs. wPPC. Datos adquiridos con alta precisión. a) (X-12). b) (X-2) [24]

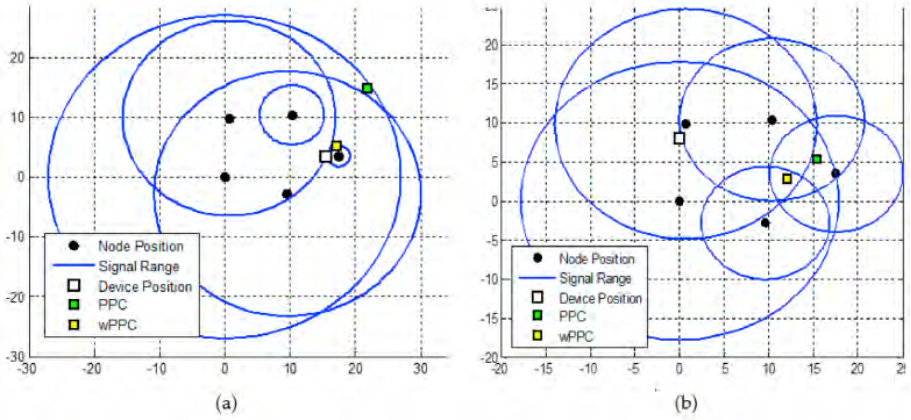

Figura 8. PPC vs. wPPC. Datos adquiridos con erros significativos. a) (X-5). b) (X-4) [24]

Para realizar la evaluación de errores de este estudio, se han utilizado los mismos datos y la misma estructura utilizados en el estudio anterior (Montanha et al., 2019), es decir, se consideraron tres conjuntos de datos de errores: (1) el error en la medición de la distancia (la distancia euclidiana entre la ubicación estimada del dispositivo $E_{xy}(E_x,E_y)$, calculado para cada método, y la posición real del dispositivo $P_n(x_n,y_n)$; (2)el error absoluto a lo largo del eje x dado por $|E_x - x_n|$ e (3) el error absoluto a lo largo del eje y dado por $|E_y - y_n$.

El resultado de este análisis puede verse en la Tabla 4, donde se evaluó el error mínimo, el error máximo y el error medio. Los errores pueden ser mayores o menores en función de la calidad de los datos adquiridos. La Tabla 4 muestra que, en el contexto general, los modelos geométricos (wPPC, PPC, CHC, PLI, MAI, TLI) presentan mejores resultados (menos errores) que los modelos numéricos (WLSm, NRm y LSm).

Tabla 4. Magnitud en metros de los errores em los casos experimentales [24]

	Minimum Error			Maximum Error			Mean Error		
	x-axis	*y*-axis	distance	*x*-axis	*y*-axis	distance	*x*-axis	*y*-axis	distance
wPPC	0.4	0.2	0.6	12.0	5.2	13.0	2.6	2.0	3.4
PPC[a]	0.4	0.2	2.7	15.5	12.5	15.7	4.5	4.4	6.9
CHC[a]	0.1	0.1	0.6	11.9	6.0	12.8	2.5	2.4	3.7
PLI[a]	0.1	0.1	0.7	12.8	15.9	16.3	2.4	3.8	5.0
MAI[a]	1.6	0.3	1.7	7.9	5.3	8.9	4.2	1.5	4.7
TLI[a]	2.3	0.3	2.3	8.3	3.9	9.2	4.1	1.3	4.4
NRm[a]	0.1	1.1	1.3	14.7	12.2	15.2	2.8	5.1	6.5
LSm[a]	0.3	1.2	1.8	14.1	22.5	23.7	3.6	6.4	7.9
WLSm[a]	0.1	0.7	1.3	13.6	15.3	17.7	3.5	4.9	6.5

[a] Available in (Montaña et al., 2019).

Considerando el error mínimo, el WPPC, presentó una media de 0,4 comparando el resultado con los métodos CHC y PLI (0,3) se puede afirmar que, cuando los datos son buenos, el WPPC produce una respuesta tan precisa como CHC y PLI. En cuanto al error máximo, los errores medios producidos por los métodos tradicionales se sitúan entre ~13 y ~20, para los métodos geométricos éstos se sitúan en torno a ~15, para wPPC y CHC promedian ~10, finalmente para MAI y TLI presentan errores medios de ~8. Considerando el error medio, WPPC presentó el error medio más bajo en comparación con todos los demás métodos. Por lo tanto, a partir de estos análisis se puede afirmar que los resultados presentados por el WPPD cuando hay una alta precisión de los datos (error mínimo) son aceptables y cuando estos datos son malos o moderados (errores moderados y medios) el WPPC presenta una respuesta más precisa que los otros métodos. El cuadro 2 presenta la variabilidad de los errores cometidos (para cada métrica de evaluación) por los métodos en función de los errores de los datos. A través de la variabilidad efectiva de los errores ( ) es posible evaluar la sensibilidad del método a la variación de la calidad de los datos. Los valores más bajos indican una menor sensibilidad a los errores en los datos y, en consecuencia, la obtención de resultados más precisos. En este sentido, los modelos geométricos (WPPC, PPC, CHC, PLI, MAI, TLI) si se comparan con los métodos tradicionales (WLSm, NRm y LSm) mostraron ser más eficientes cuando se opera con datos que tienen errores. El MAI, el TLI y el WPPC pueden destacarse como métodos con mayor capacidad para procesar datos con errores.

Tabla 5.Desviación estândar de los errores [24]

Methods	Standard Deviation of the Errors			Effective Variability of the Errors
	x-axis	*y*-axis	distance	
wPPC	3.2	1.5	3.3	2.7
PPC[a]	4.1	3.8	4.5	4.1
CHC[a]	3.1	2.1	3.4	2.9
PLI[a]	3.3	4.1	4.9	4.1
MAI[a]	2.5	1.6	2.6	2.2
TLI[a]	2.3	1.0	2.3	1.9
NRm[a]	4.0	4.0	4.9	4.3
LSm[a]	4.3	6.7	7.4	6.1
WLSm[a]	4.2	4.3	5.5	4.7

[a] Available in (Montanha et al., 2019).

Contribución 4: Un sistema basado en inteligencia artificial consciente del contexto para apoyar los cruces de calles para peatones con discapacidades visuales

Montanha, A., Oprescu, A. M., & Romero-Ternero, M.C. (2022). A Context-Aware Artificial Intelligence-based System to Support Street Crossings for Pedestrians with Visual Impairments, Applied Artificial Intelligence, 36:1, https://doi.org/10.1080/08839514.2022.2062818 [25]

Como resultado de este estudio se presenta la arquitectura del proyecto completo donde hay tres componentes principales de hardware: el smartphone, el semáforo inteligente y las antenas *WiFi*. El semáforo inteligente supervisa las intersecciones mediante cámaras IP y algoritmos de trilateración de señales y procesamiento de imágenes (basados en redes neuronales y procesos de correlación de datos). Las antenas *WiFi* instaladas en las intersecciones, utilizadas únicamente con fines de localización, se encargan de intercambiar la señal mediante la tecnología de red celular de alta velocidad, como 3G o 4G, con el smartphone (Figura 9). Se puede atender a más de un peatón con discapacidad visual, ya que los dispositivos móviles se identifican de forma exclusiva a través de la dirección *MAC*.[1]

[1] Con las nuevas políticas de anonimización, la forma de identificación ahora está vinculada a un id del software instalado en la aplicación, con la aceptación del usuario.

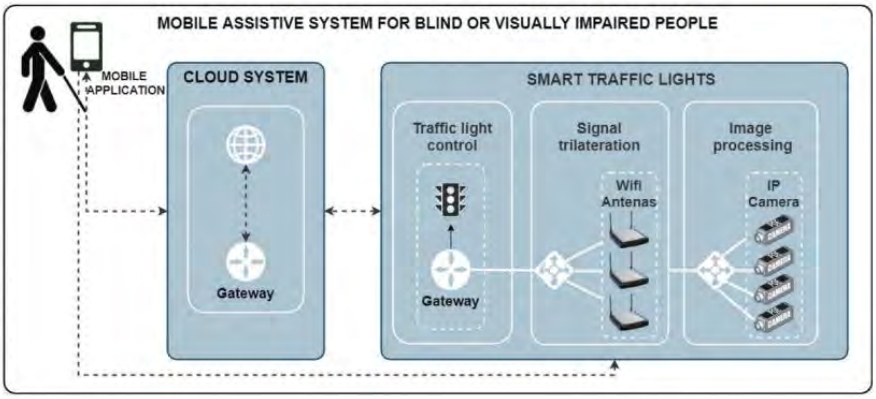

Figura 9. Visión general del diseño del sistema de asistencia móvil propuesto [25]

El semáforo *Seebot Agent* se compone básicamente de un procesador Intel I5 de 7ª generación con una interfaz de pantalla LED de alta resolución, una cámara IP Axis HD con una tasa de captura y transmisión de imágenes superior a 30 fps, un inclinómetro, un acelerómetro y un sistema de ajuste del ángulo de la cámara motorizado capaz de inclinar 80° en el eje Y (vertical). Como protocolos de conexión, utiliza *Ethernet, Bluetooth* y *WiFi.* Las imágenes captadas (Figura 10) por este dispositivo tienen una altura mínima de 5,5 metros y la distancia de la zona que se pretende atravesar es dinámica (puede cambiar en función de las características del lugar). Se utilizaron colores para resaltar los elementos más importantes de las imágenes: la zona de cruce está marcada en verde claro, el peatón en verde fluorescente y el carril de coches en rojo.

Figura 10. Imagen de paso de peatones recuperada de un Seebot Agent *instalado en una intersección [25]*

La aplicación móvil se ha desarrollado únicamente para Android debido a la mayor popularidad de los smartphones de esta plataforma. Este dispositivo ya cuenta con el hardware y el software necesarios para interactuar con el semáforo inteligente, además de ser de utilidad para muchas personas con discapacidad visual. La aplicación sigue las normas de pruebas de accesibilidad (ACT) recomendadas por el W3C (World Wide Web

Consortium, 2021) [37] y las normas internacionales de la web. La Figura 11 muestra algunas capturas de pantalla de la aplicación: la pantalla principal de inicialización de la localización del peatón, una vista de pájaro de los semáforos inteligentes instalados en una calle y su estado, y un ejemplo de alerta creada para un usuario que espera la apertura del semáforo.

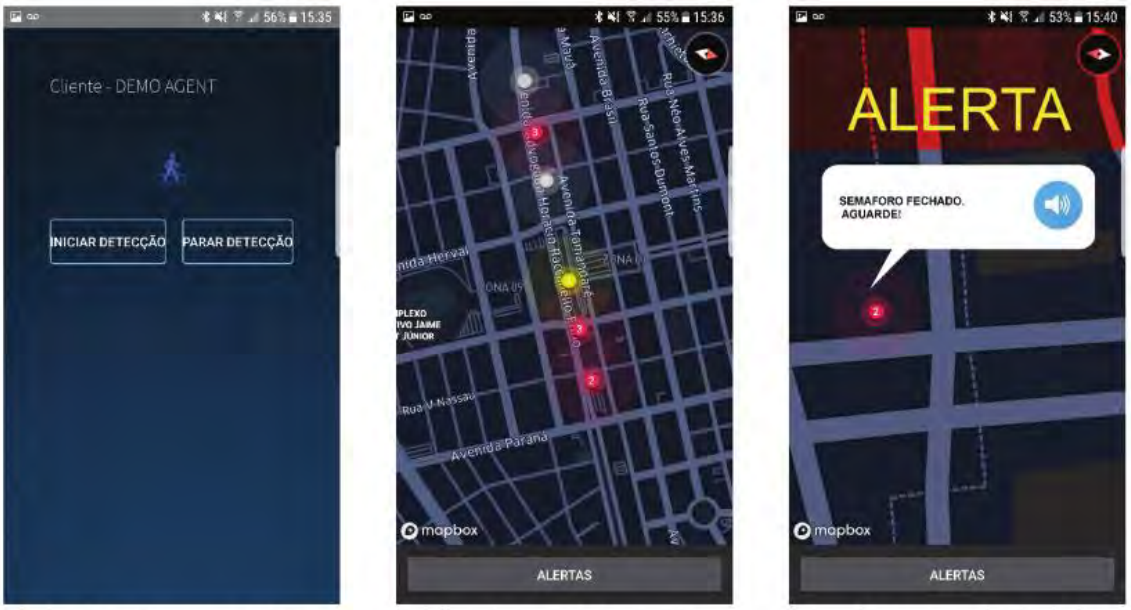

(a) App's main screen to initiate or stop localization process

(b) Aerial view of the intelligent semaphores on a street

(c) Alert to hold (closed semaphore, hold on)

Figura 11. Capturas de pantalla de la aplicación móvil de asistencia al cruce de calles [25]

El semáforo inteligente se instaló inicialmente en la ciudad de Maringá, situada en el estado de Paraná en Brasil, y se analizó durante un periodo de 3 meses (Tabla 6). En esta tabla se observa que en el primer mes (07/2019), en el que la aplicación se puso a disposición de un usuario, se produjeron 7 conexiones. Sin embargo, sólo se han realizado 6 asistencias de travesía completa y segmentación de datos. Esta diferencia se debe a que el proceso de asistencia a la travesía sólo se inicia cuando los datos resultantes del proceso de correlación entre los datos de trilateración de señales y los datos de procesamiento de imágenes superan el umbral seleccionado del 90%. En el segundo mes (08/2019), cuando se publicita la app en un grupo de redes sociales, el número de conexiones aumentó a 14. En este período, todas las conexiones dieron lugar a la asistencia a la travesía y se realizó la segmentación de los datos. En el tercer mes, se produjeron 115 conexiones y, de ellas, se completaron 93 (80,8%) asistencias de cruce y se realizaron con éxito 111 (96,5%) asistencias de segmentación de datos. Entre las 115 conexiones realizadas, el 19,2% no cruzó o lo hizo con ayuda humana y no informó de la plataforma.

Tabla 6. Número de conexiones de la app, asistencia para cruces seguros y fusión de datos exitosa del sistema operativo durante 3 meses [25]

Period	App connections	Crossing assistance completed	Segmentation (trilateration and image processing)
07/2019	7	6	6
08/2019	14	14	14
09/2019	115	93	111

Según las observaciones realizadas, para realizar la trilateración de señales se requieren pocos recursos computacionales del semáforo, este proceso consume entre el 1 y el 3% de uno de los cinco núcleos y entre 10 y 20 MB de memoria con un tiempo de procesamiento de 0,1 segundos. El procesamiento de imágenes (captura de fotogramas, procesamiento de fotogramas, detección y reidentificación de peatones) consume entre el 10 y el 30% de dos núcleos y entre 50 y 80 MB de memoria con 32 fotogramas por segundo. La detección de más de un usuario en el entorno aumenta el consumo de procesamiento en torno al 3-5% y el consumo de memoria en torno a los 10 MB. Teniendo en cuenta esta configuración y la disponibilidad de recursos, el sistema es capaz de atender hasta 5 personas simultáneamente.

Se realizó una entrevista a 11 usuarios con discapacidad visual para evaluar la usabilidad y la experiencia del usuario con la aplicación móvil. Como resultado, se obtuvo la siguiente información: el 83% estaba familiarizado con el uso de la aplicación (el 50% la usa siempre y el 36,3% la usa habitualmente), el 8,3% la usa raramente y el 8,3% no la usa nunca. En cuanto a la complejidad de uso, el 100% de los usuarios señaló que la aplicación no es compleja de utilizar ni necesita apoyo técnico para ello y el 58,3% no necesitó aprender nada más antes de utilizar la aplicación. Todos se sintieron seguros al cruzar la carretera usando la app, de estos, el 66,6% no se guiaron por otras personas para seguir el cruce, incluso usando la app. En cuanto a la usabilidad de la aplicación, el 33,3% la valoró con un 10 sobre 10, el 33,3% con un 9, el 16,6% con un 8 y el 16,6% con un 7. La pregunta sobre las formas de mejorar la aplicación dio como resultado las siguientes frases: "*Que se haga una campaña para que en más semáforos se instale la misma", "Ampliar su alcance a otros semáforos y mejoras naturales.., "Es genial", "Que hubiera una política para tener más semáforos en la ciudad", "La aplicación es simplemente perfecta y en relación con algo así, es difícil dar cualquier tipo de sugerencia", "La aplicación es excelente, pero debería tener otras formas de uso sin tener que usar el teléfono"* y *"Ninguna sugerencia"*.

Capítulo 4

Conclusiones

La primera contribución se ha logrado mediante el diseño y desarrollo de un primer prototipo de semáforo inteligente, que hemos denominado *Seebot Agent*. Este semáforo está compuesto por cámaras de vídeo, señal *wifi*, dispositivos *Bluetooth* y señal *GPS* [22]. Este dispositivo fue instalado con fines de prueba y evaluación en la ciudad de Maringá, estado de Paraná, durante un año, y en la ciudad de Campina Grande, estado de Paraíba, durante dos años.

A partir de los datos recogidos en este primer estudio, se inició el segundo estudio [23], en el que se propuso una nueva metodología, cuyo objetivo era mejorar los resultados de los métodos de localización de la posición 2D de una fuente de señal enviada por un dispositivo emisor. Este estudio ha presentado cinco modelos geométricos, a saber: (1) basado en el centroide de los puntos de la geometría polo-polar (PPC); (2) basado en la región convexa del casco entre los polos (CHC); (3) basado en el centroide de los puntos obtenidos por la intersección de las líneas polares (PLI); (4) basado en el centroide de los puntos obtenidos por la intersección de las líneas tangentes (TLI) e (5) basado en el centroide de los puntos obtenidos por la intersección de las líneas tangentes con ángulos mínimos (MAI). Los resultados de este segundo estudio muestran que el primer método (PPC) tiene un menor coste computacional $O(n)$ en comparación con los otros métodos $O(n \log n)$ donde n es el número de puntos de interés. Por último, se ha podido reducir el número de operaciones aritméticas y los errores de propagación si se compara con los métodos convencionales.

Un tercer estudio [24], ha analizado una forma de mejorar la precisión de los resultados anteriores del PPC, sin aumentar el coste computacional y el número mínimo de nodos ($m \geq 2$) en la composición de la red de localización. Se ha creado una extensión del PPC, que hemos denominado *Polo-Polar Weighted Centroid* (WPPC). Esta nueva metodología ha mejorado la exactitud de los resultados del PPC anterior, especialmente cuando tiene errores (significativos o no). Así, este nuevo método beneficia la interacción inalámbrica entre smartphones, generando una mayor precisión a la hora de estimar la localización de las señales para realizar el seguimiento de los contactos de proximidad.

En el cuarto estudio se finaliza de forma completa un sistema asistencial inteligente basado en tecnologías IoT para ciudades inteligentes, con semáforos integrados y comunicación con una aplicación para dispositivos móviles.

Preferiblemente, este dispositivo debe ser un teléfono inteligente, que, en posesión de una persona con discapacidad visual, interprete las señales enviadas y recibidas por el semáforo inteligente y lo ayude a cruzar el paso de peatones con mayor seguridad.

A continuación se presentan las principales conclusiones de cada una de las cuatro contribuciones que componen esta tesis por compendio.

Contribución 1: Una innovación tecnológica para ayudar de forma segura en la orientación espacial de personas ciegas en un entorno urbano complejo.

Montanha, A., Escalona, M. J., Domínguez-Mayo, F. J., & Polidorio, A. M. (2016, August). A technological innovation to safely aid in the spatial orientation of blind people in a complex urban environment. In 2016 IEEE International Conference on Image, Vision and Computing (ICIVC), Portsmouth, UK, 2016, pp. 102-107, https://10.1109/ICIVC.2016.7571281 [22]

Indicadores de calidad: Esta publicación, presentada en la conferencia 2016 IEEE tiene un *h-index* de 6 en el año 2016. La publicación ha recibido hasta ahora (mayo 2023) 10 citas (según la consulta de Google Scholar) y 380 visualizaciones del texto completo según el sitio web del editor (https://ieeexplore.ieee.org).

Los resultados destacables obtenidos del estudio son:

- Se ha creado el hardware de un semáforo para ciudades inteligentes, que se integró con una aplicación para smartphones mediante un agente inteligente (*Seebot Agent*) con el objetivo de ayudar a las personas con discapacidad visual a cruzar las carreteras.
- Se ha creado una solución de gestión de de *big data en el semáforo*, que proporciona un historial de información para que el sistema aprenda y pueda ayudar al proceso de cruce de carreteras de forma más fiable y segura.
- El sistema se ha probado en dos ciudades de Brasil: en la ciudad de Maringá, estado de Paraná, durante un año y en la ciudad de Campina Grande, estado de Paraíba, durante 2 años, periodo en el que se aplicaron las mejoras identificadas.
- Se identificó que los estudios futuros de este proyecto debían centrarse en métodos para localizar la posición 2D y disminuir el coste computacional.

Contribución 2: Modelos geométricos para la mejora de la triangulación de las señales.

Montanha, A., Polidorio, A. M., Domínguez-Mayo, F. J., & Escalona, M. J. (2019). 2D triangulation of signals source by pole-polar geometric models. Sensors, 19(5), 1020, https://doi.org/10.3390/s19051020 [23]

Indicadores de calidad: Este estudio fue publicado en 2019 en *Sensors*, una revista de acceso abierto cuyo factor de impacto JCR en 2021 fue de 4,05 en el año 2021, encontrándose en el Q1. La publicación ha recibido hasta ahora (mayo 2023) 6 citas (según la consulta de Google Scholar) y 4445 vistas de texto completo según el sitio web del editor (https://www.mdpi.com/journal/sensors/special_issues/Signal+InformationProcessingWSN).

Los resultados destacables obtenidos del estudio son:

- Existe una relación geométrica entre la ubicación del emisor y los elementos de la geometría polo-polar. En este contexto, se ha propuesto una solución cuyo resultado exacto (si los datos disponibles son precisos) tiene coste $O(n)$ porque es capaz de reducir el número de operaciones aritméticas requeridas por los métodos convencionales actualmente en uso.
- En caso de datos con errores, este método produjo mejores estimaciones en comparación con los métodos tradicionales como WLSm, NRm y LSm.
- Los resultados obtenidos fueron consistentes incluso en presencia de incoherencia de datos o incoherencia geométrica en la disposición del sistema receptor.

Las limitaciones de los resultados del estudio son:

- Hasta el momento la solución es 2D.
- El proceso de estimación de la localización de los métodos propuestos requiere que el dispositivo a localizar esté insertado en la zona de cobertura de los AP. Los puntos de acceso sólo pueden disponerse de forma co-lineal en algunos casos concretos.

Contribución 3: Nuevo método de ubicación de señales basado en datos de rango de señales para herramientas de rastreo de proximidad

Montanha, A., Polidorio, A. M., & Romero-Ternero, M.C. (2021). New signal location method based on signal-range data for proximity tracing tools, Journal of Network and Computer Applications, Volume 180, 103006, ISSN 1084-8045, https://doi.org/10.1016/j.jnca.2021.103006 [24]

Indicadores de calidad: Este estudio se publicó en 2021 en el *Journal of Network and Computer Applications*, una revista de acceso abierto sobre áreas relacionadas con las redes informáticas y sus aplicaciones cuyo factor de impacto JCR en 2021 es de 7,574, estando en el Q1 y con SJR de 1.145. La publicación ha recibido hasta el momento (mayo 2023) 3 citas (según la consulta de Google Scholar) y 28 vistas de texto completo según el sitio web del editor (https://www.sciencedirect.com/science/article/pii/S1084804 521000333).

Los resultados destacables obtenidos del estudio son:

- Se ha propuesto la creación de un nuevo método denominado método del centro polar ponderado (wPPC) como extensión del método del modelo del centro polar (PPC) sin aumentar el coste computacional O(m2) y el número mínimo de nodos ($m \geq 2$) en la composición de la red de localización.
- Este nuevo método, wPPC, fue capaz de producir resultados más precisos al procesar datos con errores (significativos o no).
- Esta nueva propuesta ayuda a tratar el problema de aplicación de localizar puntos 2D en una relación geométrica reduciendo el número de operaciones aritméticas requeridas por los métodos convencionales actuales y propagando los errores inherentes a los datos adquiridos.
- Este método beneficia a la interacción inalámbrica entre teléfonos móviles para el seguimiento de contactos de proximidad al mejorar la precisión de la estimación de las ubicaciones de las señales.

Las limitaciones del estudio son:

- wPPC es una solución 2D.
- Este método requiere que el dispositivo se encuentre dentro del área de cobertura de la red de nodos.
- Para la ejecución de los métodos geométricos utilizados por esta propuesta, es necesario que el dispositivo esté rodeado por los nodos de la red de localización.

Contribución 4: Un sistema basado en inteligencia artificial consciente del contexto para apoyar los cruces de calles para peatones con discapacidades visuales

Montanha, A., Oprescu, A. M., & Romero-Ternero, M.C. (2022). A Context-Aware Artificial Intelligence-based System to Support Street Crossings For Pedestrians with Visual Impairments, Applied Artificial Intelligence, 36:1, https://doi.org/10.1080/08839514.2022.2062818 [28]

Indicadores de calidad: Este estudio se ha publicado en 2022 en *Applied Artificial Intelligence*, una revista sobre aplicaciones de la inteligencia artificial en la gestión, la industria, la ingeniería, la administración y la educación, así como evaluaciones de los sistemas y herramientas de IA existentes y su impacto económico, social y cultural, cuyo factor de impacto JCR fue de 2,777 en el año 2021, estando en Q3.
La publicación ha recibido hasta el momento (mayo 2023) 1 cita (según la consulta de Google Scholar) y 1374 vistas de texto completo según el sitio web de la editorial https://www.tandfonline.com/doi/full/10.1080/08839514.2022.2062818#metrics-content).

Los resultados destacables obtenidos del estudio son:

- Se ha desarrollado un sistema asistencial inteligente para la movilidad de los peatones con discapacidad visual, concretamente para los cruces de calles. Por lo que sabemos, este es el primer estudio desarrollado para asistir a los peatones que cruzan para discapacitados visuales que combina el uso de semáforos inteligentes en ciudades inteligentes como elemento de detección del tráfico y la situación de los peatones a través de sensores, procesamiento de imágenes, técnicas de IA y dispositivos móviles.
- Se ha aprovechado el potencial de las tecnologías IoT combinadas con técnicas de inteligencia artificial, buscando la fusión de datos y el uso de infraestructuras inteligentes en ciudades inteligentes.
- El sistema de semáforos inteligentes es capaz de realizar un gran número de peticiones: adquirir y transmitir imágenes en tiempo real de sus ubicaciones de cobertura a un centro de control de tráfico, comunicarse con los peatones usuarios de dispositivos móviles o instalados en los vehículos a través de la señalización

WiFi y/o Bluetooth, y el cruce asistido para peatones con discapacidad visual, entre otras muchas tareas de regulación del tráfico.

- La solución propuesta añade como factor innovador el uso de la infraestructura existente para implementar la tecnología asistencial a los peatones con discapacidad visual.
- Se ha comprobado que hay beneficios en una solución que limita el uso del *smartphone* por parte del usuario y se basa más en una infraestructura común facilitada por el contexto de una ciudad inteligente.
- La comunicación entre el software de asistencia y el de regulación del tráfico puede ser beneficiosa para los usuarios con discapacidad visual, ya que el semáforo puede adaptarse a la situación del tráfico para garantizar un cruce seguro.

Líneas de trabajo futuras

Con el avance de las tecnologías de robots de entrega autónomos [38-39], el siguiente paso es el desarrollo de una API (Application Programming Interface) abierta para la integración con este tipo de vehículos, con el objetivo de brindarles información para que las personas ciegas puedan cruzar las carreteras con seguridad y autonomía.

La investigación futura debería contemplar la mejora de la funcionalidad del sistema por la noche, ya que sin una iluminación adecuada, la mayor parte del tiempo el sistema no es capaz de dirigirse al peatón con discapacidad visual, y se requiere el sistema de asistencia de emergencia.

El desarrollo de técnicas y algoritmos para mejorar la precisión puede llevarse a cabo dentro de la comunidad científica.

Como continuación de este estudio, se puede liberar el código fuente abierto poniéndolo a disposición en GitHub, para que investigadores de todo el mundo puedan contribuir con el código e implementar el sistema en sus ciudades.

Capítulo 5

Referencias

En esta sección se recogen las referencias que se han usado para la elaboración del presente documento. Las referencias específicas de cada artículo del compendio se pueden consultar en el apartado correspondiente a las referencias dentro de los propios artículos que se incluyen en la PARTE II: PUBLICACIONES DEL COMPENDIO.

[1] WHO. Visual Impairment and Blindness. Available online: https://www.who.int/en/news-room/fact-sheets/detail/blindness-and-visual-impairment (consultado en mayo de 2023).

[2] Alwi, S. R. A. W., & Ahmad, M. N. (2013, December). Survey on outdoor navigation system needs for blind people. In *2013 IEEE Student Conference on Research and Developement* (pp. 144-148). IEEE.

[3] El-Taher, F. E. Z., Taha, A., Courtney, J., & Mckeever, S. (2021). A systematic review of urban navigation systems for visually impaired people. Sensors, 21(9), 3103.

[4] Schroeder, B. J., Rouphail, N. M., & Emerson, R. S. W. (2006). Exploratory analysis of crossing difficulties for blind and sighted pedestrians at channelized turn lanes. *Transportation research record*, *1956*(1), 94-102.

[5] Ashmead, D. H., Guth, D., Wall, R. S., Long, R. G., & Ponchillia, P. E. (2005). Street crossing by sighted and blind pedestrians at a modern roundabout. *Journal of Transportation Engineering*, *131*(11), 812-821.

[6] Hanna, R. (2009). *Incidence of pedestrian and bicyclist crashes by hybrid electric passenger vehicles* (No. HS-811 204).

[7] Wu, J., Austin, R., & Chen, C. L. (2011). *Incidence rates of pedestrian and bicyclist crashes by hybrid electric passenger vehicles: an update* (No. HS-811 526).

[8] Tatari, O., Karaaslan, E., Noori, M., Lee, J., Wang, L., & Abdel-Aty, M. (2017). Agent-Based Simulation for Investigating the Safety Concerns of Electric Vehicles in the US.

[9] Shingledecker, C. A., & Foulke, E. (1978). A human factors approach to the assessment of the mobility of blind pedestrians. *Human factors*, *20*(3), 273-286.

[10] Warren, D. H., & Strelow, E. R. (Eds.). (2013). *Electronic spatial sensing for the blind: contributions from perception, rehabilitation, and computer vision* (Vol. 99). Springer Science & Business Media.

[11] Kay, L. (1985). Sensory aids to spatial perception for blind persons: Their design and evaluation. In *Electronic spatial sensing for the blind* (pp. 125-139). Springer, Dordrecht.

[12] Deering, M. F., & Collins, C. (1981). Real-time natural scene analysis for a blind prosthesis (Doctoral dissertation, University of California, Berkeley).

[13] Deering, M. F. (1985). Computer vision requirements in blind mobility aids. Electronic spatial sensing for the blind, 65-82.

[14] Kanwal, N., Bostanci, E., Currie, K., & Clark, A. F. (2015). A navigation system for the visually impaired: a fusion of vision and depth sensor. Applied bionics and biomechanics, 2015.

[15] Shchekotov, M. (2014, October). Indoor localization method based on Wi-Fi trilateration technique. In Proceedings of the 16th conference of fruct association (pp. 177-179).

[16] Cheng, R., Wang, K., & Lin, S. (2018). Intersection navigation for people with visual impairment. In Computers Helping People with Special Needs: 16th International Conference, ICCHP 2018, Linz, Austria, July 11-13, 2018, Proceedings, Part II 16 (pp. 78-85). Springer International Publishing.

[17] Li, X., Cui, H., Rizzo, J. R., Wong, E., & Fang, Y. (2020). Cross-Safe: A computer vision-based approach to make all intersection-related pedestrian signals accessible for the visually impaired. In Advances in Computer Vision: Proceedings of the 2019 Computer Vision Conference (CVC), Volume 2 1 (pp. 132-146). Springer International Publishing.

[18] Bai, J., Liu, D., Su, G., & Fu, Z. (2017, April). A cloud and vision-based navigation system used for blind people. In Proceedings of the 2017 International Conference on Artificial Intelligence, Automation and Control Technologies (pp. 1-6).

[19] Y'iariello, V., & Carrella, L. (2020). Everyday technology to support leisure and daily activities in people with intellectual and other disabilities. Developmental neurorehabilitation, 23(7), 431-438.

[20] Ash, R., Ofri, D., Brokman, J., Friedman, I., & Moshe, Y. (2018, December). Real-time pedestrian traffic light detection. In 2018 IEEE International Conference on the Science of Electrical Engineering in Israel (ICSEE) (pp. 1-5). IEEE.

[21] Ghilardi, M. C., Jacques, J. C., & Manssour, I. (2016). Crosswalk localization from low resolution satellite images to assist visually impaired people. IEEE computer graphics and applications, 38(1), 30-46.

[22] Montanha, A., Escalona, M. J., Domínguez-Mayo, F. J., & Polidorio, A. M. (2016, August). A technological innovation to safely aid in the spatial orientation of blind people in a complex urban environment. In *2016 IEEE International Conference on Image, Vision and Computing (ICIVC), Portsmouth, UK, 2016, pp. 102-107, https://10.1109/ICIVC.2016.7571281*

[23] Montanha, A., Polidorio, A. M., Domínguez-Mayo, F. J., & Escalona, M. J. (2019). 2D triangulation of signals source by pole-polar geometric models. *Sensors*, *19*(5), 1020, https://doi.org/10.3390/s19051020

[24] Montanha, A., Polidorio, A. M., & Romero-Ternero, M.C. (2021). *New signal location method based on signal-range data for proximity tracing tools,* Journal of Network and Computer Applications, Volume 180, 103006, ISSN 1084-8045, https://doi.org/10.1016/j.jnca.2021.103006

[25] Montanha, A., Oprescu, A. M., & Romero-Ternero, M.C. (2022). *A Context-Aware Artificial Intelligence-based System to Support Street Crossings For Pedestrians with Visual Impairments,* Applied Artificial Intelligence, 36:1, https://doi.org/10.1080/08839514.2022.2062818

[26] Intel Iot Market Ready Solutions Program. Available online: https://newsroom.intel.com.br/news-releases/intel-certifica-empresas-brasileiras-no-programa-intel-iot-market-ready-solutions-com-solucoes-para-os-setores-de-seguranca-mobilidade-urbana-e-varejo/ (consultado en mayo de 2023).

[27] IOT World Congress. Available online: https://www.iotsworldcongress.com/press_release/the-event/iotswc-2019-awards-the-solutions-by-eiffage-bioservo-cartesiam-ai-eolane-zyfra-suek-and-gft/) (consultado en mayo de 2023).

[28] Social Innovation Awards Finalist Projects. Available online: https://www.fundacionmapfre.org/en/awards-aids/awards/awards-fundacion-mapfre-innovation-social/finalist-projects-sixth-edition/ (consultado en mayo de 2023).

[29] Ahad, M., Rahman, A., Tan, J. K., Kim, H., & Ishikawa, S. (2012). Motion history image: its variants and applications. Machine Vision and Applications, 23(2), 255-281.

[30] Khan, A., & Khusro, S. (2021). An insight into smartphone-based assistive solutions for visually impaired and blind people: issues, challenges and opportunities. Universal Access in the Information Society, 20(2), 265-298.

[31] Baumgartner, A., Rohrbach, T., & Schönhagen, P. (2021). 'If the phone were broken, I'd be screwed': media use of people with disabilities in the digital era. *Disability & Society*, 1-25.

[32] Molina-Cantero, A. J., Lebrato-Vázquez, C., Merino-Monge, M., Quesada-Tabares, R., Castro-García, J. A., & Gómez-González, I. M. (2019). Communication technologies based on voluntary blinks: Assessment and design. IEEE Access, 7, 70770-70798.

[33] Balasuriya, B. K., Lokuhettiarachchi, N. P., Ranasinghe, A. R. M. D. N., Shiwantha, K. D. C., & Jayawardena, C. (2017, December). Learning platform for visually impaired children through artificial intelligence and computer vision. In 2017 11th International Conference on Software, Knowledge, Information Management and Applications (SKIMA) (pp. 1-7). IEEE.

[34] Mahmud, S., Sourave, R. H., Islam, M., Lin, X., & Kim, J. H. (2020, September). A vision based voice controlled indoor assistant robot for visually impaired people. In 2020 IEEE International IOT, Electronics and Mechatronics Conference (IEMTRONICS) (pp. 1-6). IEEE.

[35] Hakobyan, L., Lumsden, J., O'Sullivan, D., & Bartlett, H. (2013). Mobile assistive technologies for the visually impaired. Survey of ophthalmology, 58(6), 513-528.

[36] Suzuki, L. R. (2017). Smart cities IoT: Enablers and technology road map. In Smart city networks (pp. 167-190). Springer, Cham. *Disability & Society*, 1-25

[37] Caldwell, B., Cooper, M., Reid, L. G., & Vanderheiden, G. (2008). World Wide Web Consortium World Wide Web Consortium 2.0. W3C Recommendation, 11.

[38] M. A. Mohd Basri and N. H. Sahrir, "Design of Sub-Systems for GPS-Guided Autonomous Delivery Robot System", Elektrika, vol. 21, no. 3, pp. 1–5, Dec. 2022.

[39] Hossain, Mokter. (2022). Self-Driving Robots: A Revolution in the Local Delivery. California Management Review.

PARTE II:

PUBLICACIONES DEL COMPENDIO

A Technological Innovation to Safely Aid in the Spatial Orientation of Blind People in a Complex Urban Environment

A. Montanha
University of Seville.
Spain
Aleksandro.montanha@iwt2.org

M. Jose Escalona
University of Seville.
Spain
mjescalona@us.es

D. Mayo, Francisco José
University of Seville
Spain
fjdominguez@us.es

A. M. Polidorio
Maringá State University
Maringá, Brazil
ampolidorio@gmail.com

In the broader context of intelligent cities, ensure mobility of people regardless of their physical or sensory condition becomes a complex and difficult challenge to be treated. All papers referenced in this work presented as solution to equip the blind people with devices and sensors (controlled by a computational system) with ability to capture environmental structures data and somehow describe it to the understanding of the blind people. Our work explores another side of this problem: how the environment can transmit data about itself to safely-help to guide blind orientation in this environment? In other words, in our view point, the environment must report data on its structure as opposed to make the blind person try to extract these data from this environment. So, here we propose use an intelligent semaphore system (traffic lights) to communicate with a mobile system carried by the blind person and by the coherent processing of the signals sent and received between the mobile device and the intelligent semaphore, conduct the blind in the streets crossing in crosswalk safely.

Image and Signals Processing; Smart Cities; Blind-Pedestrian;

I. INTRODUCTION

The ability to travel safely, comfortably, gracefully, and independently, referred to hereafter by the term "mobility". Mobility is a factor of primary importance in the life of a blind individual. The blind person who fails to acquire this ability usually displays a life style characterized by passive acquiescence to conditions proposed and arranged by others. The blind person who has acquired this ability often displays a life style characterized by the execution of plans of his own formulation. Yet, until recent years, it was not generally recognized that mobility could be resolved into a collection of related sub-skills, and that these skills could be taught [1].

The needs of the blind both from the social view point and from the scientific and technological end has been defined and explored. Advances have been made in the areas of social adjustment, rehabilitation, communication, and learning skills. With the advancement of computer vision, even driven by the quest to bring robotizing the condition of human vision, also considering the coexistence between robots and humans [2], there have been many advances in objects segmentation and various other guidance methods in open or closed environments. This indicates that we can bring a more human view on the subject and allow the displacement or better urban mobility of an individual with visual impairment is automatically more assisted and guided by intelligent systems that can even react because of their condition.

Based on the US FARS data (National Highway Traffic Safety Administration), from 2002 and 2006 the US averaged roughly 5 blind pedestrian deaths from motor vehicle crashes (27 blind pedestrian are death) in the USA. – http://www-nrd.nhtsa.dot.gov. Given the small numbers involve, the count of blind pedestrian deaths was remarkably stable from year to year. Legally blind individuals accounted for roughly a tenth of a percent of all pedestrian deaths over this period. Was Presented a study [3] in which participants indicated when they would cross suggested that blind pedestrians miss more crossing opportunities and make riskier judgments than sighted pedestrians. [4] did an exploratory analysis of crossing difficulties for blind and sighted pedestrians at channelized turn lanes (CTL), the geometric nature of CTL facilities and the lack of signal control at the pedestrian crossing are factors that may negatively affect the delay and safety for blind pedestrians. Pedestrians waiting at the curb must judge the traffic moving in a circular motion, and they must deal with a significant amount of background traffic (i.e., noise) present at the main intersection. The findings show that crossings at all CTL crossing locations are significantly more difficult for blind pedestrians than for sighted pedestrians. Blind pedestrians tend to face a greater risk and a greater amount of delay.

How many of these individuals are guided by the noise emitted by vehicles moving or running, a new problem of difficult treatment applies with the advent of hybrid or electric vehicles, which emit low or no noise during their displacement. This problem has already been studied [US Department Transportation] and indices run over pedestrians and cyclists tend to increase, since they are not detectable. This problem is aggravated when it comes to a visually impaired pedestrian.

In the broader context of intelligent cities, ensure mobility of people regardless of their physical or sensory condition becomes a complex and difficult challenge to be treated.

Usually, the literature tries to provide the blind with devices that can capture environmental structures and somehow describe it to the understanding of the blind. Our work explores another side of this problem: which information the environment can transmit to the blind so that he can move safely. To carry out this promise, we have developed an intelligent semaphore, assembled with video cameras to provide image data to the computer vision system, *wifi signal*, Bluetooth devices and GPS signal to guide the blind when crossing a road controlled by this semaphore on the crosswalk road.

The problem treated here is to make the environment advise the blind through a mobile device when he may (or may not) cross a road (street or avenue) on the crosswalk in

the road region controlled by intelligent semaphores.

The system should detect the arrival of the blind; detect the direction and the sense of its movement; warn that it is a region controlled by intelligent semaphores and must wait for the safe time to cross the road. While crossing the road, the system must track him to ensure it walk on the crosswalk. The mobile APP, presented in this work, when properly installed, is able to communicate automatically with those intelligent semaphore to send/receive data and process these received data that are transformed into instructions which are transmitted to mobile APP that transform it in voice in the speaker connected to mobile device that tells to the blind how it need proceeding to accomplish the road crossing safely.

II. A Brief Overview of the Blind Mobility Issue

Improving the mobility of blind pedestrians will require the application of methods developed by human factors specialists. Mobility must be recognized as a complex skill, the analysis of which will provide the information that is needed for the design of mobility aids, the development of training methods, and the evaluation of both [5].

There are many different approaches to blind mobility aids. All have in common the transformation of raw environmental data into a form suitable for non-visual perception by blind user. However, when this transformation involves no direct "understanding" or complex interpretation of the data by the transforming device, the blind user is still faced with the formidable task of perceiving the data in some analog form, and must extract the complex structure of the external word from low level cues [6]

Exist a range of devices of widely varying technology, information gathering capacity, and market price shows that engineers and researchers [7, 8, 6] have not been idle, but somehow have failed to reach their goal that of providing the blind traveler with a highly acceptable electronic aid to spatial perception. That is, an aid which can be obtained readily by individuals generally with limited income, an aid which they would freely choose to use in order to get about in their daily lives or relate more effectively to their immediate environment

A real-time computer vision system designed for the limited environment of city sidewalks is presented in [10] This system is part of a prototype mobility aid for the blind. The overall device endeavors to keep blind pedestrians on a safe path down the sidewalk, and also warn of upcoming obstacles. [11] extends this idea by using more sophisticated computer vision techniques in conjunction with a depth sensor, the sensor fusion promoting.

III. The Intelligent Semaphore and the Mobile System Improving

We have developed an intelligent semaphore [Figure 1] (still on patent qualification phase) that is able to supervise the movement of vehicles in sections of roads where it is installed. This semaphore is composed of several devices interconnected by a computer system. The main of these devices are: video camera, *wifi* antenna and Bluetooth antenna. The complete system is able to receive and send signals to both vehicles and pedestrian on this supervised point.

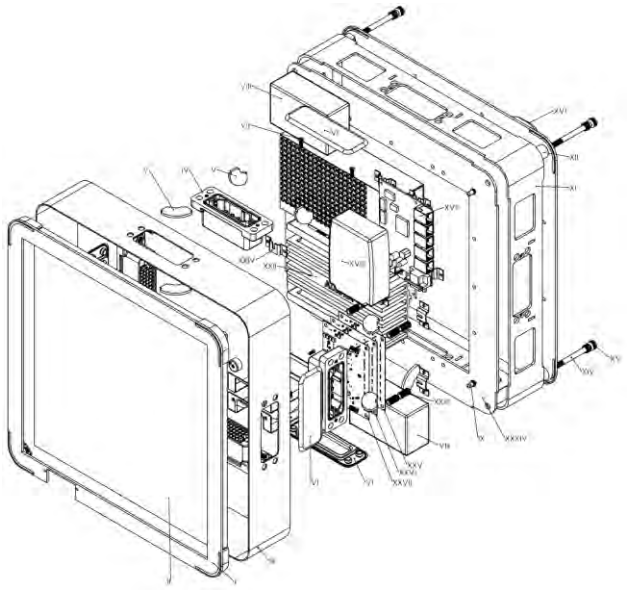

Figure 1: Intelligent semaphore design

A. *Intelligent Semaphore*

This smart device has been developed, in order, to perform a semaphoring intelligently to aid vehicles and pedestrian in an urban environment. It comprises a series of hardware and software designed to capture, process, send and receive big data platform information with purpose to optimize traffic and the urban mobility in cities. The proposed article complements the design of intelligent traffic signal, bringing the functionality to target through image processing oriented trilateration *wifi* signals and geo location (by Global Position System unit - GPS).

The proposal aims to deploy in every way connection, hotspot's that in addition to providing access to global computer network, performs authentication of its members who were on the platform. Applications for mobile devices for the visually impaired are also included in this list of applications. Using this feature, users or disabled do not only make use of transparent form of its geo location, spatial localization method based on *wifi* trilateration technique [12] and targeting images using the method shown below in this proposal.

B. *Image Processing*

In the context of this application the computational cost is extremely important, since the computational power of each traffic signal device is considered small if all the effort required rotating the device already intrinsic purpose

applications.

Therefore the consumption of computational resources with an additional process is relatively high. But, the use of low computational cost segmentation methods are best suited to perform the task of finding the pedestrian in the area now bounded by the spatial coordinates supplied by trilateration of the *wifi* signals and/or GPS. A method already used and validated in uncontrolled environments and can operate in real time, [13] is "Motion History Image ". Originally developed to detect and distinguish human motion sequences based on the composition of successive layers consist of points for the movement (silhouettes) detected inter-frame images (visible spectrum). This method allows using such layers to form a vector that represents the overall time of movement, while constituting a marker (label) capable of promoting conditions to compute a schema matching (matching) among these points and thus discriminate the movement nature (for example, to distinguish a person motion of a vehicle motion). Once movement is segmented, from an image sequence, is possible to extract parts of the overall scene and treat as a comparison model in the next frame to be analyzed. The constant search for the features extracted by edge analysis techniques, colors and geometric aspects, enable track the individual movement within specific region for a safe walking of a blind person. Since all these characteristics of movement in the scene are extracted, the system is capable to compute the space position of each object that is moving in the scene. So, if a blind person is located in an unsafe location, the system proceeds to create an alert to the blind user, as well as to the drivers that receive a luminous warning sign emitted by semaphore panel.

C. Mobile Device

The idea of bringing a mobile application to help urban mobility for visually impaired person was chosen because of the popularity of these devices and its reasonable computing power embedded coupled with the hardware and software already available (GPS, *wifi*, Bluetooth, voice system, etc). Many visually impaired have familiarity with such devices, so we was decided to then present this technological proposal for a group of blind persons that, gently, assisted us in the development of this mobile application interface. The usability of this mobile application interface has been validated by three visually impaired people already using smart phone in their daily.

For now, the interface of this application does not include visual elements, but in future versions will be available a visual interface capable of displaying a map (geo referenced) that shows the current position and the target position. This can be important because there may be the needs of the blind person ask to another not blind person to confirm if the mapped route is correct.

The current version of the application for mobile devices includes: 1) voice recognition feature; 2) vibration and; 3) message transmitted by voice, in order to create a more appropriate communication channel between the device and the blind user.

The device screen has different areas of touch that, when touched emit a sound message about its direction (Figure 2). Confirmed the direction, if the blind user to approach a crosswalk (monitored by the intelligent semaphore system), the system, installed in the mobile device, will transmit to the semaphore the direction of the movement desired by the blind user. The semaphore response (to mobile device) includes the information about the local environment conditions (if there are vehicles, if the vehicles are moving, if the semaphore is opened or closed. Even if the blind user has already started the crossing, the semaphore can guide it and, if the blind go out the correct and safe route, a route error warning message is transmitted to the blind joint with instructions to perform the correction this error. All those communication with the blind user is made by voice, sounds and vibration of the mobile device.

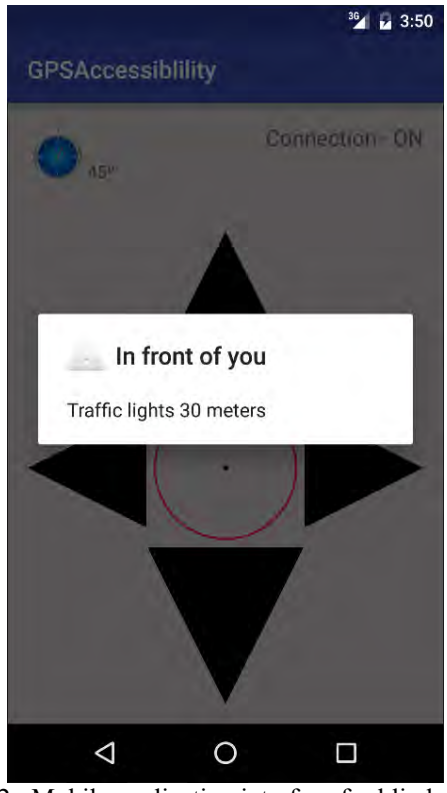

Figure 2: Mobile application interface for blind user.

D. The System Integration

Figure 3 shows the system integration - as the intelligent semaphore, the mobile device and the blind user are integrated by the proposed APP. Also, shows the data flow among different devices and the operations that are performed by the system. For the system operate correctly, the first step is detect if a blind user is close the

intelligent semaphore (region monitored). This is done by Bluetooth connection (or *wifi* or both to operate in redundancy). The APP installed in the mobile device emits a signal warning for the semaphore that a blind person is in the region monitored.

Only when the APP validate at semaphore that a blind person is in the monitored region, a communication channel between the two devices involved (semaphore-mobile) is open and the necessary data can be transmitted and received by these two devices.

E. By establishing this communication channel, the semaphore emits a signal that requests that the mobile do transmission of a historical of GPS coordinates data (previously acquired by the GPS antenna and stored in discrete periods of time while the blind walk). This historical of GPS coordinates serves to estimate the trajectory that the blind user is performing.

F. The semaphore panel changes its state by the light color changes (red, green, orange, etc.). These different colors are used to guiding and controlling the traffic of vehicles and pedestrians and it is capable to acquire and processing image data relative to movement that occurs in the monitored region. The system embedded in the mobile device is capable accomplish processing those data received from semaphore and, coherently, transforms those data into information that are transmitted to the blind by voice. The system transmits all the actions that the blind should to execute to cross safely the crosswalk.

G. The route used by pedestrian to cross the road on crosswalk is constantly monitored by video cameras installed in the intelligent semaphore. The acquired image sequence data are processed to ensure that the pedestrian always uses the crosswalk while crossing the road. If a blind, user of the system, do any deviation from a permitted route on crosswalk, the semaphore emits a warning signal to mobile user that is transformed in a voice alert "you are out of crosswalk. Stop!" So, the semaphore continues to emit signals that are transformed into voice message that explain actions that the blind user need to execute to return a safe point (on crosswalk). While the blind user do not completing the cross the road, the semaphore do not change its state (remaining closed to vehicle flux). The drivers and the others pedestrian are warned that a blind person is crossing the road (by semaphore panel).

When installed on the mobile device with GPS, wifi and Bluetooth enabled, the system (APP) starts to receive data from the GPS satellite constellation to calculate the geographic position of the blind user. This data acquisition is done in constant and continuous time interval to compose a historical of the blind user movement. Only when the mobile device connects to the semaphore, and the APP confirms this connection, the functionality to send this historical data of geographic positioning to the semaphore is executed. This transmission is done by sending an XML file. This historical data is composed of a values of geographical positioning (geo location) that was acquired in the last two minutes when there was change in the geographical position of the blind user.

H. This amount of data is sufficient to determine the direction and sense of the blind user movement. The semaphore sends a set of signals that serve to warn the blind user that it is approaching a region controlled by an intelligent semaphore, and if the road is free to the traffic of vehicle flux or not. When blind user is close enough of the semaphore, the system guides it to position yourself next to the crosswalk monitored by this semaphore. The crosswalk was duly registered, previously, by geo referencing when this semaphore was installed. In any miscommunication with the GPS when the system cannot perform the verification of latitude and longitude, it complements the spatial location data using a trilateration method of wifi signals [12]. One way to mitigate this problem is to install different of wifi access points in the region monitored by the semaphore and, so that the trilateration calculation is possible. When crossing the road, the mobile device of blind user constantly sends its geographical coordinates (transmitted by APP) to the semaphore which confers if these data are in accordance with geo referenced data that have been acquired at the moment when that semaphore was installed. Further, video camera doing acquiring data images that when processed, allows accomplish the computation of the route made by each pedestrian on the crosswalk, resulting in a redundant system.

Continuously, the system of computational vision of the intelligent semaphore processes the scenes acquired and perform the segmentation of the road lanes limits, crosswalk, vehicles stopped or in moving and pedestrian. How the system knows where the crosswalk is, anyone person who moves outside the boundaries of the crosswalk will be tracked by the vision system, and if at least one blind user is in the region monitored by the semaphore, the system will issue a warning to the blind user stop its movement. Only the blind user receives this order. If the blind user stop its movement, the vision system is capable of detect it and, in this way can guide it safely on the crosswalk.

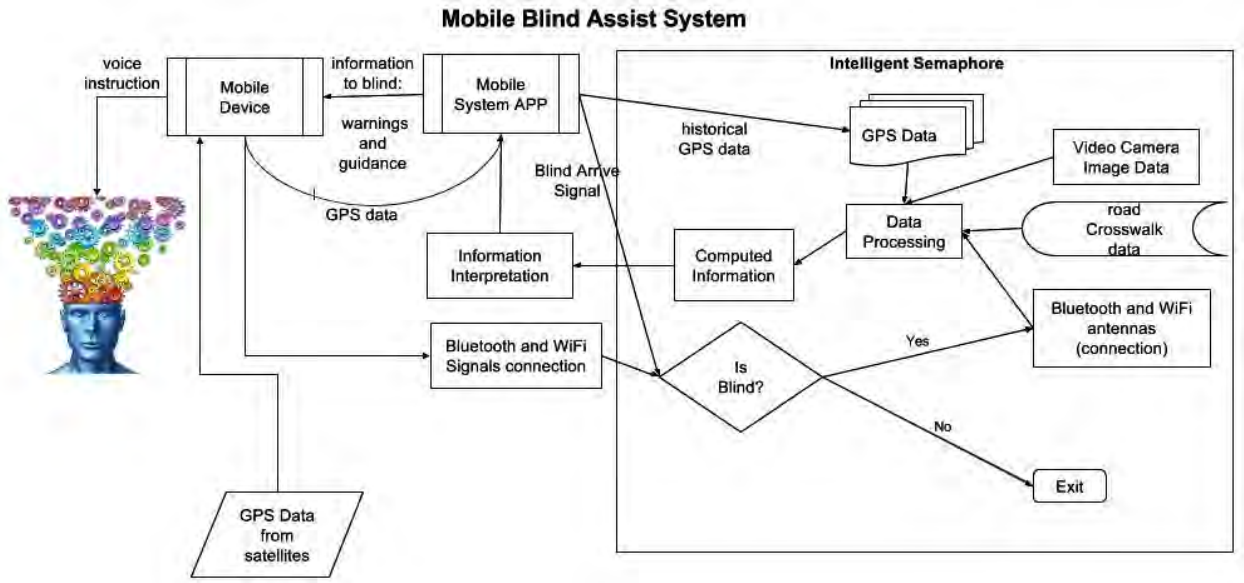

Figure 3: The system integration scheme.

FUTURE WORKS

A prototype for this intelligent semaphore was assembled. The first continuation is installing this system in a city with the objective to data collect about its functionality. After certifying that it functioning is correct and satisfactory, new possibilities can be implemented. Our idea is to install low cost systems throughout the city. Each of these systems will be able to report for the blind user what it is, how it is, what have, where it is, ... about the elements existents in environment involved in the vicinity of each point of installation. These systems can be installed in public buildings or commercial use (pharmacies, banks, bookstores, bars, clubs, museums, etc.) and, that done; we began offering accessibility and better standard of living for people with visual impairment.

REFERENCES

[1] Foulke, "The perceptual basis for mobility", Association for Education of the Visually Handicapped: Fiftieth Biennial Conference "A Look at the Child". July 1970, pp. 95 – 101.

[2] Okamoto,T.,Yamada,Y., "Study of Conditions for Safe and Efficient Traffic in an Indoor Blind Corner-based Decision Model with Consideration for Tactics and Information Uncertainty ", 2012 IEEE RO-MAN: The 21st IEEE International Symposium on Robot and Human Interactive Communication.September 2012, pp 9-13.

[3] D. Ashmead, D. Guth, R. Wall, R. Long and, P. Ponchillia,"Street crossing by sighted and blind pedestrians at a modern roundabout", 2005, J. Transp. Eng., 131(11), pp. 812–821.

[4] B. Schroeder, N. Rouphail and, R. Emerson, R. "Exploratory analysis of crossing difficulties for blind and sighted pedestrians at channelized turn lanes", Transportation Research Record: Journal of the Transportation Research Board, vol. 1956, 2014, pp. 94 – 102.

[5] A. C. Shingledecker, E. Foulke, "A human factors approach to the assessment of the mobility of blind pedestrians", Human Factors: The Journal of the Human Factors and Ergonomics Society, vol. 20, no. 3, pp. 273–286, June 1978.

[6] M. F. Deering, "Computer vision requirements", in blind mobility aids in electronic spatial sensing for the blind", Contributions from Perception, Rehabilitation, and Computer Vision. Editors: David H. Warren and Edward R. Strelow, Springer, pp. 65-82, 1985.

[7] J. T. Tou and, M. Adjouadi, "Computer vision for the blind", in Electronic Spatial Sensing for the Blind: Contributions from Perception, Rehabilitation, and Computer Vision. Editors: David H. Warren and Edward R. Strelow, Springer, pp. 83 – 124, 1985.

[8] L. Kay, "Sensory aids to spatial perception for blind persons: their design and evaluation", in Electronic Spatial Sensing for the Blind: Contributions from Perception, Rehabilitation, and Computer Vision. Editors: David H. Warren and Edward R. Strelow. Springer, pp. 125 – 139, 1985.

[9] S. R. Mackay, "Physical principles underlying blind guidance prostheses with an emphasis on the ultrasonic exploration of a region of space", in Electronic Spatial Sensing for the Blind: Contributions from Perception, Rehabilitation, and Computer Vision. Editors: David H. Warren and Edward R. Strelow. Springer, pp. 141 – 153, 1985.

[10] M. F. Deering, C. Collins, "Real-time natural scene analysis for a blind prosthesis". Proceedings of the 7th International Joint Conference on Artificial Intelligence, pp. 704 – 709, 1981.

[11] N. Kanwal, E. Bostanci, K. Currie and, A. Clark, "A navigation system for the visually impaired: a fusion of vision and depth sensor", Applied Bionics and Biomechanics - Online publication, pp. 1-16, 2015.

[12] M. Shchekotov, "Indoor Localization Method Based on Wi-Fi Trilateration Technique," Proc. of the 16th Conference on Fruct Association, 2014, pp. 177–179, ISSN 2305-7254.

[13] J. K. Tan , H. Kim ,S. Ishikawa, “Motion history image: its variants and applications”, Machine Vision and Applications ,Volume 23, Issue 2 , pp 255-281,ISSN 0932-8092.

[14] M. Shchekotov, “Indoor Localization Method Based on Wi-Fi Trilateration Technique,” Proc. of the 16th Conference on Fruct Association, 2014, pp. 177–179, ISSN 2305-7254.

sensors

Article

2D Triangulation of Signals Source by Pole-Polar Geometric Models

Aleksandro Montanha [1,*], Airton M. Polidorio [2], F. J. Dominguez-Mayo [3] and María J. Escalona [3]

[1] Web Engineering and Early Testing (IWT2) research group, Departamento de Lenguajes y Sistemas Informáticos, Escuela Técnica Superior de Ingeniería Informática, Universidad de Sevilla, Avda. Reina Mercedes s/n, 41012 Seville, Spain.

[2] Departamento de Informática Centro de Tecnologia, Universidade Estadual de Maringá, Av. Colombo, 5790 - Jd. Universitário, Maringá 87020-900, Brazil; ampolidorio@uem.br

[3] Departamento de Lenguajes y Sistemas Informáticos, Escuela Técnica Superior de Ingeniería Informática, Universidad de Sevilla, Avda. Reina Mercedes s/n, 41012 Seville, Spain.; fjdominguez@us.es (F.J.D.-M.); mjescalona@us.es (M.J.E.)

* Correspondence: aleksandro.montanha@iwt2.org; Tel.: +55-44-99998-1486

Received: 10 December 2018; Accepted: 19 February 2019; Published: 27 February 2019

Abstract: The 2D point location problem has applications in several areas, such as geographic information systems, navigation systems, motion planning, mapping, military strategy, location and tracking moves. We aim to present a new approach that expands upon current techniques and methods to locate the 2D position of a signal source sent by an emitter device. This new approach is based only on the geometric relationship between an emitter device and a system composed of $m \geq 2$ signal receiving devices. Current approaches applied to locate an emitter can be deterministic, statistical or machine-learning methods. We propose to perform this triangulation by geometric models that exploit elements of pole-polar geometry. For this purpose, we are presenting five geometric models to solve the point location problem: (1) based on centroid of points of pole-polar geometry, PPC; (2) based on convex hull region among pole-points, CHC; (3) based on centroid of points obtained by polar-lines intersections, PLI; (4) based on centroid of points obtained by tangent lines intersections, TLI; (5) based on centroid of points obtained by tangent lines intersections with minimal angles, MAI. The first one has computational cost $O(n)$ and whereas has the computational cost $O(n\ log\ n)$where n is the number of points of interest.

Keywords: signal processing; 2D point location; computational geometry; pole-polar geometry

1. Introduction

Signals can be of various natures, including sound waves, visible and non-visible light, or other electromagnetic spectrum energies (radio waves or radar waves, for instance). The position of a signal emitter or receiver device can be estimated (located) by triangulating the signal data that it sends/acquires. The signal data comprise: the nature of the own signal (as light (electromagnetic energy), sound and vibration); its intrinsic attributes (such as power, frequency, and amplitude); its extrinsic attributes (as the time when the signal arrives at each particular receiver; the strength and the propagation angle of a signal acquired at each particular receiver). Current approaches used to locate an emitter or a receiver can be deterministic, statistical or machine-learning methods. Thus, we propose to perform this triangulation by geometric models that explore elements of pole-polar geometry. Here, we are presenting five geometric models to solve the point location problem: (1) based on centroid of a set of polar-points (PPC); (2) based on a convex hull region defined by a set of interest points (CHC); (3) based on centroid of a set of interest points obtained by polar-lines intersections (PLI); (4) based on centroid of a set of interest points obtained by tangent lines

intersections, (TLI); (5) based on centroid of a set of interest points obtained by tangent lines intersections with minimal angles (MAI).

The first one has computational cost $O(n)$, whereas the others cost $O(n\,log\,n)$. The n value is the number of points of interest.

For a system composed of m receivers, the maximum of polar-points of interest generated is $p = \binom{m}{2} = m!/(2(m-2)!)$. For PPC, CHC and PLI models $n = p$. For TLI and MAI models $n = 2p$. In terms of m, the cost of proposed methods is $O(m^2)$ in accordance with the cost to perform $\binom{m}{2}$ combinations.

We use IEEE 802.11 Network infrastructures to evaluate the precision of these geometric models, with the aim to acquire strength signal data from emitter-receiver system. The acquired data was not preprocessed. The acquired raw data are used to provide better analysis of the errors committed by the five geometric methods proposed in this work (PPC, CHC, PLI, TLI, and MAI) in comparisons with the errors committed by Newton–Rapson (NRm), Least-Square (LSm), and Weighted Least Squares (WLSm) which have computational cost $\sim O(m^3)$. This paper does not address operations or methods related with signal data preprocessing. If you have particular interest in these operations, see Section 3.2 in this work. This means that there are errors in the acquired data used in this work. Such errors are due to the signal multipath; the presence of obstacles and the co-presence of other electromagnetic sources (see Section 1.1). The innovation proposed in this work is to use geometric methods to solve a geometric problem (estimation of the location of signal source or a receiver device). Obviously, in order to guarantee the accuracy of a location, it is necessary to ensure data with high quality.

Signal location estimation by range-based methods needs to solve a nonlinear equations system (quadratic equations). To facilitate this solution, the equations of this system are linearized by subtracting equations, that is, any equation of this system is chosen and is used to subtract all other ones from this system, and thus all terms of all equations that have degree two are eliminated from these equations and the system becomes linear. However, the realization of this subtraction also eliminates from the system the equation chosen to perform this linearization. For example, if there were five equations before the linearization, after the linearization there will be four equations in the system. It is important to consider that this equation that was eliminated contemplates data of radial range of the signal acquired by some device of the location network. Eliminating this equation means eliminating this device from this network and its participation on the final result of the location of a point in space becomes indirect. The most complicated fact of performing the linearization of the equations system by subtraction of its equations is in the possibility of propagation of the errors. Assume that the equation chosen to perform the linearization operation is that corresponding to the device that acquired the signal data with the highest error. By using this equation to subtract all other ones, such errors are seriously propagated to the linearized equations system, with impairment for the accuracy of the solution.

In this work we propose five geometric methods capable of estimating the location of a point (2D) without the requirement to solve a nonlinear equations system. This means that all signal radial range data acquired by all devices belonging to a positioning network are used directly to estimate the location of a desired point with computational cost $O(m^2)$ without propagating data errors among equations.

1.1. Considerations about Signal Data

In this section we briefly describe about the signal data acquisition and limitations, including the restrictive conditions involved in this acquisition. We try to associate the acquisition of data with the usual methods applied to the spatial location of a point of interest.

What locates what? There are applications which needed estimating the location of an emitter device (e.g., an airplane black box). There are applications which a receiver device needs to be located (e.g., a GPS unit). All methods presented in this paper are able to operate in any of these applications. The experimental cases (Section 3) adopt the convention for locating a receiver device.

The standard techniques range-based applied to location estimation uses a server to that aim. They perform the localization in two steps: (1) ranging, where the radial distance between two sensors (one with known positions and another with unknown position) is obtained, by some methods such as TOA (Time of Arrival), TDOA (Time Difference of Arrival), RSSI (Received Signal Strength Indicator) or AOA (Angle of Arrival) and (2) location computation, where the unknown location of a device is calculated by estimation through methods such as triangulation using the radial distance or angle data [1].

A Received Signal Strength Indicator (RSSI) is a measure of the power contained in a propagated signal. In an IEEE 802.11 system, RSSI refers to received radio signal strength (power level) in a wireless environment, measured in arbitrary units, that a particular signal is received by a receiver. Therefore, the higher the RSSI value is, the stronger the signal is received, and closer are the emitter and the receiver. RSSI-based techniques require the value of the signal magnitude attenuation to find the radial distance among a set of receiver devices. It is a practical and self-organized method that utilizes more power to send a large influx of data to the central server.

Received Signal Strength (RSS)-based fingerprinting approaches have been widely exploited for mobile device localization. The received signal strength is a function of radial distance between emitter and receiver devices. The strength magnitude of a received signal can vary because there are fonts of interferences (noise) in the signal propagation path, especially in outdoor environments [2]. Reference [3] explored signal strength data to feed a Perceptron and Decision Systems based on Learning Vector Quantization to obtain a fingerprint map of that radio strength signal. Reference [4] investigated the effects of hardware orientation, location, measurement time and duration, as well as the interference of the user presence on the RSS acquired data.

In the simplest case of free space propagation, electromagnetic waves radiate out of an isotropic antenna in all directions without being perturbed. The received power, any point in space, for such a case is provided by Friis equation [5,6] given by (1).

$$\rho_r = \rho_e g_e g_r \left(\frac{\lambda}{4\pi d}\right)^2, \quad (1)$$

ρ_r and ρ_e are the receiver and the emitter power
g_r and g_e are the receiver and emitter antennas gains
d is the radial distance between an emitter and a receiver in meters.
λ is the wavelength. For IEEE 802.11b and g to 2.4 GHz, $\lambda \approx 0.125m$ and, to 5.7 GHz, $\lambda \approx 0.06m$.

The wave propagation of Electromagnetic Radiation (EMR) in the Earth's free space conditions is compromised primarily by three phenomena [7]: (1) reflection. It happens when EMR interacts with a smooth surface with larger dimension than the wavelength; (2) diffraction, or shadowing. It takes place when the wave is obstructed by objects larger than the wavelength (a secondary wave is created behind the object); and (3) scattering. It occurs when the waves encounter a rough surface whose dimensions are of the same order as the wavelength [6]. As the wireless signal radiates out of the emitter antenna, it may interact with reflective surfaces and be reflected in different directions. If a fraction of this reflected signal reaches the receiver antenna, it will acquire signals from the same emitter that traveled by different paths. The reflected signal may be out of phase with the Line-Of-Sight (LOS) signal that can result in destructive interference and fade the receiver signal. The received signal is affected by different environment components (e.g., the own air) that promote the signal attenuation.

If the signal does not suffer external interference, it is expected an inverse exponential relationship between the radial distance d that the emitter device is there from the position of an AP and the value RSSI ρ of this signal measured in that AP [8]. In the dry air, the signal attenuation A is given by (2).

$$A = 20\, log_{10}\left(\frac{4\pi d}{\lambda}\right) \quad (2)$$

Therefore, for a signal propagation in an environment consisting of dry air, we can argue that the signal strength ρ_r received by the receiver r is dependent of the signal strength ρ_e that is

produced by the emitter e, of the gains g_r and g_e promoted by sensors antennas and of the attenuation A, (3), promoted by the dry air.

$$\rho_r = \rho_e + \rho_g - A \quad (3)$$

RSSI is used as a metric in most of distance measurement algorithms that run in indoor environments. Nevertheless, at a more basic level the reliability and precision of using RSSI to determine a spatial position in an outdoor environment has not been extensively experimented and there can be interference caused by structures. This monotonous behavior between the radial distance d and the signal strength ρ is not always observed.

Time of Flight (TOF) are time-based methods for measuring distance using signals data that propagate in a given environment with a known speed v. They consist in measuring the time interval that a wave (e.g., light, radio, or sound) needs to travel a spatial distance. Measuring radio or light wave propagations across small distance requires a clock with subnanosecond time measure; for sound it must be measured by millisecond. TOF-based methods are Time of Arrival (TOA), Time Differential of Arrival (TDOA), and Time of Transfer (TOT).

The emitter and the receiver clocks must be perfectly synchronized for using TOA approach. When an emitter sends a signal at the instant t_E, the receiver acquire this signal at instant $t_R > t_E$, so, the time interval spent for the signal arrival from emitter to receiver, $\Delta t = t_R - t_E$, allows computing the radial distance d that separates the emitter from the receiver by $d = v\Delta t$. In the 2D case, knowing the emitter distance from two receivers is sufficient to perform the triangulation of emitter location estimation. The TOT method is an unsynchronized-time approach that computes the radial distance between emitter and receivers based on the time delay of a standardized signal ξ (message) exchanged between the emitter and those receivers.

Accuracy of time acquisition is very important for any type of TOF measurements. An EMR wave travels 1 m in 3 ns in air, thus if a locating system with 1m of accuracy is desired, a 300 MHz clock (least) must be used for time acquisition. Clock accuracy depends on clock granularity, which is associated with the size of the smallest time interval measured by a clock. Larger granularity implies a small time interval, then greater precision [9]. A granularity of 20 ppm has an inaccuracy of 1.2 ms per minute, a rubidium clock has an inaccuracy of 0.06 ns per minute, and a caesium clock has an inaccuracy of 6 ps per minute. To sum up, clock precision is a source of error in TOF methods. The sources of errors can be intrinsic (i.e., related to the hardware) or extrinsic (i.e., related to the environment). Intrinsic errors are related to: (1) clock measurements accuracy; (2) printed circuit board trace (circuit impedance), that means that the electronic signal travels some distance on a printed circuit board trace and this internal path of the signal causes delay on signal propagation; (3) difference in the phases between emitter and receiver; and (4) relative velocity on signal treatment between emitter and receiver, which promotes frequency errors and, hence clock errors. Extrinsic errors comprise: (1) signal reflection; (2) diffraction; (3) scattering; (4) absorption/attenuation; (5) environmentally-dependent the speed signal propagation; and (6) physical model and computational errors (truncation and rounding). Reference [6] outlined sources of error and considerations about some methods of localization using radio frequency.

TOF-based methods suggest inaccuracy does not increase when distance increase. In general, for methods based on RSSI and angle AOA the error increases when distance increase.

To apply the TDOA approach, the clocks of the receivers system or of the emitters system need to be synchronized (e.g., for GPS, only the clocks of the satellites constellation need synchronized—this means that a mobile device GPS unit is not an expensive device). However, each satellite in this constellation needs to send in its signal the coordinates of its spatial position and the precise time registered by its clock. According [7], to estimate a position of a point using a satellite navigation system, it is thus necessary to have two things ready: the position of the satellites and the distance of the point from these satellites. Range observation equations are generated from this information and the position is estimated in 3D space by solving these equations. Therefore, two aspects are important at this point: to obtain this required range data and to solve the equations

1.2. Standard Methods and Considerations

1.2.1. RSSI Approach

The first system used for tracking and locating a mobile device by radio frequency in an indoor environment was RADAR [10]. Previously, [11,12] used the infrared to locate devices. Nevertheless, there are many limitations in the latter when using this range of the electromagnetic spectrum energy to establish communication among sensors and limited results were obtained. In contrast, the RADAR system operates by processing signal strength data at multiple base stations (AP, Access Point) geometrically positioned to provide overlapping coverage in the area of interest. The system enables estimating the location of an emitter by applying empirical measurements with signal propagation modeling.

The empirical models proposed by Equations (4) and (5) present significant disparities when confronted by actual data due to signal attenuation promoted by the floor and walls of an indoor environment. Reference [10] observed that sampled data could be filtered to achieve better results. Considering data median, model (5) provides a precision of 4.3 m, compared to 2.94 m for model (4) and 8.16 m for the strongest signal data values. For the 25th percentile, model (5) provides a precision of 1.86 m, whereas model (4) provides 1.92 m and 4.94 m for the strongest values. To summarize, this evaluation [10] shows that signals can suffer from low and high frequencies interferences (noise). Besides, [10] performed experiments to determine the impact of the data sample size on the result precision. He shows that using two data values by sample, the accuracy worsens by 11%, while using three data values it worsens by 4% (the larger the sample is, the more accurate the result is).

$$\rho(d) = \rho_0 - 10\mathcal{L}\, log_{10}\left(\frac{d}{d_0}\right) - w(nW, C), \tag{4}$$

Or

$$\rho(d) = \rho_0 - 20\, log_{10}\left(\frac{4\pi d}{\lambda}\right) + x_\sigma, \tag{5}$$

where,

$\rho(d)$ is the signal strength value (dB) expected by an AP located at a radial distance d from the signal origin.

ρ_0 is the signal strength value (dB) at some reference distance d_0.

$\mathcal{L}$ indicates the rate at which the path loss increases with distance (empirical value).

$w(nW, C)$ is the signal attenuation factor promoted by walls.

λ is the signal wavelength.

x_σ is a Gaussian noise with zero-mean and variance σ^2.

Considering $w(nW, C) = 0$, in free obstructions outdoor environment, and measure ρ_0 at $d_0 = 1m$ from the AP, by (4), the radial distance d can be computed by (6).

$$d = 10^{\frac{\rho_0 - \rho(d)}{10\mathcal{L}}}. \tag{6}$$

The parameter path-loss exponent $\mathcal{L}$ (6) depends on the frequency of signal and environment interferences (e.g., walls, buildings, cars, rain, air moisture, or people); for open free space, $\mathcal{L} \cong 2$, and for environments with obstructions, $\mathcal{L} > 2$. A more appropriate $\mathcal{L}$ value can be determined in the system calibration phase [13]. Experiments carried out by [14] showed that in an urban area, the path loss variation ranges $2.7 \leq \mathcal{L} \leq 3.5$, using a cellular radio.

1.2.2. Time-based Approaches (ToA and TDoA)

Reference [15] use sound waves to locate a receiver device using signal data based on TDoA measurements. The location computation is formulated as an optimization problem applying a set

of constraint previously determined. The basic idea is to shrink the radius of all circles at a constant step length until the intersection area reaches a small threshold. This operation needs to perform N acquisitions of data (called phase). For each set of acquired data is applied an optimization algorithm. These acquisitions of data end when the optimization algorithm finds a solution considered satisfactory. The computational complexity of the proposed method is about $O\big(10(nN^2 + n^2N)\big)$, where n is the number of nodes (emitters).

Time-based approaches are based on electromagnetic (or sound) wave propagation that moves at a speed v close to light speed,$c \approx 3 \times 10^8 m/s$ (in the vacuum). In the Earth's atmosphere $v = c/n$, n is the refraction coefficient of the atmosphere ($n = 1.000292$ to dry air at conditions 0 ℃ and $1\ atm$. The accurate value is $v = 299{,}704{,}944\ m/s$). The physical model (7) responsible for computing the radial distance d between emitter and receiver depends only on the instant t_E when the emitter sends the signal and the instant t_R when the receiver get it.

$$d = v(t_R - t_E) \tag{7}$$

The model (7) can be applied only in case that emitter and receiver are time-synchronized. Ensuring this synchronization is not always a simple task. It must be considered that v is an astronomical quantity and small deviations of precision in $(t_R - t_E)$ results in large errors (for each 1 ms error in the time registration there can be a location error higher than 300 km).

1.2.3. Generalization of 2D Location Function Range-Based

In 2D space (x, y) are two unknowns for the location of a point P. In Cartesian coordinates, the point (x, y) can be represented in terms of its range by $(x - x_1)^2 + (y - y_1)^2 = (r_1)^2$, where (x_1, y_1) is a known reference point and r_1 is the range (or radial distance) between the unknown point (x, y) and the reference point(x, y). To solve (x, y) is necessary a second observation given by another reference point (x_2, y_2) that generates the new circle equation $(x - x_2)^2 + (y - y_2)^2 = (r_2)^2$. There are two solutions for these two quadratic equations. If these two solutions are the same, then these two circles are tangent and the solution for P is found. If these two circles are secant, P has two ambiguous solutions. In this case, to obtain the correct solution is necessary known a third reference point (x_3, y_3) and its respective r_3 range to P. This is known as trilateration, the estimation of the position of a point unambiguously based on the measurements of distances from three or more known reference locations [7]. Otherwise, these three circles do not intercept at a single point because there are errors in ranges measurements. In this case, the solution for P is inaccurate and need to be estimated with error minimization. To provide this error minimization it is necessary known others reference points (x_k, y_k) and its respective ranges r_k —see Equation (8). As the Cartesian plane is concerned, the Euclidean distance between two points $P_0(x_0, y_0)$ and $P_1(x_1, y_1)$ is given by $d = \sqrt{(x_1 - x_0)^2 + (y_1 - y_0)^2}$, so, by means of (6) or (7), the relationship $(x_1 - x_0)^2 + (y_1 - y_0)^2 = \big(v(t_R - t_E)\big)^2 = 10^{2\frac{\rho_0 - \rho(d)}{10\mathcal{L}}}$ is obtained, which is the circle equation with radius $r = v(t_R - t_E) = 10^{\frac{\rho_0 - \rho(d)}{10\mathcal{L}}}$ and center (x_0, y_0). If P_0 represent the receiver position and P_1 the emitter position, the emitter belongs (best case) to this circle line and the receiver is at the circle center. Note that signal-based location methods need to know the value of the radial range of the signal r regardless of whether this value is estimated by strength data or the wave propagation speed of that signal. Despite of how the value of r is estimated, such methods do not change. Therefore, performing experiments using signal strength and signal propagation velocity data is irrelevant to compare the accuracy achieved by different methods.

The radial distance (or range data) $d = r$ between emitter and receiver is identified through (6) or (7). Using this concept to $m > 2$ receivers by one emitter, the following is obtained (8)

$$\boldsymbol{F}(x, y) = \begin{cases} (x - x_1)^2 + (y - y_1)^2 - (r_1)^2 = 0 \\ (x - x_2)^2 + (y - y_2)^2 - (r_2)^2 = 0 \\ \vdots \\ (x - x_m)^2 + (y - y_m)^2 - (r_m)^2 = 0 \end{cases} \tag{8}$$

The Equation (8) is a nonlinear equations system to solve the emitter location (x, y). If $m = 2$, this equations system is normal and can be solved either by a numerical or empirical method or applying the analytical solution showed in Figure 1a. If $m > 2$, the system is redundant and allows minimizing the solution error by means of Nonlinear Least-Squares (NLLS).

1.2.4. How to Solve the System

The following are some possible solutions for the system of nonlinear equations given in (8). Solution by Least-Squares Method—For this solution [16] proposes a linearization of the non-linear equation system (8). This linearization is achieved when an equation of the system (8) is used to subtract all the others. By performing this subtraction, the system (8) with non-linear equations results in a system of $m - 1$ linear equations. In this case, to solve a 2D location problem, $m \geq 3$ receivers are necessary. For example, if the equation 1 of (8) is chosen to perform this linearization, then the resulting linear system, written in the form $\boldsymbol{M}[x, y]^t = \boldsymbol{b}$, is given by (9). The solution of $\boldsymbol{M}[x, y]^t = \boldsymbol{b}$ is given by $[x, y]^t = M^{-1}b$, if $m = 3$, or by $[x, y]^t = (M^t M)^{-1} M^t b$, if $m > 3$.

$$\boldsymbol{M} = \begin{bmatrix} x_2 - x_1 & y_2 - y_1 \\ x_3 - x_1 & y_3 - y_1 \\ x_4 - x_1 & y_4 - y_1 \\ \vdots & \vdots \\ x_m - x_1 & y_m - y_1 \end{bmatrix}_{m-1\times 2} \quad \text{and} \quad \boldsymbol{b} = \frac{1}{2}\begin{bmatrix} b_2 - b_1 \\ b_3 - b_1 \\ b_4 - b_1 \\ \vdots \\ b_m - b_1 \end{bmatrix}_{m-1\times 1} \tag{9}$$

where $b_k = r_k^2 - (x_k^2 + y_k^2)$, for $k = 1,2,3, \ldots, m$.

Note that these solutions have any mechanism to handle errors involved with the acquired data. The position solution obtained by (9) was based upon a fundamental assumption that the ranges have no error in them. However, the same approach is valid when the range errors for all the reference points are statistically independent and identical. However, this is not true in real cases. Often, this error is neither independent nor identical. Under such conditions, the least squares position estimate does not hold good as an optimal estimate. If the range errors are Gaussian and the covariance of ranging errors is given by the matrix Σ, then the optimal estimation for location is given by the Weighted Least Squares (WLSm) provide by $[x, y]^t = (M^t \Sigma^{-1} M)^{-1}(M^t \Sigma^{-1} b)$ [7,16,17].

Solution by Numerical Method—For this specific case, the Jacobian matrix $\boldsymbol{J}$ (10) is the matrix of first order partial derivatives of $\boldsymbol{F}(x, y)$, such that, $\boldsymbol{J}(\boldsymbol{F}(x, y))$ is given by

$$\boldsymbol{J}(\boldsymbol{F}(x, y)) = \begin{bmatrix} \dfrac{\partial f_0}{\partial x} & \dfrac{\partial f_0}{\partial y} \\ \dfrac{\partial f_1}{\partial x} & \dfrac{\partial f_1}{\partial y} \\ \vdots & \vdots \\ \dfrac{\partial f_{m-1}}{\partial x} & \dfrac{\partial f_{m-1}}{\partial y} \end{bmatrix},$$

applying in (8)

$$\boldsymbol{J}(\boldsymbol{F}(x, y)) = 2\begin{bmatrix} x - x_0 & y - y_0 \\ x - x_1 & y - y_1 \\ \vdots & \vdots \\ x - x_{m-1} & y - y_{m-1} \end{bmatrix} \tag{10}$$

We look for $\boldsymbol{F}(x, y) = 0$. For $m = 2$, an interactive solution for $\boldsymbol{F}(x, y) = 0$ is found by Newton's method [18], by way (11)

$$\begin{bmatrix} x_{k+1} \\ y_{k+1} \end{bmatrix}_{2\times 1} = \begin{bmatrix} x_k \\ y_k \end{bmatrix}_{2\times 1} - [\boldsymbol{J}(x_k, y_k)]_{2\times 2}^{-1}[\boldsymbol{F}(x_k, y_k)]_{2\times 1}, \tag{11}$$

where $k = 0,1,2, \ldots$ is k^{th} iteration, $[\boldsymbol{F}(x_k, y_k)]_{m\times 1}$ is vector function, $[\boldsymbol{J}(x_k, y_k)]_{2\times m}^{-1}$ is the inverse of the Jacobian matrix, and (x_0, y_0) is the first estimative for the solution. Such solution is found when $[x_{k+1}, y_{k+1}]^t \leq [\varepsilon, \varepsilon]^t$, and ε stands for the precision value specified a priori. If $m > 2$ and $\boldsymbol{X}_k = [x_k, y_k]^t$, the system (8) can be solved by (12).

$$\boldsymbol{X}_{k+1} = \boldsymbol{X}_k - \boldsymbol{F}(\boldsymbol{X}_k)\left([\boldsymbol{J}(\boldsymbol{X}_k)]^t\ [\boldsymbol{J}(\boldsymbol{X}_k)]\right)^{-1}[\boldsymbol{J}(\boldsymbol{X}_k)]^t \quad (12)$$

Algebraic Solution—An algebraic 3D solution to locate a receiver ([19] aimed to locate a receiver using TDOA measurements and four satellites emitters) was found out by [19], Bancroft's method, which reduces the problem to solve a quadratic equation and yields the 3D Cartesian coordinate of the receiver as well as the common time of signal transmission. It also performs several algebraic manipulations to reduce the equations to a least-squares problem. The presented solution (13) considers that

$$\tilde{r}_i^2 = (r_i - \xi_i)^2 = \|p_i - \rho\|^2 = (x - x_i)^2 + (y - y_i)^2 + (z - z_i)^2, \quad (13)$$

where, r_i and $\tilde{r}_i$ are the observed and actual radial distances (pseudorange and actual range, respectively); ξ_i is the measurement noise at the receiver corresponding to the measurement between the i^{th} satellite and the receiver, respectively and ρ is the receiver position (x, y, z) to determine. A generally acceptable modeling of the ranging error ξ_i was described in [20]. Thus, using the receiver clock bias – $b = \xi_i$ as the only noise measurement and applying some algebra the following equation is obtained

$$(x_i^2 + y_i^2 + z_i^2 - r_i^2) - 2(x_i x + y_i y + z_i z - r_i b) + (x^2 + y^2 + z^2 - r^2) = 0.$$

Let $\rho = [xyzr]^t$ denotes the receiver position vector and $p_i = [x_i y_i z_i r_i]^t$ denotes the satellite position and range vectors. According to Lorentz inner product for 4-space (given by $\langle \vec{u}, \vec{v} \rangle = u_1 v_1 + u_2 v_2 + u_3 v_3 - u_4 v_4$), can be rewritten as

$$\frac{1}{2}\langle p_i, p_i \rangle - \langle p_i, \rho \rangle + \frac{1}{2}\langle \rho, \rho \rangle = 0.$$

Now, the solution can be found utilizing least-squares estimation to the organized satellites equations in the matrix $\boldsymbol{B}_{m\times 4} = [x_k y_k z_k - r_k], k = 1 \ldots m$ and the vector $\boldsymbol{a}_{m\times 1} = \frac{1}{2}[\langle p_k, p_k \rangle]$. The final solution demands a consistency analysis of the partial results found.

Analytical Solution—When two circles with centers at (x_1, y_1) and (x_2, y_2) and radius r_1 and r_2 intersect at one or two points $P(x_p, y_p)$ and $Q(x_q, y_q)$. This intersection do not always occurs due to noise and underestimation of ranges [21]. The analytical solution (x, y) is found at the median of the straight line segment s that connects P and Q points (Figure 1a), given by (14)

$$(x, y) = \left(\frac{x_p + x_q}{2}, \frac{y_p + y_q}{2}\right), \quad (14)$$

where

$$x_p = \frac{-E + G}{H}; x_q = \frac{-E - G}{H}; y_p = \frac{A - Bx_p}{C}; y_q = \frac{A - Bx_q}{C};$$

$$A = {r_1}^2 - {r_2}^2 - {x_1}^2 - {y_1}^2 + {x_2}^2 + {y_2}^2; \quad B = -2(x_1 - x_2); C = -2(y_1 - y_2); \quad L = \frac{B}{C}; D = 1 + L^2;$$

$$E = 2(L[1 - A] - x_1); \quad F = L(L - 2y_1) + {x_1}^2 + {y_1}^2 - {r_1}^2; G = \sqrt{E^2 - 4DF}; \quad H = 2L.$$

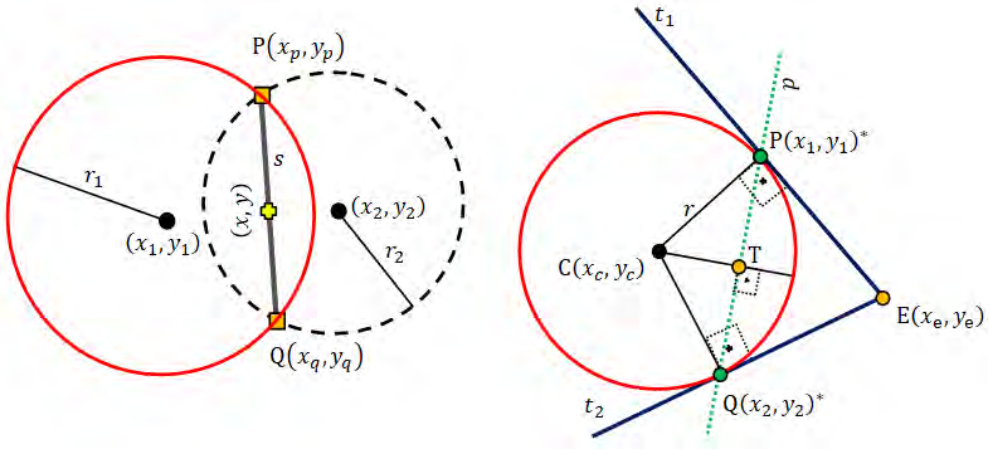

(**a**) (**b**)

Figure 1. (**a**) Analytical solution to (x, y) when there is an intersection between circles. (**b**) Possible tangential straight lines t_1 and t_2 for the circle line obtained by an external point $E(x_e, y_e)$ (pole-point). Polar-line p and its geometric relationship with the tangent lines and a given conic section (circle in this case).

For a normal equation system another analytical/algebraic solution for (8) can be obtained performing the linearization by row (equations) subtraction and then applying the Gauss–Jordan elimination method [18].

Despite the method chosen to solve this problem (analytical, algebraic, least-squares, numerical or NLLS), there are invariable errors associated with the acquired data. These errors are propagated by computational arithmetical operators, mainly multiplication and division.

It is necessary to minimize the number of arithmetic operations involved in the solution in order to improve the accuracy of the results and, therefore, reduce the computational cost to provide facilities for designing of real time systems. This work proposes a geometry-based solution with the aim to minimize the number of arithmetical operations so as to find the desired solution.

1.3. Useful 2D Geometric Definitions

This subsection describes some geometric important definitions for understanding the proposed geometric models. Such definitions are labeled as, for example, (d-9) which means the 9th definition and its uses are thus referenced in the text. References [22,23] provide these definitions and further information in this regard.

Point and Line—A coordinate $P(x, y)$ define the point P in the Cartesian plane ($\mathbb{R}^2$). The line that passes through the points $P(x_1, y_1)$ and $Q(x_2, y_2)$, $P \neq Q$, is denoted $\overleftrightarrow{PQ}$. The line segment $\overline{PQ}$ (with endpoints P and Q) is the portion of the line $\overleftrightarrow{PQ}$ between points P and Q.

(d-1) The Euclidean distance $D_{\overline{PQ}}$ between two points $P(x_1, y_1)$ and $Q(x_2, y_2)$ is given by

$$D_{\overline{PQ}} = \sqrt{(x_1 - x_2)^2 + (y_1 - y_2)^2}.$$

(d-2) For constants A, B, C (A and B not both zero) all points (x, y) satisfying the equation

$Ax + By + C = 0$ define the implicit line equation in the Cartesian plane. For two points $P(x_1, y_1)$ and $Q(x_2, y_2)$, a particular $\overleftrightarrow{PQ}$ line equation is obtained by

$$A = y_1 - y_2; \quad B = x_2 - x_1; \quad C = -Ax_1 - By_1.$$

(d-3) Two particular lines $A_1x + B_1y + C_1 = 0$ and $A_2x + B_2y + C_2 = 0$ have an interception at the point (x_+, y_+), if $d = A_1B_2 - A_2B_1 \neq 0$, given by

$$(x_+, y_+) = \left(\frac{B_1C_2 - B_2C_1}{d}, \frac{A_2C_1 - A_1C_2}{d}\right),$$

if $A_1A_2 + B_1B_2 = 0$, lines are perpendicular. If $A_1B_2 = A_2B_1$, lines are parallel or coincident.

(d-4) The angle θ formed between two particular lines is given by

$$tan\,\theta = \frac{A_1B_2 - A_2B_1}{A_1A_2 + B_1B_2}.$$

(d-5) The line equation $A_px + B_py + C_p = 0$ that passes through point $P(x_p, y_p)$ and is perpendicular to the line $Ax + By + C = 0$ is defined as

$$A_p = -B; \quad B_p = A; \quad C_p = Ax_p - By_p.$$

Circle—In the Cartesian plane the equation $(x - x_c)^2 + (y - y_c)^2 = r^2$ defines the implicit circle equation centered at the point $C(x_c, y_c)$ with radius r. Let $E(x_e, y_e)$ be an external point to a circle. By using E we can obtain two tangent lines, t_1 and t_2, to the circle (Figure 1b), which pass through points $P(x_1, y_1)^*$ and $Q(x_2, y_2)^*$, respectively. Points P and Q can be computed by applying the geometric concept of pole-polar definition.

Pole-Polar Geometry—Pole-point and polar-line are, respectively, a point and a line that have a unique reciprocal relationship with respect to a given conic section. If the point lies on the conic section, its polar-line is the tangent line to the conic section at that point [24]. If the pole-point is external to the conic section, the polar-line intercepts the conic section exactly at the points that allow passing tangent lines from this pole-point (Figure 1b). Our interest is to pass two tangent lines, t_1 and t_2, through a circle centered at point $C(x_c, y_c)$ with radius r. Moreover, these lines must pass through a known external point $E(x_e, y_e)$ (or pole-point) to this circle (Figure 1b). We need to locate the coordinates of the polar-points $P(x_1, y_1)^*$ and $Q(x_2, y_2)^*$, which define the polar-line p and lies to the tangents linest_1 and t_2. Additionally we must find the equation of the polar-line $p(Ax + By + C = 0)$.

(d-6) The general equation of a conic in the Cartesian coordinate system is given by $a_{xx}x^2 + 2a_{xy}xy + a_{yy}y^2 + 2b_x x + 2b_y y + w = 0$. We need the equation of the polar-line $p(Ax + By + C = 0)$ that can be obtained by a known pole-point $E(x_e, y_e)$. The required coefficients of the respective polar-line p is given by: $A = a_{xx}x_e + a_{xy}y_e + b_x$; $B = a_{xy}x_e + a_{yy}y_e + b_y$; $C = b_x x_e + b_y y_e + w$. In this work, the expected conic section is a circle. For the circle case, the following simplifications are helpful: $a_{xx} = 1$; $a_{xy} = 0$; $a_{yy} = 1$; $b_x = -x_c$; $b_y = -y_c$ and $w = x_c^2 + y_c^2 - r^2$.

The next step consists in placing points $P(x_1, y_1)^*$ and $Q(x_2, y_2)^*$, which are obtained by computing the intersection between the polar-line p and the circle line (Figure 1b). To compute the intersection of a line, $Ax + By + C = 0$, with a circle, $(x - x_c)^2 + (y - y_c)^2 = r^2$, the following conditions must be considered: $d_{lc} = \frac{|Ax_c + By_c + C|}{\sqrt{A^2 + B^2}}$ is the distance between the line and the circle center point $C(x_c, y_c)$,

- if $d_{lc} > r$, there is no intersection point;
- if $d_{lc} = r$, the line is tangent to the circle and has one intersection point;
- if $d_{lc} < r$, the line is secant to the circle and has two intersection points.

The algebraic solution for this intersection is an equation of degree two. Another way to solve this intersection is applying some geometric relationships, as follows. To find the intersections points $P(x_1, y_1)^*$and $Q(x_2, y_2)^*$, which are the polar-points, we have first to drop a perpendicular line (by d-5) from the center $C(x_c, y_c)$ of the circle to the line p. Let $T(x_t, y_t)$ be the intersection point and $\overleftrightarrow{CT}$ be the line that passes through C and T (Figure 1b).

The equation of line $p(Ax + By + C = 0)$ is known (by d-6). Thus, the equation of line $\overleftrightarrow{CT}$ is $\overleftrightarrow{CT}(-Bx + Ay + Ax_c - By_c)$. This way, the point $T(x_t, y_t)$ can be computed by intersection between p and $\overleftrightarrow{CT}$ lines (by d-3).

$D_{\overline{CT}}$ represents the Euclidean distance between points C and T; $D_{\overline{PT}}$ refers to the distance between points P and T; $D_{\overline{QT}}$ stands for the distance between points Q and T; and $D_{\overline{CP}} = D_{\overline{CQ}} = r$ (by d-1).

The triangles ΔCPT and ΔCQT are right-angled, and hence we prove that

$$D_{\overline{CT}}^2 + D_{\overline{PT}}^2 = r^2,$$

and

$$D_{\overline{CT}}^2 + D_{\overline{QT}}^2 = r^2.$$

(d-7) So, $D_{\overline{QT}} = D_{\overline{PT}} = h = \sqrt{r^2 - D_{\overline{CT}}^2}$; now, if we translate the point T by h units in both directions along line p, the points P and Q are determined as follows

$$(x_1, y_1)^* = \left(x_t - \frac{Bh}{\sqrt{A^2 + B^2}}, y_t + \frac{Ah}{\sqrt{A^2 + B^2}}\right),$$

and, if $h \neq 0$

$$(x_2, y_2)^* = \left(x_t + \frac{Bh}{\sqrt{A^2 + B^2}}, y_t - \frac{Ah}{\sqrt{A^2 + B^2}}\right).$$

The suggested geometric models that use the convex hull algorithm (CHC, PLI, TLI, and MAI) need to minimize the region of interest (ROI) and exclude bad points from final results. This minimization of ROI is obtained by obtaining a convex polygon defined on a set of previously computed points. A set S is convex if $\forall x, y \in S \Rightarrow xy \subseteq S$. Any region (polygon) with a "dent" is not convex [24].The convex hull of a set of points is the smallest convex set containing these points [24–26].

(d-8) The convex hull algorithm is used in this work to specify a Region of Interest (ROI).

To illustrate the use of the convex hull we must consider the existence of three receivers centered at coordinates $C_1 \neq C_2 \neq C_3$ (and these coordinates cannot all be collinear) that collect a signal from a point with distance r_1, r_2 and r_3 (radial distance), respectively. P_{kj} and Q_{kj}, $k \neq j$, represents the polar-points that lie to the circle centered in C_j that is obtained by the external point C_k (center of another circle), as Figure 2a shows. Thus, the smallest convex polygon that contains all obtained polar-points is the convex hull for these points and this minimal polygon defines our ROI. This region in red-color lines is used to illustrate the ROI for the proposed geometric models presented below (always representing a convex hull to define a ROI).

(d-9) The location estimation of the emitter, $E_{xy}(E_x, E_y)$, is based on a set S that contains n points, (x, y), which are collected in a defined ROI. This location is given by the centroid point among all points in S, by

$$E_x = \frac{\sum_{x \in S} x}{n}, \qquad E_y = \frac{\sum_{y \in S} y}{n}.$$

Section 2 presents the models (methods) proposed in this work. All examples illustrated in Section 2 are generated in a simulator system (MatLab code) that implements the respective proposed models. This simulator is available for download (see Supplementary Materials Section for details). The simulated cases presented in this work use systems composed by three, four, or five receivers, but the simulator is able to operate with any number (>1) of receivers.

The Figure 2b presenting a Cartesian system to locate points in meters. In all figures bellow that involves example of location problems the description of the axes (label) were omitted. The axes x and y represents the Cartesian system to locate a point in the plan. The coordinate values are free of linear unit (meters, feet, or geographic coordinates).

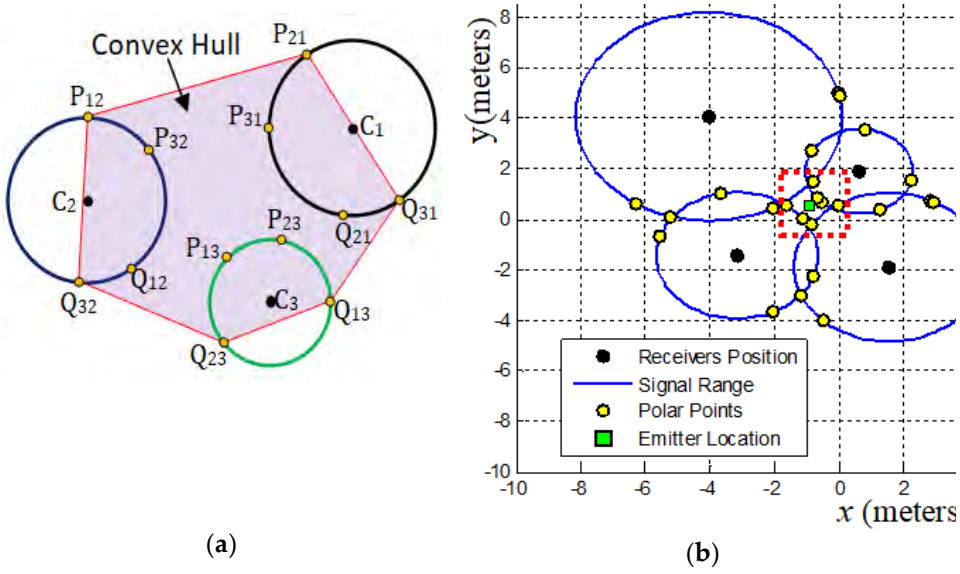

(**a**) (**b**)

Figure 2. (**a**) Illustration of Convex Hull algorithm applied to a set of polar-points. (**b**) An example of signal data and it respective signal ranges with its polar points. This case represents sets of signal data with satisfactory quality. The red dotted rectangle mark a region where a set of polar points enveloping the location of an emitter device.

2. The Proposed Geometric Models

The proposed geometric models are applicable to $m \geq 2$ receivers and one emitter. A system comprises m receivers to triangulate the emitter location $E_{xy}(E_x, E_y)$ by geometric relationship applying elements of pole-polar geometry.

Our algorithmic descriptions (and the simulator) use as input data the coordinates of each receiver position $C_k(x_k, y_k)$, $k = 1,2, \ldots, m$ and its respective signal range r_k. In real world, these signal ranges values are computed from acquired signal data by each receiver using, for example, a time-based or strength-based model. Only after can be applied a method capable to triangulate the signal emitter device location.

In this Section we present the proposed geometric methods. To evaluate such methods, we developed an experiment, in an outdoor environment, capable of acquiring signal strength data (Section 3). In this environment we define a local coordinate system that allows controlling the geometry of the localization system and guarantees precision in the positioning of the emitters and the receiver. The analyses of the acquired data in this experiment, the results produced by the application of the proposed methods and comparisons with results obtained by other three methods are in Sections 3.2 and 3.3.

2.1. Accurate Data, Exact Result

Before presenting the five proposed geometric models to solve the problem of locating a signal source, we present now the perfect solution, if the acquired signal data are accurate and if the spatial geometric arrangement among the receivers be symmetric along the x-axis and y-axis. This exact solution has complexity $O(n)$.

All the geometric models proposed in this work are based on the calculation of polar points, which belong to a circle line (signal range). If it is certain that the data acquired from the signal are accurate, the solution for the location of the signal source is immediate. According to ISO 5725-1, the term "accuracy" is used to describe the closeness of a measurement to the actual value.

The Figures 2b, 3c, 4b and 4c illustrate some cases that involve accurate signal data and therefore must have exact solutions. The Figure 3c is the perfect case using a system composed by $m = 3$ receivers. The Figure 4b and c show perfect cases using a system with $m = 4$ receivers. In fact, the case presented in Figure 3c is almost perfect. The signal data has been purposely shifted from perfection to being able to see that in the red dotted rectangle there is more than one polar point (there are four). If the data were accurate, these four polar points would self-overlap at the intersection point among the lines of these three circles. See in Figure 3c that the solution pointed out by the geometric model PPC (green rectangle) is not exact. The reason for this divergence is explained in the description and analysis of the PPC model (Section 2.2). For the case illustrated in Figure 3c, the exact solution is obtained by the set of polar points that overlap the point of intersection among the lines of the circles.

If the signal data are accurate, the exact solution is given by a single point, among all the polar points, that having the property to belongs at the same time to all circles lines (signal ranges). The formal proof for this exact solution is obtained by construction, or proof by example, which requires the construction of a concrete example with exact solution to show that some polar point is the exact solution because have the property to belongs to all circles lines. To verify this proof, use the proposed PPC method (Section 2.2) provided in the simulator system (see Section Supplementary Material). Using the simulator, you can construct examples of ideal situations (all lines of circles must intersect at a single point and the geometric arrangement of the receivers in the plane must respect aspects of non-collinearity and neither all them can be located in the range of another receiver). If these conditions are met, the PPC method will determine one or more polar-points over that single point of intersection among all circle lines and/or determine the solution over that intersection.

To obtain the exact solution we must discover at least one polar point that has the property of belonging to all circles lines. The number of polar points that have this property depends on the geometric arrangement among the position of the receivers. For example, the arrangement

presented in the Figure 3c has four polar points with this property. For Figure 4b, there are eight polar points. For Figure 4c, although the data is perfect, there is no polar point that has this property. Regardless of the number of receivers m used in the system, the maximum number of polar points that can have this property is eight.

The Figure 2b shows a system composed of four receivers. As you can see the lines of all circles do not intersect at a single point. In this case, there is some error associated with the signal data. Even so, we can admit that the data quality is satisfactory.

If the geometric arrangement among the position of the receivers is favorable and if the quality of the signal data is high there will always be an expressive set of polar points involving the location of the signal-emitting device. If the system consists of $m \geq 3$ receivers, find all polar points that are closest to each other. The centroid point (green rectangle in Figure 2b) among these selected points is the best solution to estimate the location of the signal emitter device. This can be done by stipulating a distance value as a threshold (acceptable error value) and verifying that each polar point is located a distance less than that threshold with respect to the lines of all circles (signal range). If there is a single circle line that is at a distance greater than the stipulated threshold from the point-candidate under analysis then that point must be discarded, otherwise it is selected.

However, receiving high signal data is an almost unlikely task. In this way, this work does not consider this eventual possibility as a solution. Our intention is to present new methods applied to signal triangulation problems and to analyze their behavior in the face of the errors inherent in the signal data.

2.2. Polar-Points Centroid Model (PPC)

The Figures 3 and 4 show a set of possible cases of signal data and the respective application of PPC model (Algorithm 1). Figures 4a and 4c presents an intrinsic example of data incoherence, when the spatial position of a receiver is inside the signal range of another receiver, due to the presence of noise or excessive gain applied to the antennas. Even so, the results produced are consistent with data and no singularity was generated. If this case is possible, then some polar-points are complex numbers in the form $a + bi$. However, the proposed models have their origins in the polar geometry projection, which is also used to represent complex numbers. This means that the real part, $real(a + bi) = a$, of a complex polar-point can be used as an approximate value to represent an actual polar-point. Another way is to exclude all generated complex numbers from partial results. In this work, those complex numbers are not excluded. This option shows that the proposed geometric models are capable to solve these data incoherence producing a consistent result (Figures 4a and c, 8b and 13).

Figure 3c displays the optimal case for real application. The emitter location should be in the common intersection point among the three receiver range circles. Although the result was close to this point, there is no perfect match, because there are polar-points that do not have the pattern responsible for symmetrically enveloping the emitter location. These polar-points are bad points. Using redundant data, by applying $m > 3$ receivers to the system, these non-symmetrical points will have low influences on results (Figure 4b).

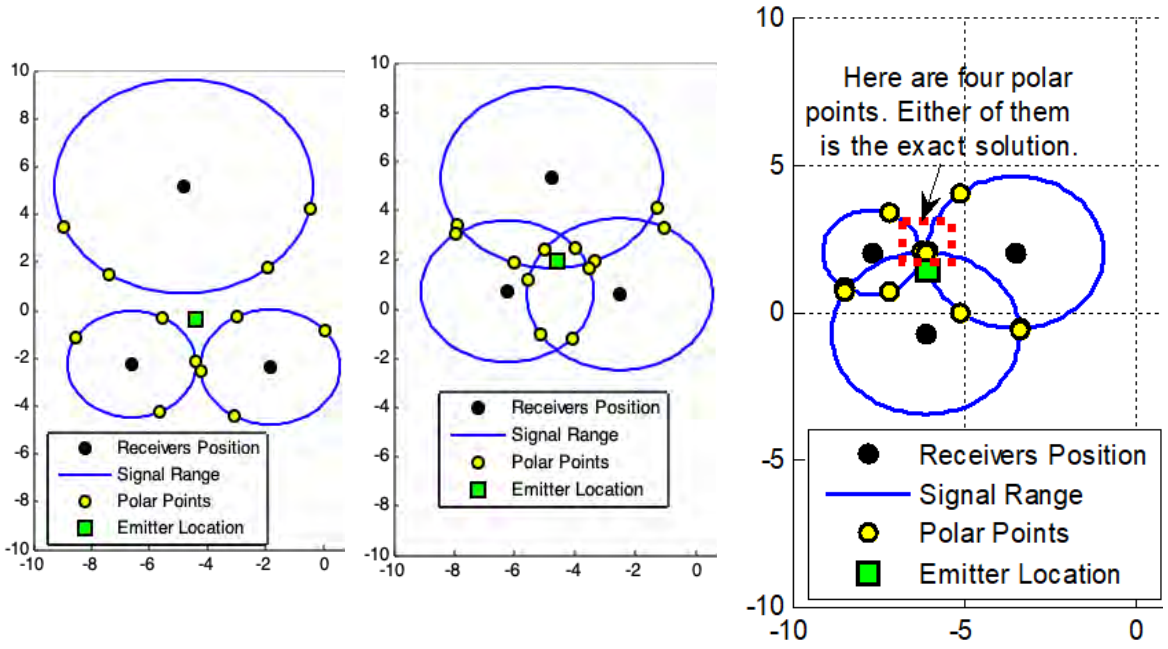

(**a**) (**b**) (**c**)

Figure 3. Results produced by Polar-Points Centroid Model (PPC). (**a**) and (**b**) show the possible presence of noise in acquired data. (**c**) Represents the best case for acquired data because the signal data are *quasi*-exact. The red dotted rectangle mark all (four) polar points that belong to all circle lines (signals range). The exact solution is one of these points (see Section 2.1).

Figure 4c present an atypical geometric arrangement for a system used to solve signal triangulation problems. All receivers are arranged in a straight line (they are collinear). It is not all triangulation methods that can solve the problem with this arrangement. The PPC resolves and, if the data is accurate, the solution can be exact.

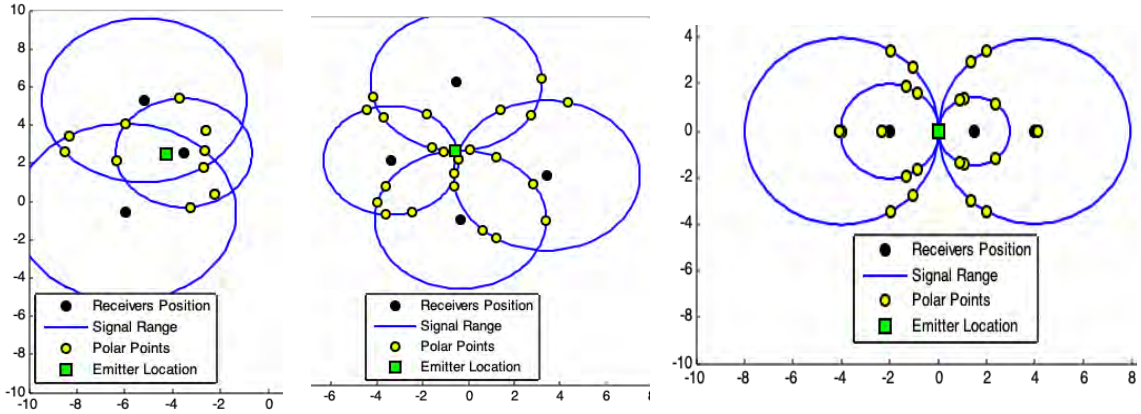

(**a**) (**b**) (**c**)

Figure 4. (**a**) Incoherence in data. The spatial position of a receiver is inside of range of another receiver. In this case, some polar-points are complex numbers (see the polar-points out of the line circles)—but their real parts belong to the region of interest (ROI). (**b**) Accurate data. Exact solution produced by PPC using redundant data (four receivers). For this case, is better applying the exact solution providing by Section 2.1. (**c**) Accurate data. A collinear arrangement among receivers (geometric arrangement not recommended) and the exact solution provided by PPC. The solution to

this problem is impossible for Weighted Least Squares (WLSm), Least-Square (LSm), and Newton–Rapson (NRm).

Algorithm 1 PPC – Polar-Points Centroid Model

Data Input

$m \geq 2$ is the number of receivers.
$C_k(x_k, y_k)$, $k = 1,2, \ldots, m$, is the planar position of each receiver.
$r_k, k = 1,2, \ldots, m$, is the signal range of each receiver to an emitter.

Procedure

1: **for** each $k = 1,2,3, \ldots, m$
2: $\forall k, j: 1,2, \ldots, m/k \neq j$, by (d − 6) and (d − 7), for each receiver position C_k, used as pole-points, **compute** all combinations of polar-points $P_{kj}\left(x_{pkj}, y_{pkj}\right)$ and $Q_{kj}\left(x_{qkj}, y_{qkj}\right)$ with the respective receiver at position C_j and signal range r_j.
3: **store** the points P_{kj} and Q_{kj} in the set $(S \leftarrow S \cup \{P_{kj}, Q_{kj}\})$.
4: **end for**
5: **Apply** (d – 9) in the set S, compute the location estimation, $E_{xy}(E_x, E_y)$, of the emitter.

Information Output

6: Emitter location estimation $E_{xy}(E_x, E_y)$.

2.3. Convex Hull Centroid Model (CHC)

Figures 5a and 5b shows results closer to the solutions together with those shown in Figures 3a and 3b. Nonetheless, the result shown in Figure 6 is better than that of Figure 3c and 5c. This improvement in accuracy is related to the exclusion of non-symmetrical polar-points (called bad points) to the emitter actual location.

It must be noticed that in Figure 6 the set of polar-points, adding a new receiver to the system, allows obtaining a region (ROI) more symmetrical to the emitter actual position. Accuracy in results improves by adding new receivers to the system. This filtered ROI is more symmetrical, both PPC and CHC (Algorithm 2) produce the same correct result.

Algorithm 2. CHC – Convex Hull Centroid Model Algorithm

Data Input

$m > 2$ is the number of receivers.
$C_k(x_k, y_k)$, $k = 1,2, \ldots, m$, is the planar position of each receiver.
$r_k, k = 1,2, \ldots, m$, is the signal range of each receiver to an emitter.

Procedure

1: **Execute** the steps 1 until 4 of algorithm Polar Points Centroid Model.
2: **Apply** (d − 8), **find** the convex hull polygon for all polar-points in S. The obtained polygon is the minimal convex polygon that involves all interest points in S. This polygon constitutes the ROI.
3: **Exclude** all polar-points on the boundary of this convex polygon, called bad polar-points, from S.
4: **Apply** (d – 9) in S, **compute** the location estimation, $E_{xy}(E_x, E_y)$, of the emitter.

Information Output

5: Emitter location estimation $E_{xy}(E_x, E_y)$.

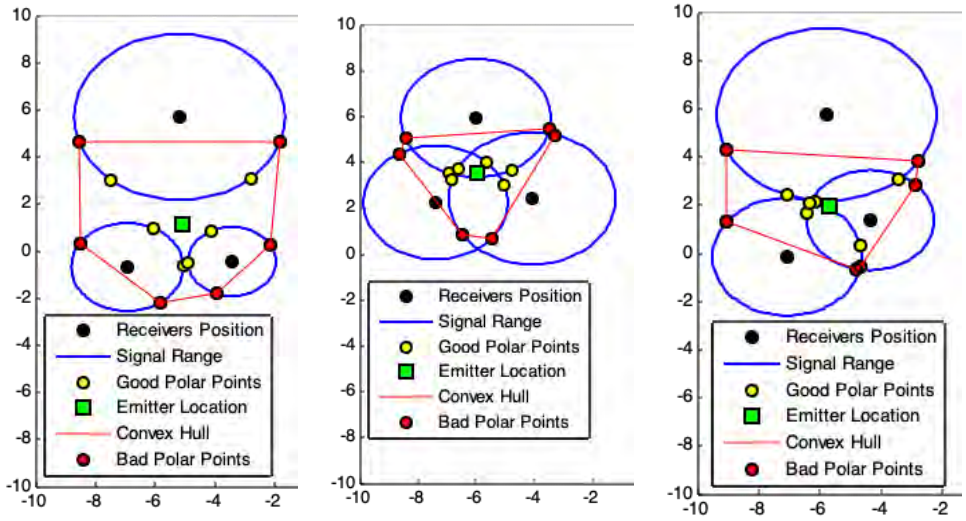

Figure 5. Results produced by Convex Hull Centroid Model (CHC). (**a**) and (**b**) highlight the possible presence of noise in acquired data. (**c**) Represents the best case for acquired data. For this case, is better applying the exact solution provided by Section 2.1.

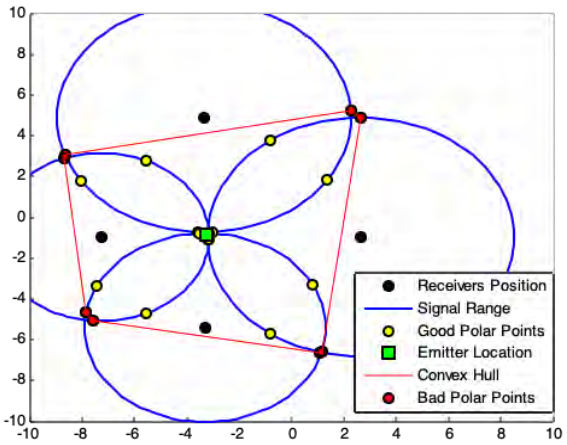

Figure 6. Results produced by CHC using satisfactory redundant data (four receivers). For this case, is better applying the exact solution provided by Section 2.1.

When the acquired data are coherent, the responses produced by the two models are similar (Figure 7b). If there are some discrepancies on the data, there may be divergences among the results (Figure 7a). Consequently, data errors promote differences in results. In this work, we do not evaluate data quality, but show consistency of results presented by the proposed models, whenever there is guarantee on the data quality.

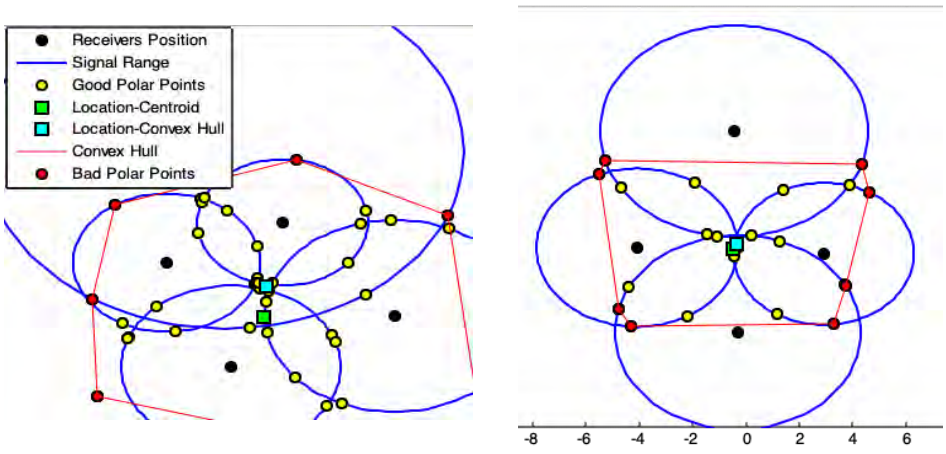

(**a**) (**b**)

Figure 7. Different cases and respective responses of the PPC and CHC models. (**a**) Five receivers system. The data has some discrepancies. (**b**) Four receivers system. The data has small inconsistencies. For both cases, is better applying the solution provided by Section 2.1.

2.4. Polar Lines Intersections Model (PLI)

The polar-line p is a line that passes through two corresponding polar-points $P(x_1, y_1)^*$ and $Q(x_2, y_2)^*$ that belongs to a line of a conic section (circle in this case). These polar-points are obtained by a given pole-point $E(x_e, y_e)$ (Figure 1b). The PLI model (Algorithm 3) consists finding all combinations of pole-polar lines using as pole-points the position of each receiver at a time. After, we must compute the points of intersection among all these lines.

Figure 8a represents cases of data underestimation provide by sensors. Figure 8b shows a good case for real application. The emitter location should be on the common intersection point among the receiver range circles. Figure 8c shows the exact result. Reliable data quality improves accuracy.

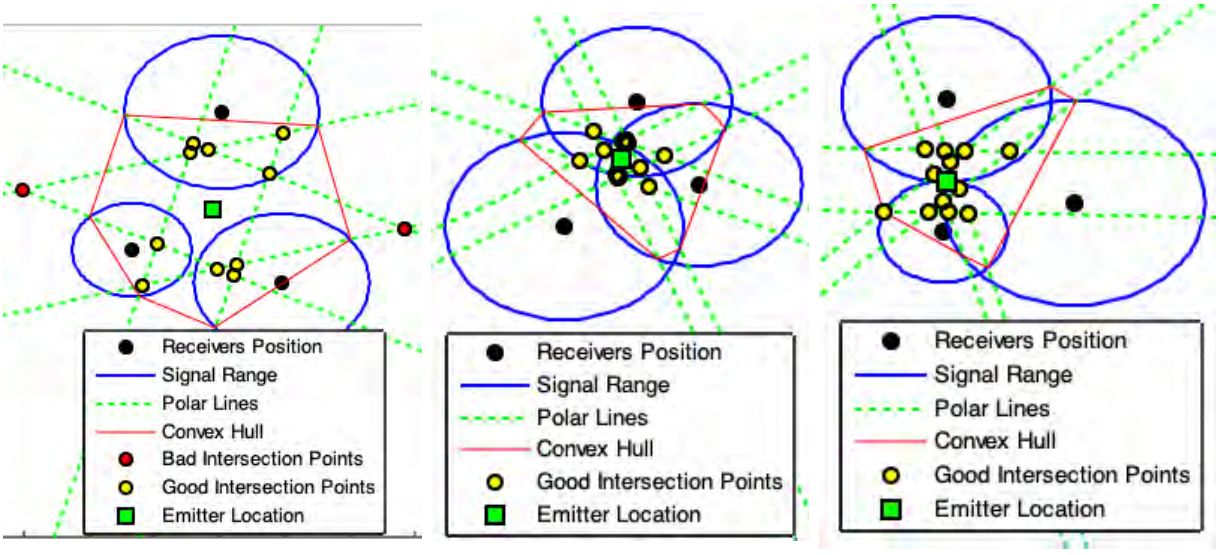

(**a**) (**b**) (**c**)

Figure 8. Results produced by Polar Lines Intersections Model (PLI). (**a**) and (**b**) show the possible presence of noise in acquired data. (c) Represents the best case for acquired data. For this case is better applying the exact solution provided by Section 2.1.

A lot of pole-polar lines pairs, in the geometry arrangement with m receivers, are parallel lines (Figures 8 and 9); this minimizes the number of intersection points. For $m > 3$ receivers, several bad

intersections points are generated. The convex hull among polar-points establishes a ROI that ensures better symmetry among the points of interest. For large values of m, many intersections will occur very far from the ROI, breaking then the desired symmetry among these points (Figure 9). The Pole-Polar Lines Intersections model achieves accurate values for emitter location because it generates significant symmetrical points of interest.

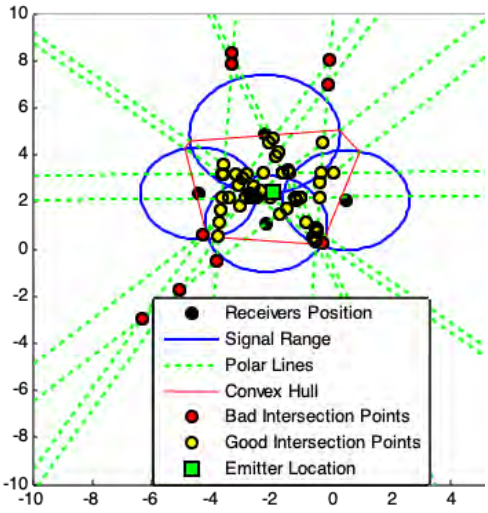

Figure 9. Result produced by PLI four receivers system. The non-symmetrical points are removed from the ROI by the use of Convex Hull. For this case is better applying the exact solution provided by Section 2.1.

Algorithm 3. PLI – Polar Lines Intersections Model Algorithm

Data Input

$m \geq 3$ is the number of receivers.
$C_k(x_k, y_k)$, $k = 1,2, \dots, m,$ is the planar position of each receiver.
$r_k, k = 1,2, \dots, m,$ is the signal range of each receiver to an emitter.

Procedure

1: **for** each $k = 1,2,3, \dots, m$
  2: $\forall k, j$: $1,2, \dots, m/k \neq j$, by (d − 6) and (d − 7), for each receiver position C_k, used as pole-points, **compute** all combinations of polar-points $P_{kj}\left(x_{pkj}, y_{pkj}\right)$ and $Q_{kj}\left(x_{qkj}, y_{qkj}\right)$ with the respective receiver at position C_j and signal range r_j.
  3: **Stores** the corresponding points P_{kj} and Q_{kj} in the set R $\left(R \leftarrow R \cup \{P_{kj}, Q_{kj}\}\right)$.
  4: For each corresponding P_{kj} and Q_{kj} points, by (d – 6), **compute** the p_{kj} polar-line equation.
4: **end for**
5: For all p_{kj} polar-lines, by (d − 3), **compute** the intersections points, (x_+, y_+), among all others polar-lines. **Stores** these intersections points in S.
6: **Apply** (d − 8), **find** the convex hull polygon for all polar-points in R. The obtained polygon is the minimal convex polygon that involves all interest points in R. This polygon constitutes our ROI.
7: **Exclude** from S all intersections points among all polar-lines on the boundary, or out, of the ROI, called bad intersections points.
8: **Apply** (d – 9), **compute** the location estimation, $E_{xy}(E_x, E_y)$, of the emitter.

Information Output

9: Emitter location estimation $E_{xy}(E_x, E_y)$.

2.5. Tangent Lines Intersections Model (TLI)

Using each center circle point C_k as pole-point, one by one, all polar-points $P_{kj}(x_{pkj}, y_{pkj})$ and $Q_{kj}(x_{qkj}, y_{qkj})$ can be computed for each other circle $j \neq k$ (Figures 1b, 3 and 10). It is possible to draw two lines for a particular C_k point (tangent lines to a circle $j \neq k$): one passing through by P_{kj} and another by Q_{kj} (Figures 10 and 11a). If m is the number of receivers in the system (there are m circles), so, $2(m-1)$ tangent lines (Figures 10 and 11a) pass through each circle and generate a large set of intersections points among these lines, but most of these points are bad points that are eliminated by the convex hull ROI. The convex hull among polar-points establishes a ROI that ensures better symmetry among the points of interest. For large values of m, many intersections will occur very far from the ROI, breaking the desired symmetry among these points.

There are intersections of tangent lines in each circle center because they pass by each circle center (receiver position) C_k. Whether these center points must be used in the estimation of emitter location depends on the geometric arrangement among receivers. While the results produced by TLI model (Algorithm 4) are consistent (Figure 10), $m \geq 4$ receiver usage is recommended (Figure 10d) for best accuracy.

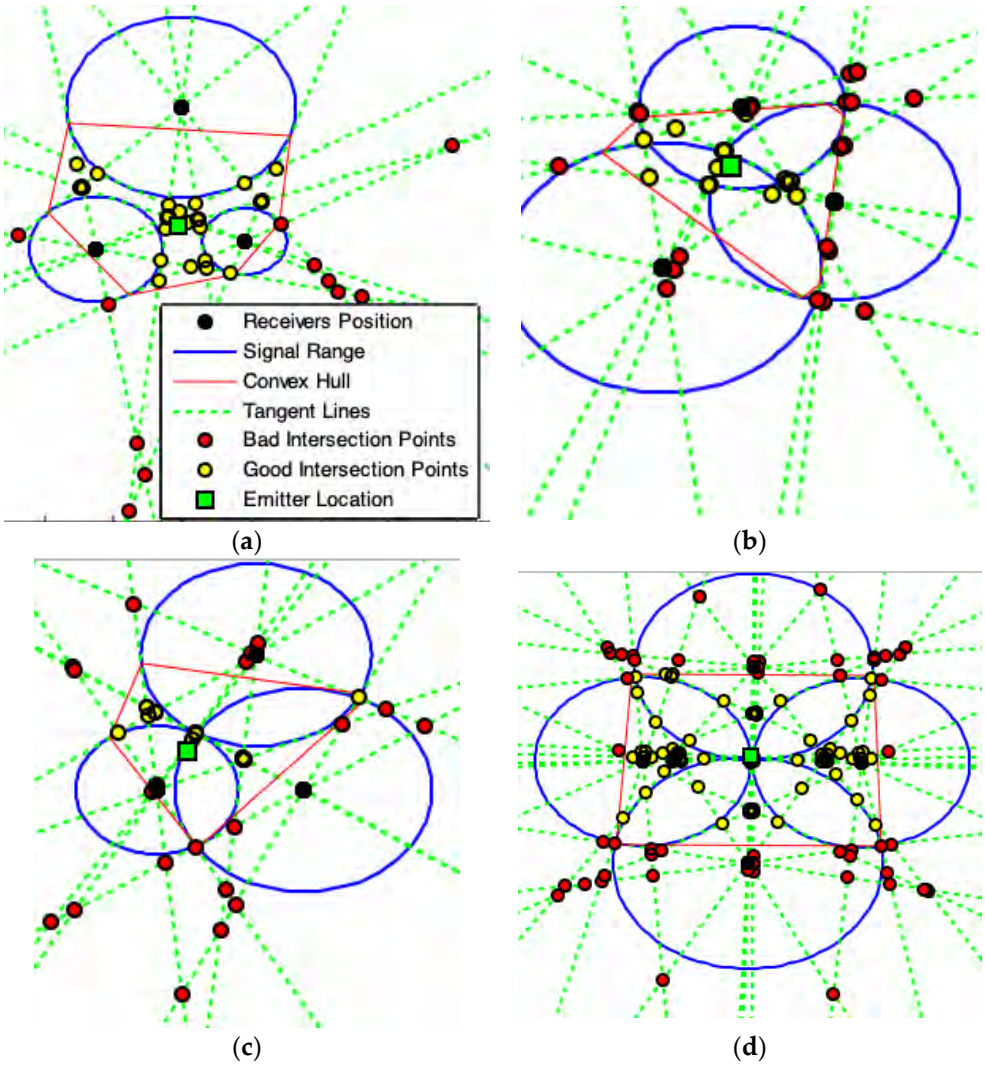

Figure 10. Results produced by Tangent Lines Intersections (TLI) model. (**a**) and (**b**) show the possible presence of noise in acquired data. (**c**) and (**d**) represents the best case for acquired data. (d)

Use of four receivers (the legend box is omitted for best view). For cases (c) and (d) is better applying the exact solution provided by Section 2.1.

Algorithm 4. TLI – Tangent Lines Intersections Model Algorithm

Data Input

$m \geq 2$ is the number of receivers.
$C_k(x_k, y_k)$, $k = 1,2,\dots,m$, is the planar position of each receiver.
$r_k, k = 1,2,\dots,m$, is the signal range of each receiver to an emitter.

Procedure

1: **for** each $k = 1,2,3,\dots,m$
  2: $\forall k, j: 1,2,\dots,m/k \neq j$, by (d – 6) and (d – 7), for each receiver position C_k, used as pole-points, **compute** all combinations of polar-points $P_{kj}\left(x_{pkj}, y_{pkj}\right)$ and $Q_{kj}\left(x_{qkj}, y_{qkj}\right)$ with the respective receiver at position C_j and signal range r_j.
  3: **Stores** the points P_{kj} and Q_{kj} in the set R $\left(R \leftarrow R \cup \{P_{kj}, Q_{kj}\}\right)$.
  4: For each corresponding P_{kj} and Q_{kj} polar-points, by (d – 6), **computes** the respective two tangent lines equation t_{Pkj} and t_{Qkj} that passes by each C_k.
5: **end for**
6: For all t_{Pkj} and t_{Qkj} tangent-lines, by (d – 3), **computes** the intersections points, (x_+, y_+), among all tangent-lines. Store these intersections points in S.
7: **Apply** (d – 8**), find** the convex hull polygon for all polar-points in R. The obtained polygon is the minimal convex polygon that involves all interest points in R. This polygon constitutes our ROI.
8: **Exclude** from S all intersections points among all tangent-lines on the boundary, or out, of the ROI, called bad intersections points.
9: **Apply** (d – 9), **compute** the location estimation, $E_{xy}(E_x, E_y)$, of the emitter.

Information Output

10: Emitter location estimation $E_{xy}(E_x, E_y)$.

2.6. Tangent Lines with Minimal Angles Model (MAI)

A complementary explanation is necessary before presenting this model. We have to consider three disjoint circles centered at $C_0(x_0, y_0)$, $C_1(x_1, y_1)$, and $C_2(x_2, y_2)$, as Figure 11a shows. Two

tangent lines pass by C_0 through the circle at C_1 and two more through to the circle at C_2. Consider the angles θ_k, $k = 0,1,2,3$, formed between two tangent line pairs that touch the circles at C_1 and C_2. The tangent lines that touch the same circle are not important to this analysis. Discard all combinations of tangent lines pairs that touch the same circle. For the illustration presented by Figure 11a, four angles can be obtained by combining all possible pairs of tangent lines that touch different pairs of circles.

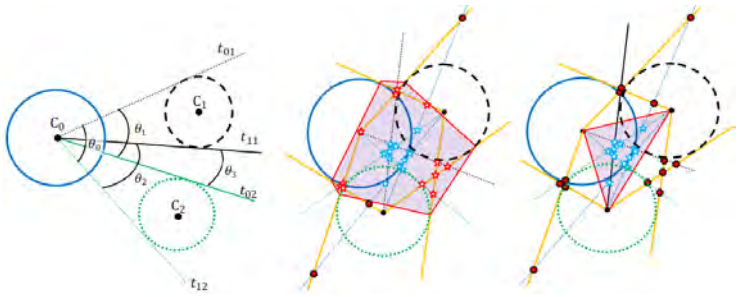

(**a**) (**b**) (**c**)

Figure 11. (**a**) Illustrations that define the Tangent Lines with Minimal Angles Model (MAI). (**b**) All intersections (red-star) with non-minimal angle tangent lines (orange-lines) must be eliminated. (**c**) All points inside the ROI formed by the convex hull polygon among the circle centers are the required points (blue-star).

For each circle pair, the two tangent lines that form the lowest angle must be preserved, while others must be removed. These two preserved lines are used by MAI (Algorithm 5). Figure 11a shows that the two lines combinations with lowest angle are the tangents lines t_{11} and t_{02}. Repeat this process to obtain all combinations of Tangent Lines with Minimal Angle that pass by different circles center to other $m - 1$ circles for each different pair of circle. Executing this procedure, Figure 11b and 11c show in orange-color the lines that must be eliminated.

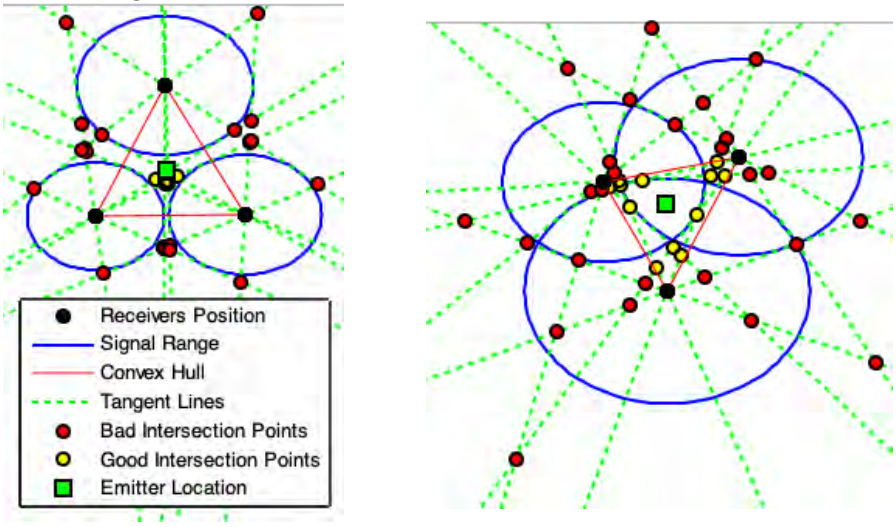

(**a**) (**b**)

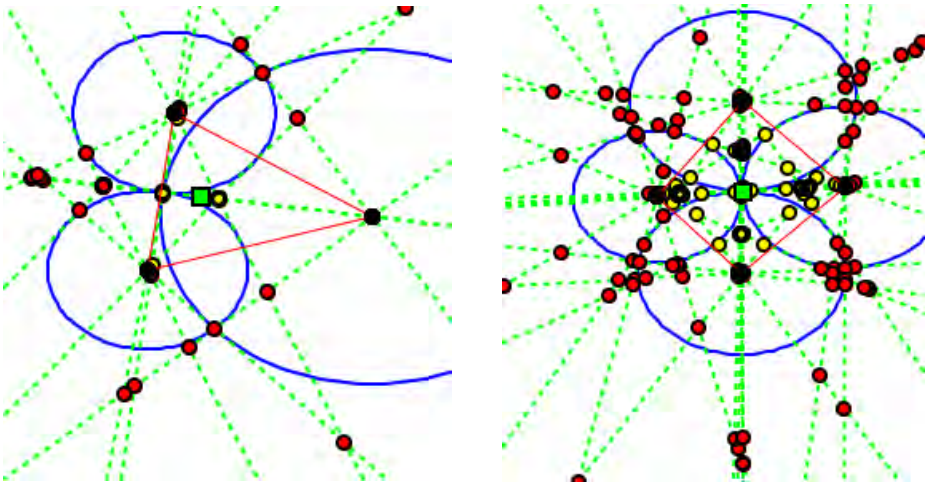

(**c**) (**d**)

Figure 12. Results produced by MAI model. (**a**) and (**b**) show the possible presence of noise in acquired data. (**c**) and (**d**) represents the best case for acquired data. (d) Application using four receivers (the legend box is omitted for best view). For the cases (c) and (d) is better applying the exact solution provided by Section 2.1.

Figures 12 e13 shows some examples of results produced by applying the MAI. The results 12a, 12b and 13 are consistent with the expected results due to the signals range errors.

The signal range used in Figures 12c and 12d are accurate and the solutions are exact. But, for 12c the MAI do not found this exact solution. MAI did not find the exact solution because the geometric arrangement of the devices of the localization system is not symmetrical. In case 12d there is this geometric symmetry and the exact solution was found. However, it can be seen both in 12c and 12d that there are polar points marking the exact solution and, if the exact solution exists, the best way to find it is to apply the solution provided in Section 2.1 of this work.

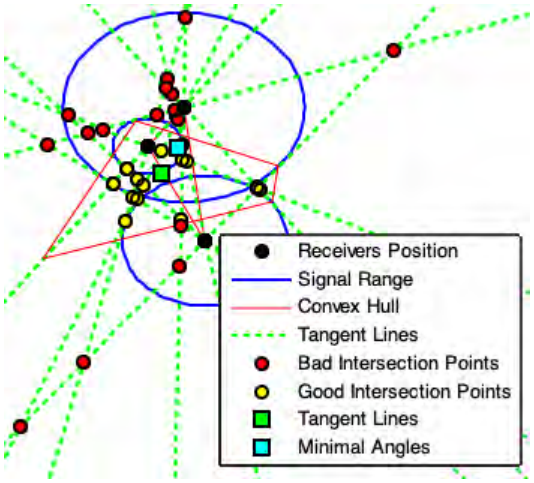

Figure 13. Geometric incoherence. The receiver is placed inside the range of another receiver. The geometric models TLI and MAI are able to overcome this data inconsistency and produce a satisfactory result.

Algorithm 5. MAI – Tangent Lines with Minimal Angles Intersections Model Algorithm

Data Input

$m \geq 2$ is the number of receivers.
$C_k(x_k, y_k)$, $k = 1,2, \ldots, m,$ is the planar position of each receiver.
$r_k, k = 1,2, \ldots, m,$ is the signal range of each receiver to an emitter.

Procedure

1: **for** each $k = 1,2,3, \ldots, m$
  2: $\forall k, j: 1,2, \ldots, m/k \neq j$, by (d − 6) and (d − 7), for each receiver position C_k, used as pole-points, **compute** all combinations of polar-points $P_{kj}\left(x_{pkj}, y_{pkj}\right)$ and $Q_{kj}\left(x_{qkj}, y_{qkj}\right)$ with the respective receiver at position C_j and signal range r_j.
  3: **Stores** the points P_{kj} and Q_{kj} in the set R $\left(R \leftarrow R \cup \{P_{kj}, Q_{kj}\}\right)$.
  4: For each corresponding P_{kj} and Q_{kj} polar-points, by (d − 6), **compute** the respective two tangent lines equation t_{Pkj} and t_{Qkj} that passes by C_k.
5: **end for**
6: For all t_{Pkj} and t_{Qkj} tangent-lines, by (d − 3), **compute** the intersections points, (x_+, y_+), among all tangent-lines. **Stores** these intersections points in S.
7: **Apply** (d − 8)**, find** the convex hull polygon for all center circles points C_k. The obtained polygon is the minimal convex polygon that involves all interest points in S. This polygon constitutes our ROI.
8: **Exclude** from S all intersections points among all tangent-lines on the boundary, or out, of the ROI, called bad intersections points.
9: **Apply** (d − 9), **compute** the location estimation, $E_{xy}(E_x, E_y)$, of the emitter.

Information Output

10: Emitter location estimation $E_{xy}(E_x, E_y)$.

3. Experimental Cases

3.1. Methodology Applied to Real Data Acquisition

In order to carry out our experiments, a structure composed of five APs devices to compose the emitters system (AP4, AP5, AP6, AP7, and AP8) is set up in an outdoor environment that covers an area of 150 m² on the ground (Figure 14). Each AP is positioned at the Cartesian coordinate (x, y) and the respective value (in meters) is registered alongside the respective AP (e.g., the AP5 is at $(9.60, -2.84)$—Figure 14). These Cartesian coordinate (2D) design the set of C_k points (centers of range signals circles computed for the *kth*-AP) and defines the geometric arrangement of the covered area on the ground.

An AP is the interface between wireless and wired section of the network. Its task is supported by the IEEE 802.11 Network Infrastructures and mainly consists in a translation of the frames from wireless framing format into a wired network framing format like Ethernet. This experiment uses the AP Tp-Link Wireless N 300Mbps TL-WR849N to compose the system of emitters that emits signals of radio frequency of 2.4 GHz.

The receiver device is a commercial cell phone operating with the operational system Android. A previously developed application capable of receiving, identifying and measuring the strength of the signal sent by each emitter (APs of interest) was installed in this cell phone (our mobile device).

To calibrate the mobile device it is placed at a distance of one meter away from each AP to acquire the respective signal strength of reference (ρ_0^k) sent by the *kth*-AP.

Next, a set of coordinatesE_p, marked and identified as known ground points, is located on the covered region. The mobile device is positioned on each of these marked ground points to receive the signals sent by each AP of interest. In this position, the strength of the signal $\rho_k(d)$sent by the *kth*-AP is measured by the mobile device application.

By means of Equation (6), the radial signal-range $d = r_{kp}$ is computed for each *k*-AP located at C_k using the signal strength ρ_{kp} sent by the respective *k*-AP and received by the mobile device located at E_p at each ground coordinate. The value $\mathcal{L} = 2.2$ is adopted for the path-loss factor in order to use the Equation (6),

Thus, we know the position of each emitter k given by $C_k(x_k, y_k)$; the radial signal-range at each AP given by r_{kp} and; the real receiver position given by $E_p(x_p, y_p)$ (Figure 15).

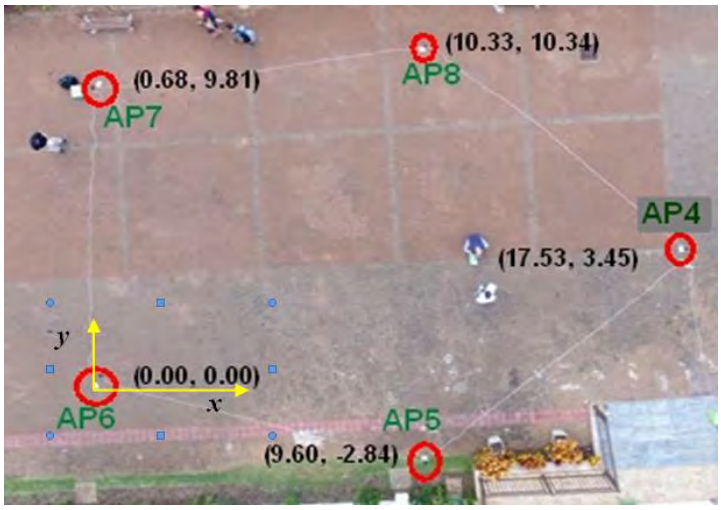

Figure 14. Structure composed of five Access Point (AP) devices and their respective position on an outdoor environment.

Now, through the proposed geometrical models, using $C_k(x_k, y_k)$ and r_k as input data, the location estimation $E_{xy}(E_x, E_y)$ of the receiver can be computed and the distance between this emitter location approximation E_{xy} to its known (real) position E_p can be calculated.

The acquired data in this analysis cases are not preprocessed. Raw data are used to verify the behavior of the proposed geometric models in cases of works with data incoherency.

3.2. Quality of Acquired Data

Figure 15 shows three sets of acquired data quality. Figure 15a and b are poor data quality and Figure 15c shows satisfactory data quality. Figure 15a shows that AP6 and AP7 overestimate and AP4 e AP5 underestimate the respective radial signal range. Although AP8 is more specific, the incoherence of data diverts the solution from the desired precision, independent of the method used to formulate the estimation. In light of this, [27] provided an alternative to improve the quality of the acquired data, [28] discussed the limits of localization using signal strength by a comparative study and [29] performed sensor localization under limited measurement capabilities. References [15,30] confirm that an optimal solution involves high computational cost, but obtaining the optimal solution is not guaranteed. This is because the errors are not in the methods that perform the triangulation of the signal data. The errors are in the signal data.

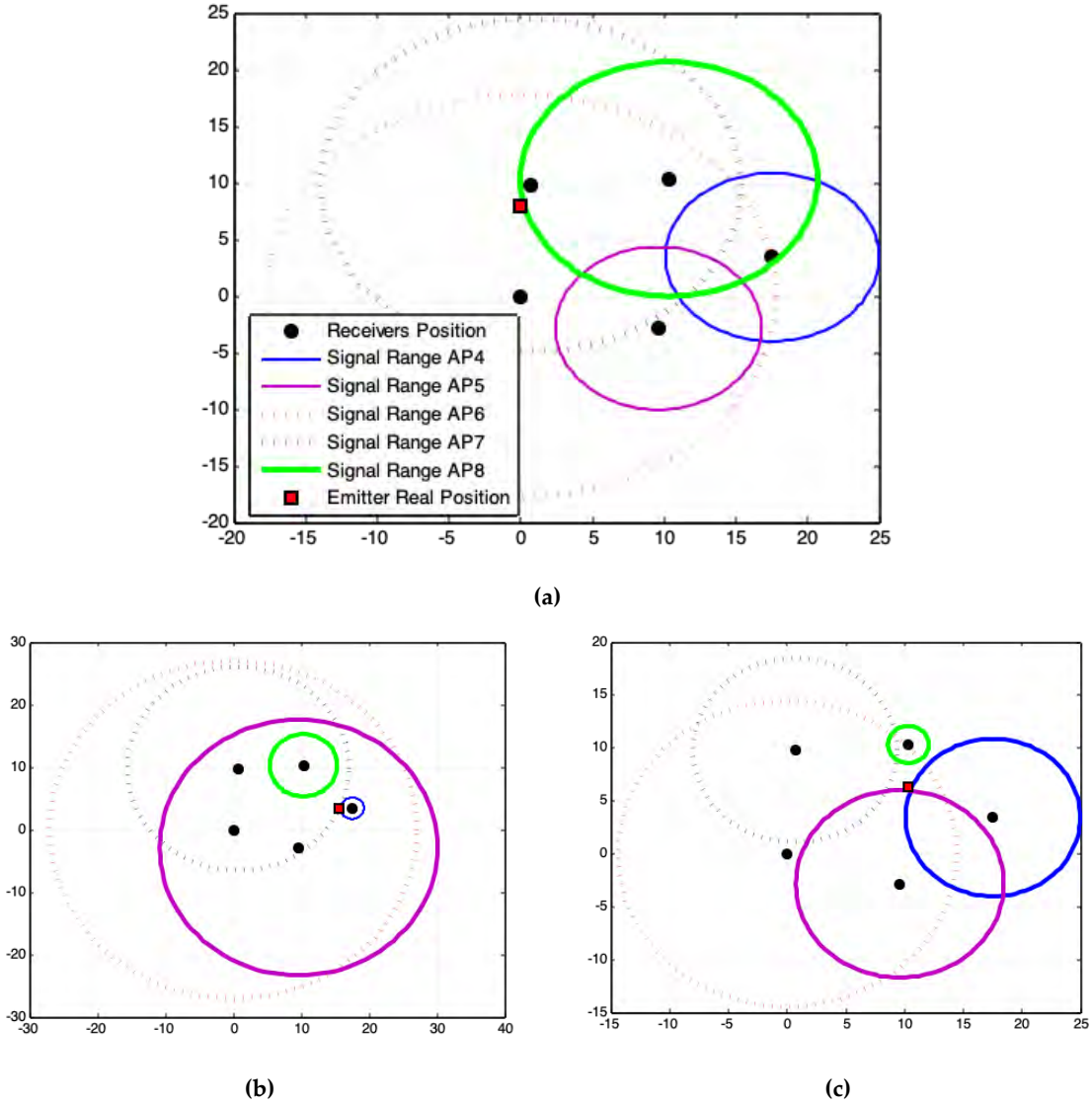

Figure 15. Acquired data quality (graphical units in meter). (**a**) and (**b**) worst quality data. (**c**) Satisfactory data quality.

With regard to the problem of localization in wireless sensor networks [31–34] presented alternative approaches and concerns regarding signal data behavior. To achieve better results, [34] preprocessed data after processing a set of partial results to decide which the best one was. As it can be noticed, acquiring accurate signal data is an arduous task. References [35,5] proposed methods for sampling signal data acquisition and discussed uncertainty and signal location. Besides, the environment is not predictable with multipath, fading, interference and shading effects [16].

In Figure 15a, AP6 generates a signal range that covers an area of ≈1200 m² on the ground, while the area covered by the APs system is ≈150 m² (Figure 14). Therefore, this data incoherence leads to solutions with larger errors.

3.3. Results and Analyses

Three experimental cases are chosen to show the results produced by the application of the proposed geometric models: (1) one that produces the worst result; (2) one that produces result with intermediate precision; and (3) one that generates more accurate result. The accuracy achieved in these cases is due solely to the quality of the data acquired. For more result, see Appendix A.

These analyses consider three metrics: (1) the error in distance measurement (Euclidean distance between the estimated location of the emitter $\mathrm{E}_{xy}(E_x, E_y)$ and the real emitter position

$E_p(x_p, y_p)$); (2) the error along x-axis given by $|E_x - x_p|$;and (3) the error along y-axis given by $|E_y - y_p|$.

The nomenclature used on the graphics legend box is:

- PPC—Polar Points Centroid Model (proposed).
- CHC—Convex Hull Centroid Model (proposed).
- PLI—Polar Lines Intersections Model (proposed).
- TLI—Tangent Lines Intersections Model (proposed).
- MAI—Tangent Lines with Minimal Angles Model (proposed).
- NRm—Newton–Rapson Method (for comparison).
- LSm—Least Square Method (for comparison).
- WLSm—Weighted Least Square Method (for comparison).

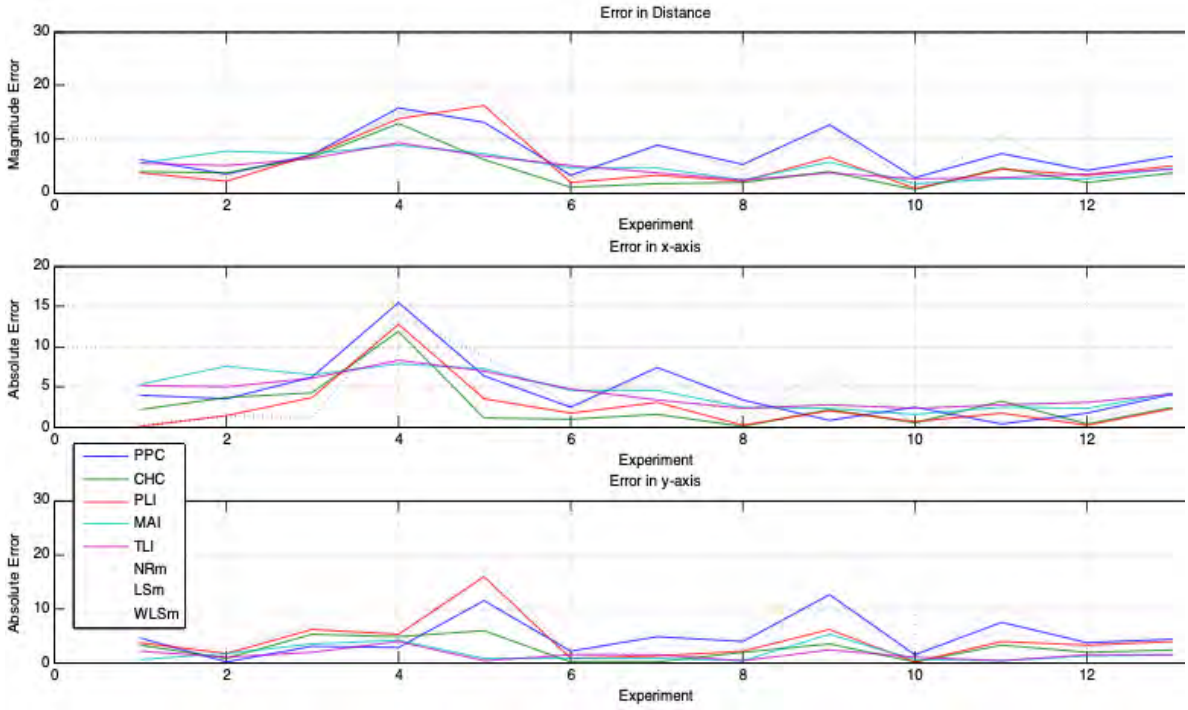

Figure 16. Magnitude error analyses.

For accomplishing the analyses, twelve experimental cases are generated (Figure 14) and the proposed geometric models (PPC, CHC, PLI, TLI, and MAI) are utilized in each acquired data set. We also use WLSm, NRm, and LSm methods to demonstrate the superior quality of the proposed geometric models. The metrics of analyses (distance error, x-axis error, and y-axis error) are computed for each result obtained from the geometric models and numerical methods. Figure 16 shows the magnitude of these errors for each experimental case. In these graphs, the 13th case represents the arithmetic mean of the magnitude errors for the respective metric and model/method.

Table 1 presents a global evaluation of the error values considering all experiments for each geometric model and numerical method. These values explain that some geometric model produce results with errors equivalent to those produced by numerical methods. MAI and TLI models promote larger errors on the x-axis, but smaller on the y-axis and distance (dist). They also promote smaller errors and produce smaller maximum errors, which show that MAI and TLI achieve better results when there is inconsistency in the data. CHC and PLI miss the least on the x-axis and get most significant result on the y-axis and distance. Errors committed by PPC are equivalent to those committed by numerical methods (WLSm, NRm, and LSm). We can observe that errors may be larger or smaller depending on the quality of the acquired data, but in the general context, geometric models present better results than numerical methods.

Table 2 displays a global mean error committed by the geometric models against numerical methods. That is to say, these values are the result of minimizing the errors reached by solving the problem of signal location. Errors are not committed by methods, but they are present in data, as Figure 15 displays. Table 2 shows that the proposed geometric models can achieve better results than those achieved by numerical methods.

Table 3 displays the variability of the errors committed by each method. The column Effective Variability of the Errors is the arithmetic mean of the standard deviation of the errors committed on the *x*-axis, *y*-axis and in distance by each method.

The Effective Variability of the Errors (Table 3) allows analyzing how a method is sensitive to the variation of data quality. In other words, this value is a metric to define how much a method can approach the exact solution when it operates on data with errors. The lower this value, the less sensitive is the method to the errors in the data and therefore has the ability to produce more accurate results. A simple analysis of the data in Table 3 shows that the proposed geometric models are more robust when they operate on data with errors than the traditional WLSm, NRm, and LSm methods. Among the geometric methods, the TLI has greater capacity to process data with errors.

Table 1. Magnitude of errors in the experimental cases.

Methods	Magnitudes Errors (in Meters)								
	Minimum Error			Maximum Error			Mean Error		
	x-axis	*y*-axis	distance	*x*-axis	*y*-axis	distance	*x*-axis	*y*-axis	distance
PPC*	0.4	0.2	2.7	15.5	12.5	15.7	4.2	4.4	6.9
CHC*	0.1	0.1	0.6	11.9	6.0	12.8	2.5	2.4	3.7
PLI*	0.1	0.1	0.7	12.8	15.9	16.3	2.4	3.8	5.0
MAI*	1.6	0.3	1.7	7.9	5.3	8.9	4.2	1.5	4.7
TLI*	2.3	0.3	2.3	8.3	3.9	9.2	4.1	1.3	4.4
NRm	0.1	1.1	1.3	14.7	12.2	15.2	2.8	5.1	6.5
LSm	0.3	1.2	1.8	14.1	22.5	23.7	3.6	6.4	7.9
WLSm	0.1	0.7	1.3	13.6	15.3	17.7	3.5	4.9	6.5

* Geometric Models proposed in this work

In order to analyze these results in a particular context, Figure 15 prove that the fourth experiment is the worst case of acquired signal data, since it promotes bigger errors, both for the numerical methods and for the geometric models (Figure 17a). An intermediate result is achieved by the eleventh (Figure 17b) experiment and the best result is obtained in tenth (Figure 17c).

Figure 17c shows that when satisfactory data make all methods and models works with relative precision, whereas data incoherencies (dotted circle lines in Figure 17) make results divert of the expected solution, and Figures 17a, b and c confirms that the proposed geometric models point to a location closer to the exact position of the signal source than the numerical methods used and can better solve the existing problem of data inaccuracy.

Table 2. Global mean errors (Geometric Models × Numerical Methods).

	Mean Errors (in Meters)		
	***x*-axis**	***y*-axis**	**Distance**
Geometric Models	3.7	2.9	5.3
NRm + LSm+ WLSm	3.5	4.1	6.0

Table 3. Standard deviation of the errors.

Methods	Standard Deviation of the Errors	Effective Variability

	x-Axis	*y*-Axis	Distance	of the Errors
PPC*	4.1	3.8	4.5	4.1
CHC*	3.1	2.1	3.4	2.9
PLI*	3.3	4.1	4.9	4.1
MAI*	2.5	1.6	2.6	2.2
TLI*	2.3	1.0	2.3	1.9
NRm	4.0	4.0	4.9	4.3
LSm	4.3	6.7	7.4	6.1
WLSm	4.2	4.3	5.5	4.7

*Geometric Models proposed in this work.

The worst case, Figure 17a, deals with the case of inconsistency of acquired data. Even, if the use of such data does not show the precise location of the emitter, the results produced by the geometric models are consistent with the geometric arrangement among data. The solution is found on the region where most of signals range (circles) intersects. The solution is inaccurate because of the serious deviations in the acquired data. If data inconsistency is moderate (Figure 17b), the proposed geometric models generate higher quality results than those produced by numerical methods.

The Appendix A presents six other experimental results.

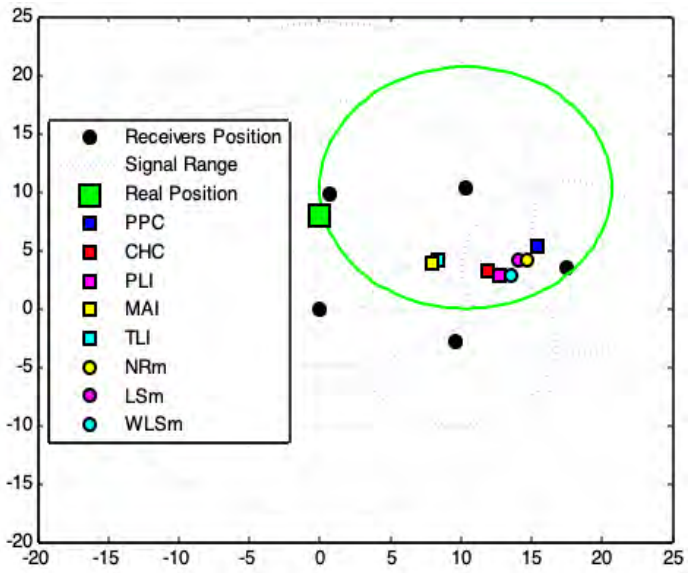

(a)

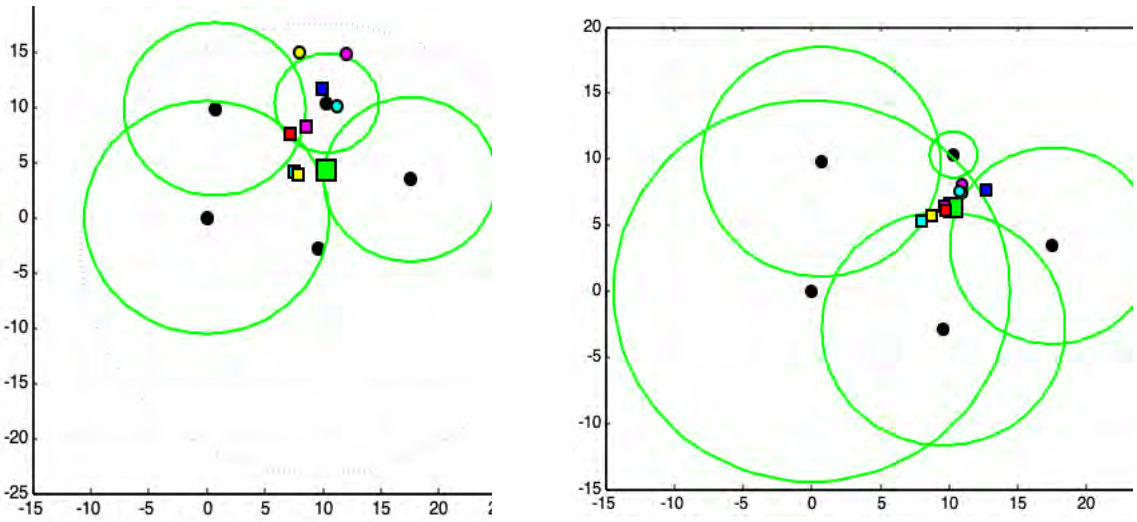

Figure 17. Some particular experimental results. (**a**) The worst case. (**b**) An intermediate case. (**c**) The best case. The blue-dotted circle lines show the receivers/emitters that suffered severe interferences and promoted the acquisition of data with errors.

4. Conclusion

Our results show that there is a geometrical relationship between the emitter location and elements of pole-polar geometry. For this aim, we propose geometric models to solve a geometric problem: 2D location of a signal source and, if accurate data are available, an exact solution is found with cost $O(n)$ (Section 2.1). If the data quality is satisfactory, the proposed models obtain the best estimative for the problem of locating the signal emitter source and are more robust when they operate on data with errors than the traditional WLSm, NRm, and LSm methods.

This work contributes to cope with the problem of applying 2D point location in a geometric relationship by reducing the number of arithmetic operations needed by the current conventional methods in use and the inherent propagation errors in the acquired data. The proposed geometric models have low computational cost $O(n\,log\,n)$. The obtained results are consistent even when there is incoherence in the data or when there is incoherence geometric in the arrangement of the receivers system.

When analyzing these results, we observe that the solutions given by the geometric models are located around the region of intersections of the radial signals ranges for all cases. Thus, a linear combination of all these solutions is also a solution. Consequently, we have computed the mean among the five solutions to derive this linear combination with no special motivation. This new solution minimizes the global error (Table 2).

Five geometric models have been presented and experimented with displayed solutions that are located around the region of intersection of the radial signals range for all cases. A comparison of results with numerical methods Weighted Least-Square, Least-Square, and Newton–Rapson has been carried out and results achieved by the proposed geometric models have improved, especially in cases of moderate data incoherence.

The proposed geometric models have the following limitations: (1) 2D solution (we are developing a 3D solution). (2) Proposed methods for estimating location require that the device to be located be inserted into the coverage area of the APs. We are developing a solution to this limitation in conjunction with the 3D solution. (3) APs may be arranged collinearly only for a few specific cases.

To develop this work we have built a simulator in MatLab code and used the implemented functions to construct a prototype that processes real data [36]. All code and data used are at anyone's disposal. Go to www.coding2change.org/articles/GeometricModels.zip. Consult User's Manual for more instructions.

Author Contributions: A.M. and A.P conceived, designed and performed the experiments; proposed the geometrical models; analyzed the data and results; developed the MatLab code; wrote the paper. M.E. and F.D. conceived the experiments; analyzed the results; provided mathematical contributions; wrote the paper; acted as peer reviewers.

Funding: This research has been supported by the Pololas project (TIN2016-76956-C3-2-R) of the Spanish Ministry of Economy and Competitiveness and by the particular research plan of the University of Seville (VPPI-US).

Acknowledgments: Special thanks to the University of Seville—Spain and the State University of Maringá—Brazil.

Conflicts of Interest: The authors declare no conflict of interest. The founding sponsors had no role in the design of the study; in the collection, analyses, or interpretation of data; in the writing of the manuscript, and in the decision to publish the results.

Appendix A—Complementary Results

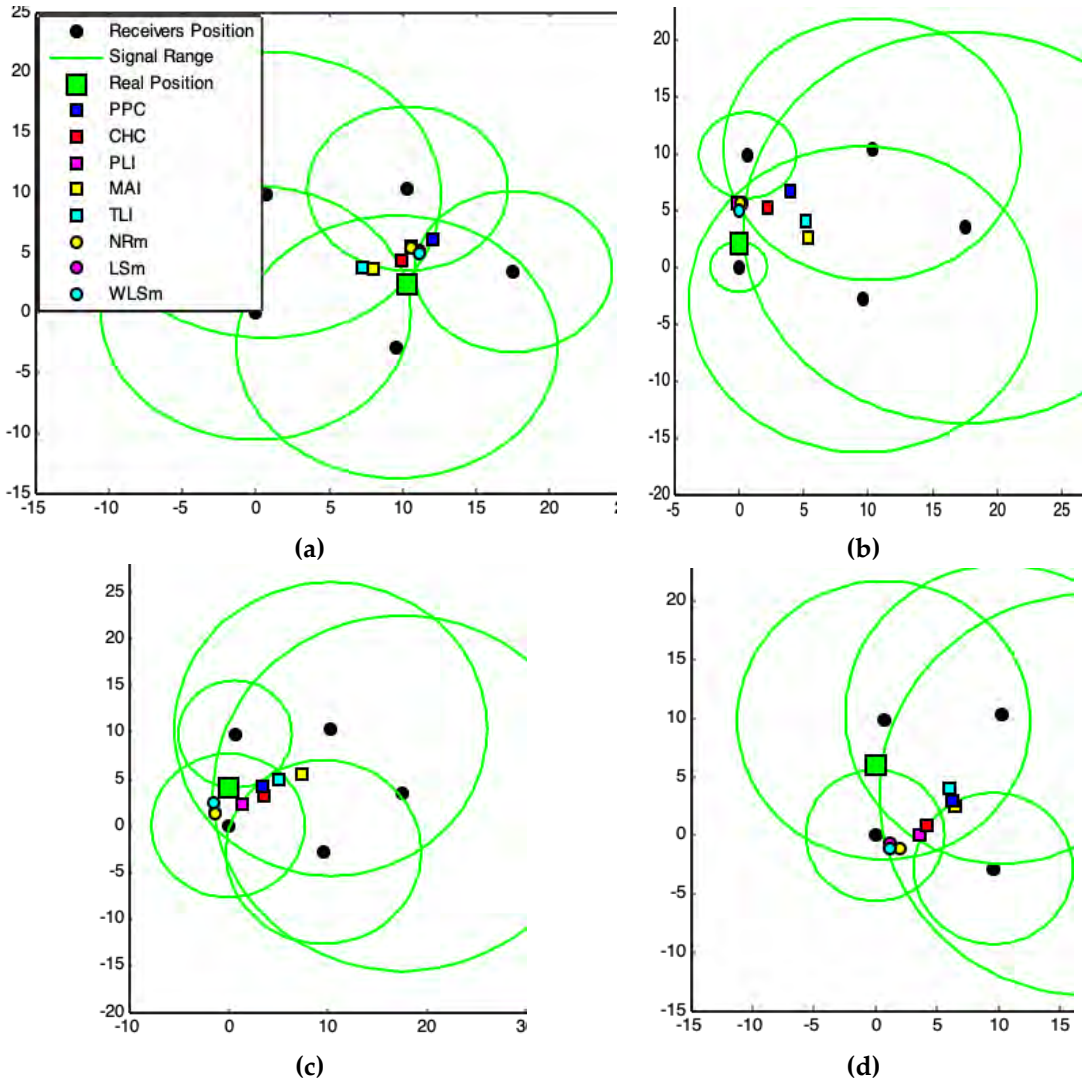

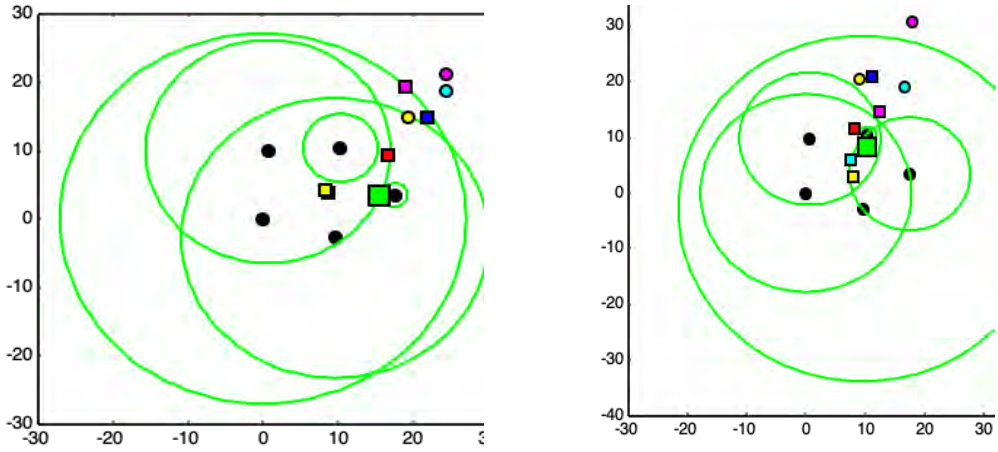

Figure A-1. Complementary experimental results.

References

1. Wang, H.; Gao, Z.; Guo, Y.; Huang, Y. A Survey of Range-Based Localization Algorithms for Cognitive Radio Networks. In Proceedings of the Second International Conference on Consumer Electronics, Communications and Networks, Yichang, China, 21–23 April 2012; pp. 844–847, doi:10.1109/CECNet.2012.6201449.
2. O'Hara, B.; Petrick, A. *The IEEE 802.11 Handbook: A Designers Companion*, 2nd ed.; IEEE Press: New York, NY, USA, 2005; ISBN 0-7381-4449-5.
3. Ahmad, U.; Gavrilov, A.V.; Lee, S.; Lee, Y.-K. A modular classification model for received signal strength based location systems. *Neurocomput. Lett.* **2008**, *71*, 2657–2669, doi:10.1016/j.neucom.2007.11.045.
4. Kaemarungsi, K.; Krishnamurthy, P. Analysis of WLAN's received signal strength indication for indoor location fingerprinting. *Pervasive Mob. Comput.* **2012**, *8*, 292–316, doi:10.1016/j.pmcj.2011.09.003.
5. Balanis, C.A.; Polycarpou, A.C. *Antennas. Wiley Encyclopedia of Telecommunications*; J. G. Proakis Ed.; John Wiley & Sons: New York, NY, USA; 2003, pp. 179-188, doi:10.1002/0471219282.eot124.
6. Goswami, S. *Indoor Location Technologies*; Springer: Heidelberg, Germany, 2013; ISBN 978-1-4614-1377-6.
7. Acharya, R. *Understanding Satellite Navigation*; Elsevier Inc.: Atlanta, GA, USA; 2014; Chapters 6–7, ISBN 978-0-12-799949-4. doi:10.1016/B978-0-12-799949-4.00001-4.
8. Wu, R.H.; Lee, Y.H.; Tseng, H.W.; Jan, Y.G.; Chuang, M.H. Study of characteristics of RSSI signal. In Proceedings of the IEEE International Conference on Industrial Technology, ICIT 2008, Chengdu, China, 21–24 April 2008; doi:10.1109/ICIT.2008.4608603.
9. Fosdick, L.D.; Jessup, E.R.; Schauble, C.J.C.; Domik, G. *An Introduction to High-Performance Scientific Computing*; The MIT Press: Cambridge, MA, USA, 1996; ISBN 0-262-06181-3.
10. Bahl, P.; Padmanabhan, V.N. RADAR: An in-building RF-based user location and tracking system. *Proc. IEEE Infocom* **2000**, *2*, 775–784.
11. Maass, H. Location-Aware Mobile Applications based on Directory Services. In Proceedings of the 3rd Annual ACM/IEEE International Conference on Mobile Computing and Networking, MobiCom '97, Budapest, Hungary, 26–30 September 1997; pp. 23–33, ISBN 0-89791-988-2, doi:10.1145/262116.262123.
12. Nelson, G.J. Context-Aware and Location Systems. Ph.D. Thesis, University of Cambridge, Computer Lab, Cambridge, UK, January 1998.
13. CISCO. Wi-Fi Location-Based Services 4.1 Design Guide. 2014. Available online: http://www.cisco.com/c/en/us/td/docs/solutions/Enterprise/Mobility/WiFiLBS-DG.html (accessed on 13 February 2018).
14. Mehra, R.; Singh, A. Real Time RSSI Error Reduction in Distance Estimation Using RLS Algorithm. In Proceedings of the IEEE 3rd International Advance Computing Conference, IACC 2013, Ghaziabad, India, 22–23 February 2013; pp. 661–665, doi:10.1109/IAdCC.2013.6514305.
15. Luo, M.; Chen, X.; Cao, S.; Zhang, X. Two New Shrinking-Circle Methods for Source Localization Based on TDoA Measurements. *Sensors* **2018**, *18*, 1274; doi:10.3390/s18041274.

16. Beutel, J. Location Management in Wireless Sensor Networks. In *Handbook of Sensors Networks: Compact Wireless and Wired Sensing Systems*; Ilyas, M., Mahgoub, I., Eds.; CRC Press: New York, NY, USA; 2005; ISBN 0-8493-1968-4.
17. Tarrío, P.; Bernardos, A.M.; Casar, J.R. Weighted Least Squares Techniques for Improved Received Signal Strength Based Localization. *Sensors* **2011**, *11*, 8569–8592; doi:10.3390/s110908569
18. Atkinson, K.E. *An Introduction to Numerical Analysis*, 2nd ed.; John Wiley & Sons: New York, NY, USA; 1988; ISBN 978-0-471-62489-9.
19. Bancroft, S. An algebraic solution of the GPS equations. *IEEE Trans. Aerosp. Electron. Syst.* **1985**, *AES-21*, 56–59, doi:10.1109/TAES.1985.310538.
20. Strang, G.; Borre, K. *Linear Algebra, Geodesy, and GPS*; Wellesley Press: Cambridge, UK; 1997; ISBN 0961408863.
21. Rahman, M.Z. *Beyond Trilateration: GPS Positioning Geometry and Analytical Accuracy, Global Navigation Satellite Systems: Signal, Theory and Applications*; Jin, S., Ed.; InTechOpen: London, UK, 2012; Chapter 10, pp. 241–256, ISBN 978-953-307-843-4. Available online: http://www.intechopen.com/books/global-navigation-satellite-systems-signal-theory-and-applications (accessed on 10 January 2018). doi:10.5772/30602.
22. WCIPEG—Programming Enrichment Group. Computational Geometry. Woburn Collegiate Institute's. Available online: http://wcipeg.com/wiki/Computational_geometry (accessed on 13 February 2018).
23. Gibson, C.G. *Elementary Euclidean Geometry: An Introduction*; Cambridge University Press: Cambridge, UK, 2004; ISBN 978-0-521-83448-3.
24. Knuth, D.E. *Axioms And Hulls: Lecture Notes in Computer Science*; Springer: Heidelberg, Germany, 1992; ISBN 978-3-540-55611-4.
25. Barber, C.B.; Dobkin, D.P.; Huhdanpaa, H.T. The Quickhull Algorithm for Convex Hulls. *ACM Trans. Math. Softw.* **1996**, *22*, 469–483, doi:10.1145/235815.235821.
26. O'Rourke, J. *Computational Geometry in C*, 2nd ed.; Cambridge University Press: Cambridge, UK; 1994; ISBN 978-0521649766.
27. Halder, S.J.; Choi, T.Y.; Park, J.H.; Kang, S.H.; Park, S.W.; Park, J.G. Enhanced ranging using adaptive filter of ZIGBEE RSSI and LQI measurement. In Proceedings of the 10th International Conference on Information Integration and Web-Based Applications & Services, iiWAS '08, Linz, Austria, 24–26 November 2008; pp. 367–373, ISBN 978-1-60558-349-5, doi:10.1145/1497308.1497374.
28. Elnahrawy, E.; Li, X.; Martin, R.P. The limits of localization using signal strength: A comparative study. In Proceedings of the Sensor and Ad Hoc Communications and Networks, Santa Clara, CA, USA, 4–7 October 2004; p. 406–414.
29. Wang, C.; Xiao, L. Sensor Localization under Limited Measurement Capabilities. *IEEE Netw.* **2007**, *21*, 16–23, doi:10.1109/MNET.2007.364254.
30. Mensing, C.; Plass, S. Positioning algorithms for cellular networks using TDOA. In Proceedings of the 2006 IEEE International Conference on Acoustics, Speech and Signal Processing, Toulouse, France, 14–19 May 2006; pp. IV-IV. doi:10.1109/ICASSP.2006.1661018.
31. Wu, D.; Bao, L.; Li, R. UWB-Based Localization in Wireless Sensor Networks. *Int. J. Commun. Netw. Syst. Sci.* **2009**, *2*, 407–442, doi:10.4236/ijcns.2009.25046.
32. Sahoo, P.K.; Hwang, I.-S. Collaborative Localization Algorithms for Wireless Sensor Networks with Reduced Localization Error. *Sensors* **2011**, *11*, 9989–10009, doi:10.3390/s111009989.
33. Amitangshu, P. Localization Algorithms in Wireless Sensor Networks: Current Approaches and Future Challenges. *Netw. Protoc. Algorithms* **2010**, *2*, 45–73, doi:10.5296/npa.v2i1.279.
34. Schneider, C.; Zutz, S.; Rehrl, K.; Brunaue, R.; Gröchenig, S. Evaluating GPS sampling rates for pedestrian assistant. *J. Locat. Based Serv.* **2016**, *10*, 212–239, doi:10.1080/17489725.2016.1259509.
35. Lam, L.D.M.; Tang, A.; Grundy, J. Heuristics-based indoor positioning systems: A systematic literature review. *J. Locat. Based Serv.* **2016**, *10*, 212–239, doi:10.1080/17489725.2016.1232842.
36. Montanha, A.; Escalona, M.J.; Domínguez-Mayo, F.J.; Polidorio, A. Technological Innovation to Safely Aid in the Spatial Orientation of Blind People in a Complex Urban Environment. In Proceedings of the International Conference on Image, Vision and Computing (ICIVC), Portsmouth, UK, 3–5 August 2016; IEEE Publisher: New York, NY, USA; 2016; pp. 102–107. doi:10.1109/ICIVC.2016.7571281.

Journal of Network and Computer Applications 180 (2021) 103006

Contents lists available at ScienceDirect

Journal of Network and Computer Applications

journal homepage: www.elsevier.com/locate/jnca

New signal location method based on signal-range data for proximity tracing tools

Aleksandro Montanha [a], Airton M. Polidorio [b], María del Carmen Romero-Ternero [c,*]

[a] PhD. Student, Programa Doctorado Ingeniería Informática, Escuela Técnica Superior de Ingeniería Informática, Universidad de Sevilla, Avda. Reina Mercedes S/n, 41012, Seville, Spain
[b] Departamento de Informática Centro de Tecnologia, Universidade Estadual de Maringá, Av. Colombo, 5790 - Jd. Universitário, Maringá, 87020-900, Brazil
[c] Departamento de Tecnología Electrónica, Escuela Técnica Superior de Ingeniería Informática, Universidad de Sevilla, Avda. Reina Mercedes S/n, 41012, Seville, Spain

ARTICLE INFO

Keywords:
2D signal location
Wireless network
Method
Signal processing
Computational geometry
Pole-polar geometry
IEEE 802.11
Contact tracing

ABSTRACT

Several technological solutions have emerged over the last several months to support proximity contact tracing to fight the COVID-19 pandemic. For this reason, today more than ever, accurate signal location is needed, even in indoor public areas (supermarkets, public transport, etc.). In a previous work, we proposed five methods to solve the problem of signal localization using elements of pole-polar geometry. The proposals were innovative, since they solved a geometric problem (locating a point in a coordinate system) only by applying concepts of geometry. Among these developed methods, the PPC (Pole-Polar Centroid model) was also presented. Although the PPC solves the problem of locating a device with better precision than conventional methods (based on numerical or optimization methods), its accuracy was found to be the worst among the five proposed geometric methods. In this context, this work proposes an extension to our PPC method, called the weighted Pole-Polar Centroid method (wPPC), which improves the accuracy of the previous PPC results. Such an extension does not change the complexity O(m^2) or the minimum dimensionality ($m = 2$) of nodes, which integrate a location network to perform the triangulation of such signals. Moreover, this extension estimates a device's location coordinates by means of the interaction, via signals, of this device with the network nodes distributed in any coordinate system. An IEEE 802.11 network infrastructure is used to accomplish the experiments. Errors in signal data are common, and our new proposed method, the wPPC, can mitigate the influence of these errors, produce more accurate results than the PPC, and outperform some of the other four proposed geometric methods and current numeric methods. Despite the use of an IEEE 802.11 network infrastructure for testing here, this range-based method for signal triangulation can be applied to any signal type (such as Wi-Fi, Bluetooth, and light and sound propagation).

1. Introduction

The impact of non-pharmaceutical interventions (NPIs) to reduce COVID-19 mortality is globally significant (Wang et al., 2020; Eubank et al., 2020). One of these NPIs is contact tracing, which has become an essential tool for helping public health and local communities to prevent virus spread (Cho et al., 2020), and its use is also recommended by the World Health Organization (onsiderations in the, 2020). Besides manual contact tracing, several technological initiatives have emerged in recent months based on mobile phone apps to track exposures after an infected individual is identified [3] (Klonowska et al., 2020)[eHealth Network Mobile ap, 2020], such as the Trace Together app (Singapore) (Ng et al., 2020), the Pan-European Privacy Preserving Proximity Tracing (PEPP-PT) (-Pan-European Priv), the New Zealand initiative (Rapid Audit of Contact Tr, 2020), and the Apple & Google partnership (Apple and Google partner, 2020). One of the distributed approaches is based on the smart device interaction using tokens and messages through wireless communication by proximity.

2. Today, most people carry mobile phones that are connected through wireless communication technologies, such as Bluetooth or Wi-Fi (the IEEE 802.11 protocol family). One of the problems of using these interactions to keep track of contacts based on proximity is the possibility of communication or signal data errors, which cause the

* Corresponding author.
E-mail addresses: aleksmontanha@gmail.com (A. Montanha), ampolidorio@uem.br (A.M. Polidorio), mcromerot@us.es (M.C. Romero-Ternero).

https://doi.org/10.1016/j.jnca.2021.103006
Received 10 June 2020; Received in revised form 10 November 2020; Accepted 29 January 2021
Available online 20 February 2021

location of the device to achieve an accuracy that is lower than it should be (Ahvar et al., 2016; Gandotra et al., 2017; Pedhadiya et al., 2019; Yassinet al., 1327; Hassan et al., 2015; Lau et al., 2019).

3. The present work proposes a new signal location method based on weighted pole-polar geometry that improves the estimation accuracy of signal location.
4. The paper is structured in five sections. Section 2 describes the initial considerations from our previous work. Section 3 presents a new method called the weighted Pole-Polar Centroid (wPPC). Section 4 shows details experimental cases and their results. Section 5 presents the conclusions of this work.

2. Considerations and algorithm formalization from previous work

6. Signal location estimation by range-based methods needs to solve a nonlinear system with m-many equations, if obtained the numbers of nodes of the location network. The solution of this system can be obtained by the linearization of these equations. The linearization process can be accomplished by subtracting equations. One equation of this system is chosen and is used to subtract all others from this system. Thus, the terms of all equations of degree two are eliminated, and the system becomes linear. However, the realization of this subtraction also eliminates from the system the equation chosen to perform this linearization. For example, if there were five equations before the linearization, after the linearization, there will be four equations in the system. It is important to consider that this equation that was eliminated contemplates data of the radial range of the signal acquired by a device of the location network system. Eliminating this equation means eliminating this device from the network, and its participation in the final result of the location of a point in space becomes indirect. The most complicated fact of performing the linearization of the equations system by the subtraction of its equations is the possibility of error propagation. Assume that the equation chosen to perform the linearization operation is that corresponding to the device that acquired the signal data with the highest error. By using this equation to subtract all other ones, such error is substantially propagated to the linearized equation system, damaging the accuracy of the solution.
7. Based on these two problems that the linearization operation causes to the location system, (1) a device is eliminated from the location network, which reduces the redundancy of that network and compromises the ability to minimize errors in the result of the location estimate, and (2) the choice of an equation for this system to perform linearization by subtraction can substantially propagate the signal data errors contained in this chosen equation for the other equations, leading to the proposal of geometric solutions to the problem of 2D signal location (Montanha et al., 2019).
8. The geometric solutions previously proposed have the following advantages over conventional methods: (1) there is no need to linearize the system of equations, (2) there is no need to remove a node from the location network, and (3) the complexity of geometric methods is of order $O(m^2)$ instead of order $O(m^3)$ of the conventional methods.
9. Our previous work [17] proposed five geometric methods to estimate the location of sources emitting/receiving signals based on the signal range: (1) PPC, based on a centroid of a set of polar points; (2) CHC, based on a convex hull region defined by a set of interest points; (3) PLI, based on a centroid of a set of interest points obtained by polar line intersections; (4) TLI, based on a centroid of a set of interest points obtained by tangent lines intersections; and (5) MAI, based on a centroid of a set of interest points obtained by tangent line intersections with minimal angles.
10. All of these methods have been shown to be capable of estimating a position in a coordinate system, by geometrically manipulating signal range data, with better precision than traditional methods such as Newton–Raphson (NRm) [17][S and Atkinson, 1990], Least-Squares (LSm) [17][19][Acharya, 2014], and Weighted Least-Squares (WLSm) [17][19][Tarrío et al., 2011], leading to the conclusion that the proposed geometric methods are able to handle errors in signal data more adequately.
11. In this context, this work proposes an extension to the PPC method [17]: the weighted Pole-Polar Centroid model (wPPC) method. It provides the PPC with the ability to process signal data with errors and obtain better accuracy in location estimation, without changing the complexity $O(m^2)$ or the minimum dimensionality ($m = 2$) of nodes in the location network system required by the original PPC method.
12. This paper does not address operations or methods related to signal data preprocessing. This means it is assumed that there are errors in the acquired data. Such errors are due to the signal multipath, the presence of obstacles, and the co-presence of other electromagnetic sources. Obviously, in order to guarantee the accuracy of location estimation, it is necessary to ensure accurate data.
13. To analyze the results produced by wPPC, this work uses the same data provided by previous work [17]. Such data, not preprocessed, were acquired using the IEEE 802.11 network infrastructure in a system of radio signal emission and reception devices. Each device in this network allows one to extract the strength value of the emission/reception of a radio signal, supported by IEEE 802.11 by access to the Received Signal Strength Indicator (RSSI). These strength data allow for estimations of the radial distance (signal range) between the sending device and each receiving device (or vice versa). The respective computed radial distances allow for estimations of the location of a specific device in this network. Despite using an IEEE 802.11 network infrastructure for testing here, this range-based method for signal triangulation can be applied to any signal type (such as Wi-Fi, Bluetooth, and light and sound propagation).

2.1. Useful 2D geometric definitions

14. This subsection describes some important geometric definitions for understanding the proposed geometric models PPC and wPPC. These definitions were listed and organized in the previous work (Montanha et al., 2019). Such definitions are labeled as, for example, (d-9), which means the 9th definition, and its uses are thus referenced in the text. Other definitions and further information in this regard are provided by WCIPEG (Woburn Collegiate Institu, 2018) and Gibson (2004).

2.1.1. Point and line

A coordinate $P(x, y)$ define the point P in the Cartesian plane ($\mathbb{R}^2$). The line that passes through the points $P(x_1, y_1)$ and $Q(x_2, y_2)$, $P \neq Q$, is denoted as $\overleftrightarrow{PQ}$. The line segment $\overline{PQ}$ (with endpoints P and Q) is the portion of the line $\overleftrightarrow{PQ}$ between points P and Q.

(d-1) The Euclidean distance $D_{\overleftrightarrow{PQ}}$ between two points $P(x_1, y_1)$ and $Q(x_2, y_2)$ is given by

$$D_{\overline{PQ}} = \sqrt{(x_1 - x_2)^2 + (y_1 - y_2)^2}$$

(d-2) For constants A, B, and C (A and B not both zero), all points (x, y) satisfying the equation $Ax + By + C = 0$ define the implicit line equation in the Cartesian plane. For two points P(x_1, y_1) and Q(x_2, y_2), a particular line equation is obtained by

$$A = y_1 - y_2; B = x_2 - x_1; C = -Ax_1 - By_1$$

(d-3) Two particular lines $A_1x + B_1y + C_1 = 0$ and $A_2x + B_2y + C_2 = 0$ have an intercept at the point (x_+, y_+) if $d = A_1B_2 - A_2B_1 \neq 0$, given by

$$(x_+, y_+) = \left(\frac{B_1C_2 - B_2C_1}{d}, \frac{A_2C_1 - A_1 \quad - C_2}{d}\right)$$

If $A_1A_2 + B_1B_2 = 0$, the lines are perpendicular. If $A_1B_2 = A_2B_1$, the lines are parallel or coincident.

(d-4) The line equation $A_px + B_py + C_p = 0$ that passes through point P(x_p, y_p) and is perpendicular to the line $A_x + B_y + C = 0$ is defined as

$$A_p = -B; \quad B_p = A; \quad C_p = Ax_p - By_p.$$

2.1.2. Circle

In the Cartesian plane, the equation $(x\text{-}x_c)^2 + (y\text{-}y_c)^2 = r^2$ defines the implicit circle equation centered at the point $C(x_c, y_c)$ with radius r. Let E (x_e, y_e) be an external point to a circle. By using E, we can obtain two tangent lines, t_1 and t_2, to the circle (Fig. 1a), which pass through points P(x_1,y_1)* and Q(x_2,y_2)*, respectively. Points P and Q can be computed by applying the geometric concept of pole-polar definition.

(d-5) The distance $\delta_{\overline{PC},r}$ between a point $P(x_1, y_1)$ and a circle line centered at the point C(x_c, y_c) with radius r is given by

$$\delta_{\overline{PC},r} = |r - D_{\overline{PC}}|,$$

where $D_{\overline{PC}}$ is the Euclidean distance between the point P(x_1, y_1) and the point C(x_c, y_c) computed by definition (d-1).

2.1.3. Pole-polar geometry

A pole point and polar line are, respectively, a point and a line that have a unique reciprocal relationship with respect to a given conic section. If the point lies on the conic section, its polar line is the tangent line to the conic section at that point (Wyk and O'Rourke, 1995). If the pole point is external to the conic section, the polar line intercepts the conic section exactly at the points that allow passing tangent lines from this pole point (Fig. 1a). Our interest is to pass two tangent lines, t_1 and t_2, through a circle centered at point C(x_c, y_c) with radius r. Moreover, these lines must pass through a known external point E(x_e, y_e) (or pole point) to this circle (Fig. 1a). We need to locate the coordinates of the polar points P(x_1, y_1)* and Q(x_2, y_2)*, which define the polar line p and lie on the tangents lines t_1 and t_2. Additionally, we must find the equation of the polar line $p(A_x + B_y + C = 0)$.

(d-6) The general equation of a conic in the Cartesian coordinate system is given by

$$a_{xx}x^2 + 2a_{xy}xy + a_{yy}y^2 + 2b_xx + 2b_yy + w = 0.$$

We need the equation of the polar line $p(A_x + B_y + C = 0)$ that can be obtained by a known pole point E(x_e,y_e). The required coefficients of the polar line p are given by

$$A = a_{xx}x_e + a_{xy}y_e + b_x; B = a_{xy}x_e + a_{yy}y_e + b_y; \; C = b_xx_e + b_yy_e + w$$

In this work, the expected conic section is a circle. For the circle case, the following simplifications are helpful: $a_{xx} = 1$; $a_{xy} = 0$; $a_{yy} = 1$; $b_x = -x_c$; $b_y = -y_c$; $w = x_c^2 + y_c^2 - r^2$.

The next step consists in placing points P$(x_1, y_1)^*$ and Q$(x_2, y_2)^*$, which are obtained by computing the intersection between the polar line p and the circle line (Fig. 1a). To compute the intersection of a line, t : $Ax + By + C = 0$, with a circle, $(x - x_c)^2 + (y - y_c)^2 = r^2$, the following conditions must be considered using the parameter $d_{tc} = \frac{|Ax_c + By_c + C|}{\sqrt{A^2 + B^2}}$, which is the distance between the polar line t and the circle center point C(x_c,y_c):

- if $d_{tc} > r$, there is no intersection point;
- if $d_{tc} = r$, the line is tangent to the circle and has one intersection point;

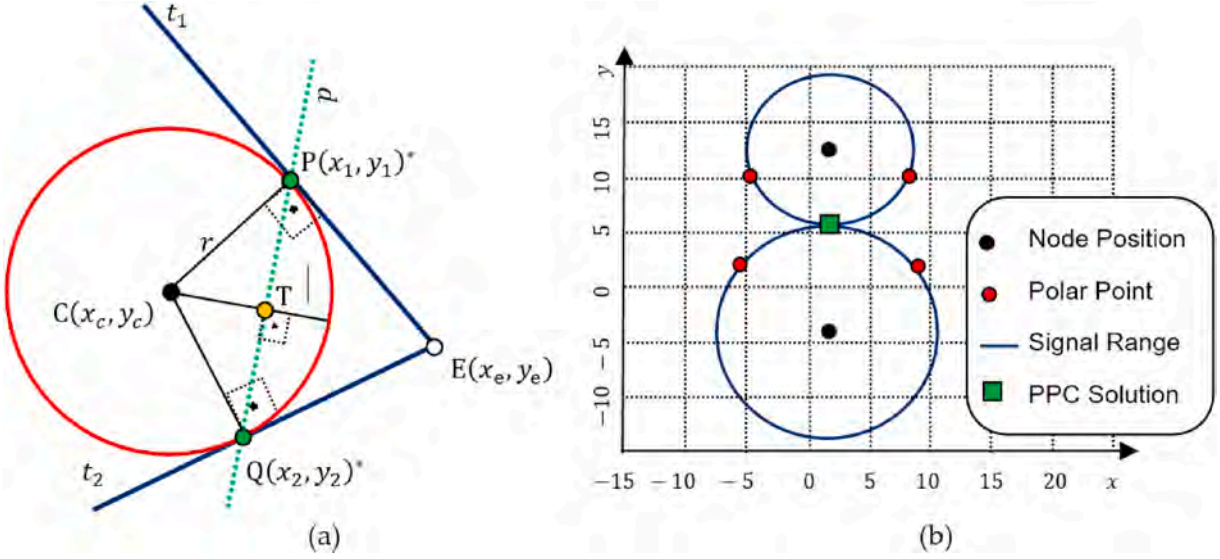

Fig. 1. (a) Possible tangential straight lines t_1 and t_2 for the circle line obtained by an external point E(x_e, y_e) (pole point) (Montanha et al., 2019). Polar line p and its geometric relationship with the tangent lines and a given conic section (a circle in the case of this work). (b) A location system composed by two nodes and one device. Computation of the polar points (red dots) using as pole points (black dots) the respective centers of the signal range (blue lines). The green faced square is the exact emitter location computed by the PPC method in this coordinate system.

○ if $d_{tc} < r$, the line is secant to the circle and has two intersection points.

The algebraic solution for this intersection is an equation of degree two. Another way to solve this intersection is to apply some geometric relationships, as follows. To find the intersections points $P(x_1, y_1)^*$ and $Q(x_2, y_2)^*$, which are the polar points, we first have to drop a perpendicular line (by (d-4)) from the center $C(x_c, y_c)$ of the circle to the line p. Let $T(x_t, y_t)$ (Fig. 1a, yellow dot) be the intersection point and $\overleftrightarrow{CT}$ be the line that passes through C and T (Fig. 1a).

The equation of line $p(Ax + By + C = 0)$ is known (by (d-6)). Thus, the equation of line $\overleftrightarrow{CT}$ is $\overleftrightarrow{CT}(-Bx + Ay + Ax_c - By_c)$. This way, the point $T(x_t, y_t)$ can be computed by intersection between p and $\overleftrightarrow{CT}$ lines (by (d-3)).

$D_{\overline{CT}}$ represents the Euclidean distance between points C and T; $D_{\overline{PT}}$ refers to the distance between points P and T; $D_{\overline{QT}}$ stands for the distance between points Q and T; $D_{\overline{CP}} = D_{\overline{CQ}} = r$ (by (d-1)).

The triangles ΔCPT and ΔCQT are right-angled, so we prove that

$$D_{\overline{CT}}{}^2 + D_{\overline{PT}}{}^2 = r^2$$

and

$$D_{\overline{CT}}{}^2 + D_{\overline{QT}}{}^2 = r^2.$$

(d-7) Therefore, $D_{\overline{QT}} = D_{\overline{PT}} = h = \sqrt{r^2 - D_{\overline{CT}}{}^2}$; now, if we translate the point T by h units in both directions along line p, the polar points P and Q (Fig. 1a) are determined as follows:

$$(x_1, y_1)^* = \left(x_t - \frac{Bh}{\sqrt{A^2 + B^2}}, y_t + \frac{Ah}{\sqrt{A^2 + B^2}}\right).$$

If $h \neq 0$, there is a second point of tangency given by

$$(x_2, y_2)^* = \left(x_t + \frac{Bh}{\sqrt{A^2 + B^2}}, y_t - \frac{Ah}{\sqrt{A^2 + B^2}}\right).$$

(d-8) The location estimation of a device, $E_{xy}(E_x, E_y)$, is based on a set S that contains n points, (x, y), which are collected in a defined Region Of Interest (ROI). This location is given by the centroid point among all points in S, by

$$E_x = \frac{\sum_{x \in S} x}{n}, E_y = \frac{\sum_{y \in S} y}{n}.$$

In this work, it is not necessary to define an ROI. All polar points are used for estimating a location point.

An arbitrary 2D coordinate Cartesian system used for positioning a location system composed by two nodes (receiver devices) is shown in Fig. 1b. This coordinate Cartesian system is arbitrary (no units are necessary). The black dots define the positions, previously defined, of the location network nodes. The blue circle lines represent the radial range of the signal, perceived at each node, emitted by a device that needs to be located by this network with two nodes. The red dots are the respective polar points, which were computed using the positions of the nodes (the centers of each circle) as pole points, applying the definition (d-7). By the definition (d-8) and the set S containing all (four in this case) the polar points computed, the location of the respective device (green-faced square) was estimated by the PPC method. The location solution provided in previous work uses the nomenclature $E_{xy}(E_x, E_y)$ (Montanha et al., 2019). This work uses the nomenclature $E^{P}_{xy}(E_x, E_y)$ to indicate that this solution is relative to the PPC method and $E^{W}_{xy}(E_x, E_y)$ for the wPPC solution.

2.2. The PPC method and Considerations

The PPC model is a method proposed to triangulate the position of a device emitting/receiving signals using specific points computed in an arbitrary coordinate system. These specific points, polar points, are computed with the aid of definitions of pole-polar geometry. Basically, pole-polar geometry relates the lines of a circle (or any other conical section) with center $C(x_c, y_c)$ and radius r with any point $E(x_e, y_e)$, arranged in a same Cartesian coordinate system. One of the questions that pole-polar geometry answers is: if a spot observer is over point E, what fraction of the circle with center C and radius r (Fig. 1a) can they see?

The PPC method explores the solution of this problem to perform triangulation and estimate a location of a specific device inserted in the environment covered by the coordinate system that supports the distribution of the triangulation network nodes. Through signals of some nature (e.g., sound or radio), the network nodes and the device interact (communication). These interactions allow for the extraction of data, such as angles and radial distances, in relation to the device's posture with the physical disposition of each node in the network (Fig. 2a).

PPC uses the radial distance r_k (radial range) indicated in each node k of the network to perform the triangulation. Fig. 2b illustrates the case in which Node 2 observes the radial range of Node 1, and Fig. 2c the case in which Node 2 observes the radial range of Node 1. These observations allow for the computation of the respective polar points that provide the "vision" constraint on each node over the radial range of the other node.

For a network consisting of m nodes, PPC requires that pairs of nodes be combined among all these nodes. The number p of possible node pairs is given by Equation (1). The number of polar points obtained when combining pairs of nodes is $n = 4p$ (each pair of the combination provides four polar points). If the location network has $m = 4$ nodes, there are $p = 6$ combinations of pairs of nodes and therefore $n = 24$ polar points. In terms of m, the computational cost of PPC is $O(m^2)$ in accordance with the cost to perform these combinations.

$$p = \binom{m}{2} = \frac{m!}{2(m-2)!} \quad (1)$$

2.2.1. The PPC method and the exact solution

The exact solution of any location system depends exclusively on the quality of the data acquired from the signals used in the interaction of the device to be located with the nodes of the location network. If the data are perfect, the solution must be accurate. In the case of methods based on the data of radial ranges of the nodes (lines of the circles), to obtain the exact solution, these radial ranges derived from all nodes of the network must intersect at a single point in the coordinate system.

PPC is based on the computation of the centroid among all polar points. In practice, the centroid is a geometric mean (see definition (d-8)). The greater the radius of a circle is, the more distant, among them, the polar points are. These great distances move the centroid to the circle neighborhood with the greatest radius, and, if there is no symmetry in the distribution of the network nodes, the PPC can lead the result to a location with a significant error (see Fig. 3).

When an exact solution exists, it can be given by a polar point. In this case, there is no need to compute the centroid. This exact solution is obtained with a sequential search on the set of polar points. If there is at least one polar point in that set that belongs to all lines of the circle at the same time, that point is the exact solution. This solution was addressed in previous work (Montanha et al., 2019), but it has not been formalized. The number of polar points that marks the exact solution depends on the number and geometric arrangement of the nodes in the plane of the coordinate system of the location network. For example, with three nodes (Fig. 3a), there are two polar points indicating the exact solution. With four nodes, there are eight (Fig. 3b). If using only two nodes, there is no polar point marking the solution, but in this case the PPC marks the exact solution (Fig. 1b). Even if there is an exact solution and the network has more than two nodes, there is a dependence on the

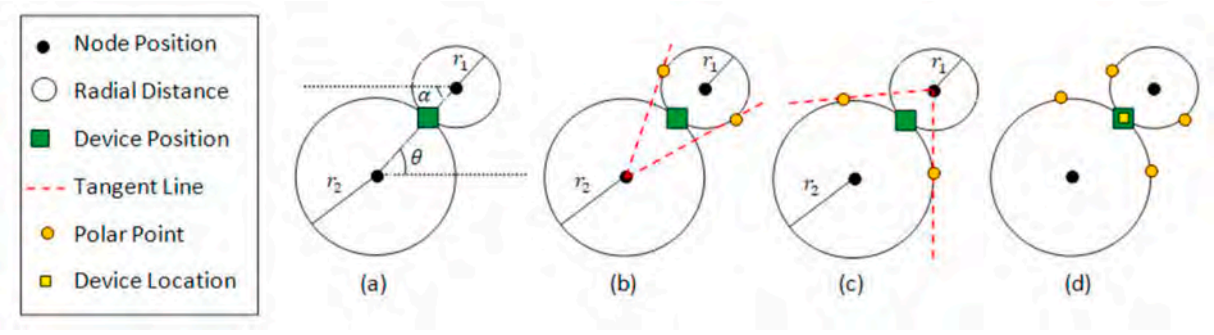

Fig. 2. Triangulation network with two nodes and a device to be located. (a) Possible data extracted from the signal interaction between the device and each node. (b) The Node 2 "view" limitation on the radial range of Node 1 fixed by the polar points. (c) The Node 1 "view" limitation on the radial range of Node 2 fixed by the polar points. (d) The centroid computed on the union of all polar points estimates the device location.

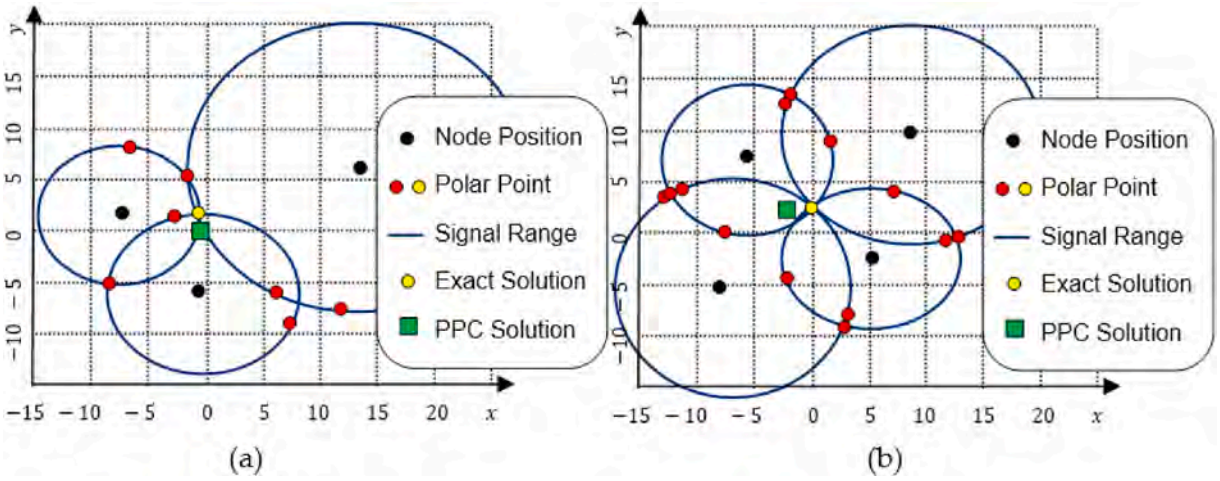

Fig. 3. Exact PPC solutions. Asymmetric distribution of nodes in the location network and the PPC solution shifted from accuracy (green faced square). In this case, the exact solution is given by the polar point highlighted in yellow. (a) Network with three nodes. (b) Network with four nodes.

geometric arrangement of the nodes for a polar point to mark that solution. Fig. 5c shows a case in which the solution is exact, but no polar point marks such a solution. Fig. 6 also illustrates this situation of an absence of a polar point indicating the exact solution. In the case illustrated by Fig. 5c, PPC finds the exact solution. In the case of Fig. 6, the PPC does not find an exact solution. When there is an exact solution, but there is no polar point marking or the PPC does not find such a solution, a precision value T capable of minimizing the error of the location estimation is needed.

In computational practice, two real numerical values computed by different paths are not always the same. Even if they are mathematically equal, computationally, they may be slightly different due to the performance of truncation and rounding operations. This means that there is a risk of applying definition (d-5) with the unique condition of obtaining zero in the result when searching for the exact solution marked by a polar point. It is most appropriate to establish a threshold value T that specifies an acceptable precision value to solve the problem of location. In this case, the polar point is considered an exact solution, if it exists, closer to all lines of the radial ranges of the nodes of the location system; at the same time, it is less than or equal to the pre-established T value (see Equation (2)).

Let $m > 2$ be the number of nodes in the location network. Let P_k be the set of all polar points that belong to the radial range of node k. Consider that all polar points are stored in a list (a function) S indexed by the value k, $S_k : k \rightarrow P_k$, and that k is an index identifying any node in the network, $k \in \{1, 2, \ldots, m\}$. The S_k operation accesses all the polar points stored in S that are on the line of the radial range of node k with center C_k and radius r_k. Let E^P_{xy} be an undefined point in the coordinate system. If in the set of polar points there is at least one point that is the exact solution, or with an acceptable precision, E^P_{xy} is associated with that point by Equation (2).

$$E^P_{xy} = \begin{cases} undefined, & \Delta^\star = \varnothing \\ \wp, \ (\Delta^\star \neq \varnothing) \bigwedge (\wp \in dom\ \Delta^\star) \bigwedge (\wp, \min(ran\ \Delta^\star)) \end{cases} \quad (2)$$

where $\Delta^\star = \cup(\{k \in \{1, 2, \ldots, m\} \bullet \overline{\Delta}_k\})$;

$$\overline{\Delta}_k = \left\{ P \in S_k \Big/ \left(\forall j \in \{1, 2, \ldots, m\} \Big/ (j \neq k) \bigwedge \left(\delta_{\overline{PC_j}, r_j} \leq T \right) \right) \bullet \left(P, \delta_{\overline{PC_j}, r_j} \right) \right\}$$

$\delta_{\overline{PC_j}, r_j}$ is the distance between point P and the radial range of node j centered at C_j with radius r_j (definition (d-5));

$\cup(\_)$ is the generalized union of a set of sets, e.g., if $s = \{\{1, 2\}, \{2, 4\}\} \Rightarrow \cup(s) = \{1, 2, 4\}$;

$dom(\_), ran(\_)$, and $min(\_)$ are, respectively, the domain and codomain (range) of a relationship and the minimum value of a set of real values.

Fig. 4 illustrates an example of how Equation (2) works. Consider the radial ranges r_1 and r_2 of two nodes, 1 and 2, centered at C_1 and C_2, the permissible precision value T, and the respective polar points P_1, P_2, P_3, and P_4, among which only P_2 and P_3 comply with the solution condition given by Equation (2).

For all cases where Equation (2) produces the value $\Delta^\star \neq \varnothing$, E^P_{xy} will store the value of the exact solution, or with acceptable precision T.

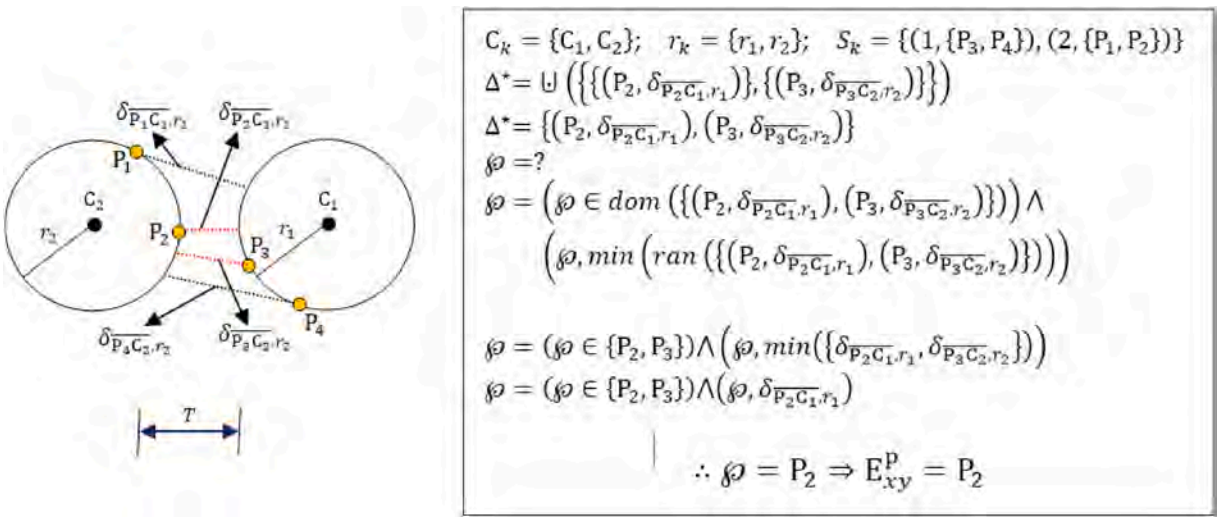

Fig. 4. Example illustrating how Equation (2) works.

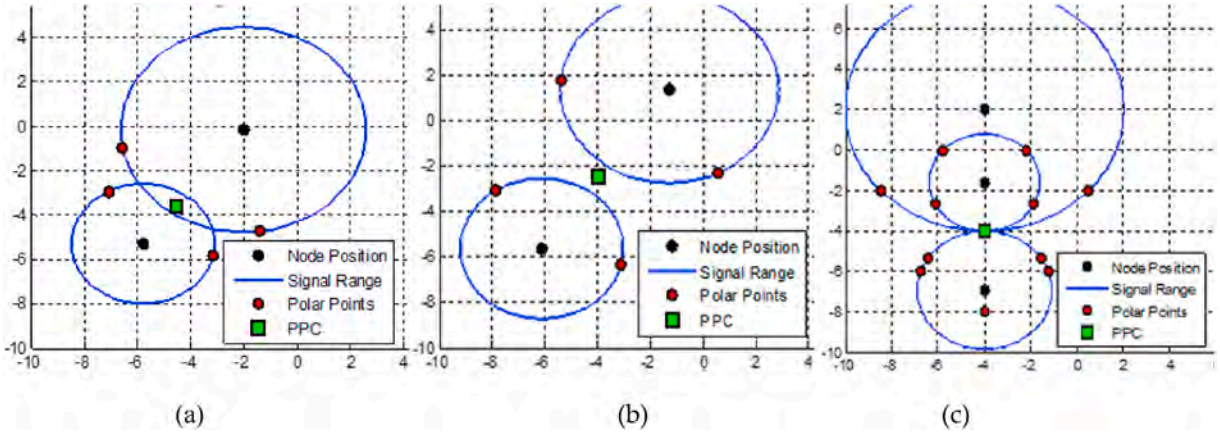

Fig. 5. Restricted solutions. (a) Two nodes with secant ranges. This can be solved algebraically (Montanha et al., 2019). (b) Two nodes without intersection of ranges. This can be solved by optimization (Luo et al., 2018). (c) Three vertical collinear nodes. This can be solved algebraically (Montanha et al., 2019) or by optimization (Luo et al., 2018).

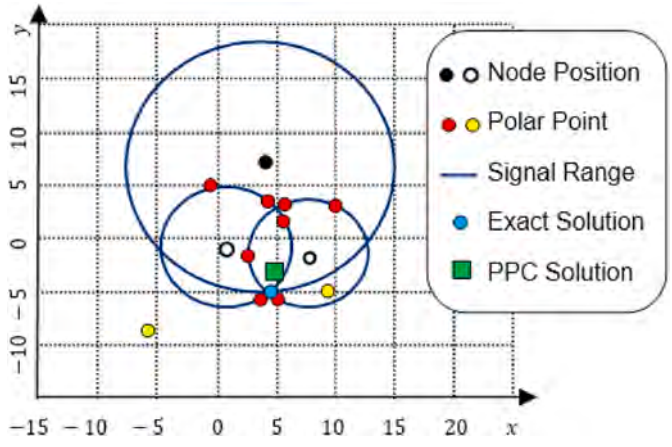

Fig. 6. Limitation of the PPC. The two nodes (white and black) are inserted into the radial range of the node with the greatest radial range. The polar points, yellow and black, are complex numbers.

When producing the value $\Delta^\star = \varnothing$, E_{xy}^{P} is undefined.

2.2.2. *The PPC method and restricted solutions*

Not all location methods can be applied to all location system configurations. Fig. 5 illustrates some of these cases. There is a dependence on the methods in relation to the number of nodes used in the location network and the geometric arrangement of these nodes in the coordinate system. All these cases of restricted solution are solved by the PPC method with good precision.

Fig. 1b shows a location network consisting of only two nodes. Methods that need to perform the linearization of the system of equations, such as LSm and WLSm, cannot solve the unknown (x, y) coordinates of the device's estimated location because, after linearizing the system with two equations, only one equation will be left to solve the two unknowns.

However, as shown in Fig. 1b, if the lines of the two circles touch each other (touch one point), or if they are secant (touch two points—Fig. 5a), there is a direct algebraic solution. Such a solution was addressed in the previous work (Montanha et al., 2019).

When the line of two circles does not intersect (Fig. 5b), the algebraic method also fails and, in this case, it is necessary to have a solution by optimization.

If the geometric arrangement of the network nodes is collinear,

parallel to one of the axes of the coordinate system (Fig. 5c), LSm, WLSm, and NRm cannot solve by eliminating all equations from the system of equations.

2.2.3. Limitations of the PPC method

The PPC method is based on obtaining polar points using a pole point that is outside the radial range of the network node (Figs. 1 and 2). However, pole-polar geometry does not preclude that the pole point does not belong to the region covered by the radial range of the node (Figs. 5c and 6). PPC combines all nodes in pairs and alternately uses the positions of these nodes as pole points to observe the radial range of the other nodes in the network. There may be situations of inclusion of one or more nodes in the radial range of other nodes. When this occurs, complex numbers are generated as polar points (Fig. 6).

When this problem occurs, two possibilities are recommended (Montanha et al., 2019): discard those points represented by complex numbers, or use only the real part of those numbers as a solution for the respective polar points.

The points highlighted in yellow and black in Fig. 6 correspond to the real part of the generated complex numbers. Note that these points are outside the context of the radial ranges of any node (the polar points must be on lines of circles). The result presented (the green square) was computed without excluding these points represented by complex numbers. The real part of these complex numbers was used. Even if these points are very much out of context, the solution obtained is close to the exact solution. However, the best alternative to solving this problem is to apply the exact solution search (Section 2.1.1) with a predefinition of an acceptable precision value T. Note that, in Fig. 6, there are two polar points near the exact solution and the search for the exact solution chooses one of these points as a solution to estimate the location.

2.2.4. The PPC algorithm

The proposed PPC method in the previous work (Montanha et al., 2019) is applicable to the location network with $m \geq 2$ nodes. The estimation of the location of a device $E^{P}_{xy}(E_x, E_y)$ is based on elements of pole-polar geometry.

Polar-Points Centroid Model (PPC).

Data Input

$m \geq 2$ is the number of nodes arranged in the location network.
$C_k(x_k, y_k)$, $k = 1, 2, \ldots, m$ is the planar position of each node (geometric arrangement).r_k, $k = 1, 2, \ldots, m$ Is the radial signal range of each node.
T is the specification of the minimum precision value acceptable.

Procedure

1: for each node $k = 1, 2, 3, \ldots, m$
2: $S \leftarrow \{(1, \varnothing), (2, \varnothing), \ldots, (m, \varnothing)\}$;
3: $\forall j : 1, 2, \ldots, m/k \neq j$, by (d – 6) and (d – 7), for each node position C_k, used as pole points, compute polar points $P_{kj}(x_{pkj}, y_{pkj})$ and $Q_{kj}(x_{qkj}, y_{qkj})$ given by the combination of jth and kth, nodes pair with the respective centers at positions C_k and C_j and signals radial range r_k and r_j. join the points P_{kj} and Q_{kj} in $S_j \leftarrow S_j \cup \{P_{kj}, Q_{kj}\}$;
4: end for 5: compute $\Delta^{\star}$ (defined in the description of expression (2));
6: if $\Delta^{\star} = \varnothing$ then //there is not exact or acceptable solution.
7: compute E^{P}_{xy} using the definition (d-8); //the centroid among the polar points is the PPC solution.
8: *flag*←FALSE;
9: else //there is exact or acceptable solution. A polar point is the PPC solution.
10: compute E^{p}_{xy} using the expression (2);
11: *flag*←TRUE;
12: end if

Information Output

Device location estimation $E^{P}_{xy}(E_x, E_y)$. S set of polar points indexed by nodes.
flag.

The PPC algorithmic proposed in the previous work (Montanha et al., 2019) use as input data the coordinates of each node, $C_k(x_k, y_k)$, $k = 1, 2, \ldots, m$, positioned on a coordinate system previously defined and the respective radial signals ranges r_k.

Formally, the presented work, which adds to the initial algorithm, suggested that the PPC can find the exact solution, when possible, or can estimate locations based on a criterion of minimum desired precision T. We then insert this innovation in the original algorithm. This new PPC requires a specification for T that acts as input data and is used to establish the criterion for achieving location estimation responses with acceptable precision. The gray typed text lines are instructions that help the original PPC algorithm to obtain the exact solution given by Equation (2) and to organize the data for the wPPC algorithm. The PPC algorithm returns E^{P}_{xy}, a point solution given by a polar point or by the centroid of the polar point set.

3. The proposed weighted Pole-Polar Centroid method (wPPC)

A new method, called the wPPC method, is proposed to be applicable to $m \geq 2$ nodes that integrate a location network. By arranging these nodes in a known coordinate system, a system for estimating device locations based on data from sent/received signals among these nodes and devices is defined.

wPPC is a complement to PPC. Its use is recommended when the signal data are compromised. In uncontrolled environments, receiving high quality data is extremely difficult. In this way, this work does not consider this eventual possibility as a solution. Our intention is to present new methods applied to signal triangulation problems and to analyze their behavior facing the inherent errors in data signals. Regarding the problem of localization in wireless sensor networks, several alternative approaches and concerns have been presented about data signal behavior (Wang and Li, 2009; Sahoo and Hwang, 2011; PAL, 2010). In order to achieve better results, pre-processed data were used to process a set of partial results that were analyzed to determine between them the more suitable solution (Schneider et al., 2016). As can be seen, acquiring accurate data signals is an arduous task. Schneider et al. (2016) and Lam et al. (2016) proposed methods for sampling data signal acquisition and discussed uncertainty and signal location. In addition, the environment is not predictable with multipath, fading, interference, and shading effects (Ilyas and Mahgoub, 2005).

There is a consensus that signal data with greater radial range are responsible for propagating more significant errors in estimating the location of a device. Such observation is due to the fact that the greater the signal radial range, the greater distance separates the node from the device. Thus, the signal has to travel longer and suffers greater attenuation by the elements of the environment (e.g. atmosphere and obstacles).

These elements interact and degrade the signal by the action of several mechanisms, such as scattering, reflection, absorption, multipath, and the co-presence of other signal sources.

In this context, if there is no exact solution for the position of a device caused by errors in the signal data, data with errors are assumed, and a coordinate that minimizes the location error is estimated. Assuming that it is possible that radial ranges with a larger radius contribute the largest portion of the error in estimating the location of a device in a location system, an alternative to minimize the error of this estimation is to decrease the influence of the largest radial ranges when computing the coordinate location. A second alternative, through error analysis, is to eliminate these greater ranges of location computation, which is possible if there is a redundancy of nodes in the location network. Let us consider Equation (3):

$$E^{W}_{xy} = \frac{\sum_{k=1}^{m}\left(w_k \sum_{j=1}^{n} S_{k,j}\right)}{n\sum_{k=1}^{m} W_k} \tag{3}$$

where: $n = 2(m - 1)$; the pole point r_k places two polar points on each radial range of the nodes, except on the line of its own range;

$w_k = \frac{1}{r_k}$, for $k = 1, 2, \ldots, m$;

$S_k : k \rightarrow \mathrm{P}_k$ k is an index identifying any node in the network, and $k \in \{1, 2, \ldots, m\}$ is the set of all polar points that are over the radial range of node k;
S_{kj}, $j = 1, 2, \ldots, n$ is the jth polar point that belongs to the range of node k.

Equation (3) can be written in matrix form:

$$E_{xy}^{\mathrm{W}} = \frac{\mathrm{w}\Pi}{n\mathrm{O}\mathrm{w}^t} \tag{4}$$

$$\text{where} \begin{cases} \mathrm{w} = \begin{bmatrix} \frac{1}{r_1} & \frac{1}{r_2} & \cdots & \frac{1}{r_m} \end{bmatrix}_{1\times m} \text{ and } \Pi = \begin{bmatrix} \sum_{j=1}^{n} S_{1,j} \\ \sum_{j=1}^{n} S_{2,j} \\ \vdots \\ \sum_{j=1}^{n} S_{m,j} \end{bmatrix}_{m\times 1} \\ \mathrm{O} = \begin{bmatrix} 1 & 1 & \cdots & 1 \end{bmatrix}_{1\times m} \end{cases}.$$

The wPPC method, described by Equation (3) or (4), uses the alternative that minimizes the error of the estimated location by decreasing the influence of the largest radial ranges in computing this location. Such a decrease in influence is made by reducing the values of the polar points that are over the range of a given node by a weight value equal to the inverse of the range (radius) of that same node. The greater the range is, the more drastic this reduction is.

Weighted Polar-Points Centroid Model (wPPC)

Data Input

$m \geq 2$ is the number of nodes arranged in the location network.
$\mathrm{C}_k(x_k, y_k)$, $k = 1, 2, \ldots, m$, is the planar position of each node (geometric arrangement).
r_k, $k = 1, 2, \ldots, m$, is the radial signal range of each node.
T is the specification of the minimum acceptable precision value.

Procedure

1: $[\mathrm{E}_{xy}^{\mathrm{P}}, S, flag] = \mathrm{PPC}(m, \mathrm{C}, r, T)$; **call** PPC and **return**: E_{xy}^{P}, location by PPC; S, set of polar points by node and a *flag* indicating whether an exact, or acceptable, solution was found by PPC or not.
2: **if** not *flag* **then** //PPC no found satisfactory solution. Do not have polar point that solves the location.
3: **if** $\mathrm{E}_{xy}^{\mathrm{P}}$ is not solution **then** //verify, by (2), if PPC solution $\mathrm{E}_{xy}^{\mathrm{P}}$ is not satisfactory.
5 4: **compute** $\mathrm{E}_{xy}^{\mathrm{W}}$ by Equation (3) or (4); //solve the location using wPPC.
5: **else**
6: $\mathrm{E}_{xy}^{\mathrm{W}} = \mathrm{E}_{xy}^{\mathrm{P}}$; //PPC solves location. The centroid among the polar points is the solution.
7: **end if**
8: **else**
9: $\mathrm{E}_{xy}^{\mathrm{W}} = \mathrm{E}_{xy}^{\mathrm{P}}$; //PPC found satisfa ctory solution. One polar point solves the location.
10: **end if**

Information Output

Device location estimation $\mathrm{E}_{xy}^{\mathrm{W}}(E_x, E_y)$.

19 The wPPC algorithm uses the PPC to compute and to organize the polar point data. wPPC and PPC require the same input data: the coordinates of each node, $\mathbf{C}_k(x_k, y_k)$, $k = 1, 2, \ldots, m$, the respective radial ranges $\mathbf{r_k}$, the specification of the minimum precision value T acceptable, and the number of nodes $\mathbf{m} \geq 2$ arranged in the location network to return the location estimation $\mathbf{E}_{xy}^{\mathbf{W}}$.

4. Experimental cases and results

To perform the experimental cases, the present work uses the same dataset used in the previous work (Montanha et al., 2019). It is detailed in Appendix A.

Using the IEEE 802.11 Network Infrastructures, we define a location system composed of a local coordinate system, a set of nodes (Access Points – AP Tp-Link Wireless N 300 Mbps TL-WR849 N) arranged on the coordinate system, thus defining the network of location nodes. Such nodes emit radio signals with a 2.4 GHz frequency.

The location system developed in the previous work used five nodes, which were geometrically distributed (location network) in a region of space (coordinate system) (see Table A1). The device to be located was positioned at different coordinates (see Table A3), in that region (12 cases) and the respective radial distances (see Table A3) between that device and each node in the network was estimated using Equation (5) based on the signal strength measured by the device in each experimental case (see Table A2).

A signal receiving device (a commercial cell phone with the Android operational system) was used to acquire the signals emitted by the nodes of the network. The receiving device, the cell phone, has the ability to identify the source of the signal (the device knows that a given signal was emitted by a specific node—BSSID) and to measure the reception strength ρ_k (see Table A2), in dBm, of each of these signals (RSSI).

Using this signal strength data emitted by the nodes, the device can estimate the radial distances (signal ranges) r_k, $k = 1, 2, \ldots, m$ (see Table A3). This is from each node k of the network in Equation (5). Fig. 7 shows the preprocessed data generated by the 10th experiment (see Table A3).

$$r_k = 10^{\frac{\rho_0^k - \rho_k}{10\mathscr{L}_k}} \tag{5}$$

where

ρ_k is the signal strength value (dBm) emitted by the kth node and measured by the receiver device placed on a specific position on the coordinate system;

ρ_0^k is the signal strength value (dBm) at some reference distance d_0 (the calibration of the device with the kth node). The authors of (Montanha et al., 2019) used $d_0 = 1\mathrm{m}$ for all nodes;

$\mathscr{L}_k$ is an empirical value that defines the attenuation factor of the signal (path-loss parameter) emitted by the kth node. The authors of (Montanha et al., 2019) used the value $\mathscr{L}_k = 2.2$ for all nodes.

4.1. Results

This section presents the results comparing PPC and wPPC. The experimental cases used in this work are the same as those used in the previous one (Montanha et al., 2019), which provided 12 study cases. In

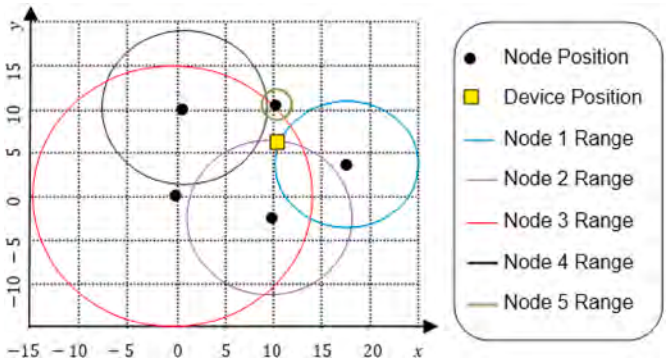

Fig. 7. The 10th experimental case performed in the previous work (Montanha et al., 2019). The location system consisting of a location network with five nodes and the respective coordinate system is defined in Table A1. The signal strength data for each node measured on the device to be located are in Table A2 (10th row), and the actual position of this device and the respective radial ranges of each node are in Table A3 (10th row).

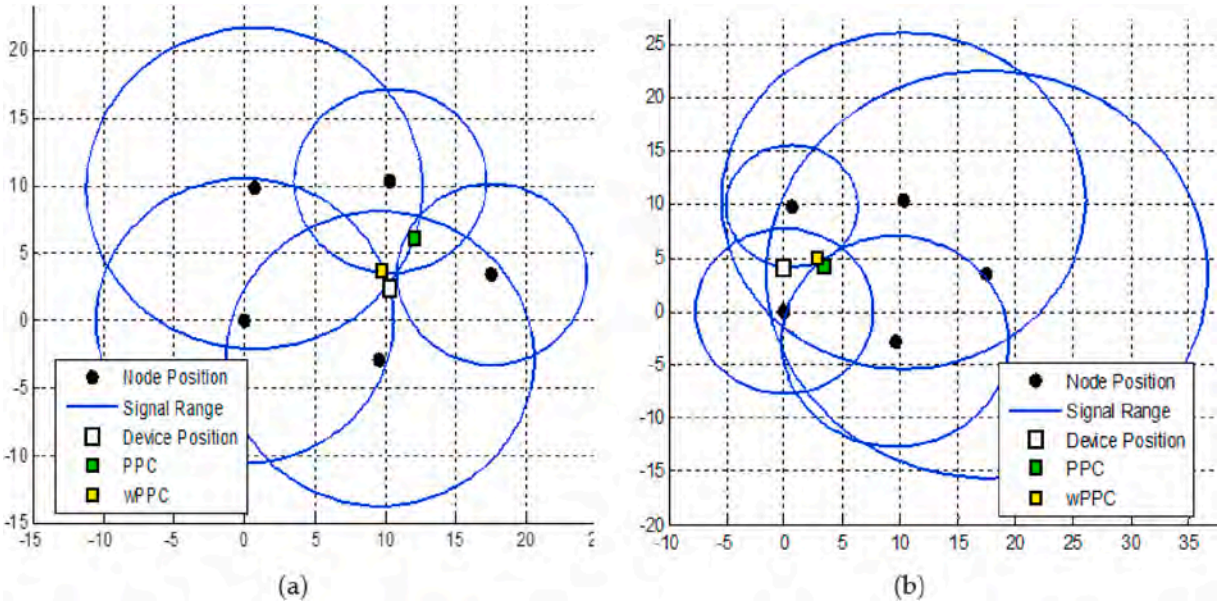

Fig. 8. PPC vs. wPPC. Acquired data with high accuracy. a) (X-12). b) (X-2).

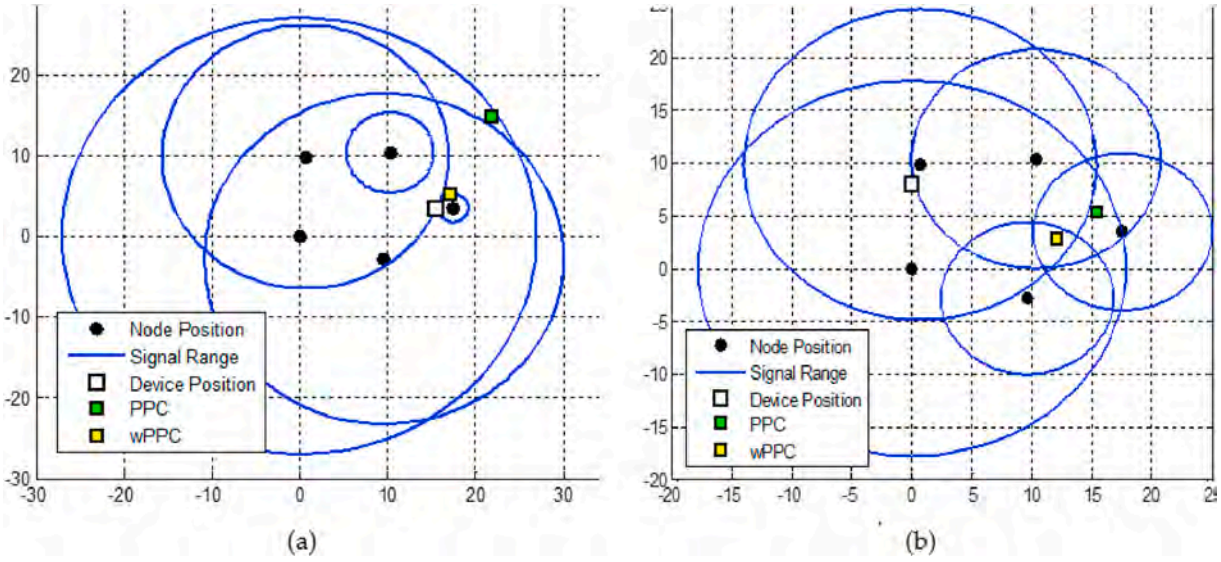

Fig. 9. PPC vs. wPPC. Acquired data with significant errors. a) (X-5). b) (X-4).

this section, four cases are presented. The other eight cases are described in Appendix B. The captions of Figs. 8 and 9, used to show the results, also reference the index of experimental data provided in the previous work (Montanha et al., 2019) and recorded in Table A3. For example, (X-7) refers to the data from the 7th experimental case that are found in Row 7 of Table A3.

Fig. 8a and b shows how PPC and wPPC work when operating on high-quality data. Fig. 9a and b shows how PPC and wPPC work when operating on low-quality data. In both cases, wPPC produced location estimation results more accurately than PPC.

4.2. Results analysis

Figs. 8 and 9 and all those presented in Appendix B show the 12 experimental cases, with actual data, used in the previous work (Montanha et al., 2019). It can be seen in these figures that the wPPC method is able to compute these data (with errors) more accurately than the PPC. In all these cases, there are errors in the acquired signal data.

As we mentioned before, the previous work (Montanha et al., 2019) proposed five variations of geometric methods (PPC, Polar-Point Centroid, CHC, Convex Hull Centroid, PLI, Polar Line Intersection Centroid, TLI, Tangent Line Intersection Centroid, and MAI, Minimal Angle Tangent Line Intersection Centroid) and compares the results achieved by the methods that we developed with the results produced by traditional methods (NRm, the Newton-Rapson method, LSm, the Least Squares method, and WLSm, the Weighted Least Squares method). Extensive error evaluation was performed on the actual data acquired in the experiment carried out. In order to analyze the results produced by the methods previously proposed, statistical metrics were applied to compare the results produced by the new proposed methods with the results produced by other methods. The same data and the same structure generated in the previous work to analyze the results are used in this case (Tables 1 and 2). The only difference is the inclusion of the results produced by the wPPC method in this analysis.

This analysis performed in the previous work considers three datasets of errors: (1) the error in distance measurement (the Euclidean

Table 1
Magnitude in meters of errors in the experimental cases.

	Minimum Error			Maximum Error			Mean Error		
	x-axis	*y*-axis	distance	*x*-axis	*y*-axis	distance	*x*-axis	*y*-axis	distance
wPPC	0.4	0.2	0.6	12.0	5.2	13.0	2.6	2.0	3.4
PPC[a]	0.4	0.2	2.7	15.5	12.5	15.7	4.5	4.4	6.9
CHC[a]	0.1	0.1	0.6	11.9	6.0	12.8	2.5	2.4	3.7
PLI[a]	0.1	0.1	0.7	12.8	15.9	16.3	2.4	3.8	5.0
MAI[a]	1.6	0.3	1.7	7.9	5.3	8.9	4.2	1.5	4.7
TLI[a]	2.3	0.3	2.3	8.3	3.9	9.2	4.1	1.3	4.4
NRm[a]	0.1	1.1	1.3	14.7	12.2	15.2	2.8	5.1	6.5
LSm[a]	0.3	1.2	1.8	14.1	22.5	23.7	3.6	6.4	7.9
WLSm[a]	0.1	0.7	1.3	13.6	15.3	17.7	3.5	4.9	6.5

[a] Available in (Montanha et al., 2019).

distance between the estimated device location $E_{xy}(E_x, E_y)$, computed for each method, and the actual device position $P_n(x_n, y_n)$ (see Table A3)), (2) the absolute error along the *x*-axis given by $|E_x - x_n|$, and 3) the absolute error along the *y*-axis given by $|E_y - y_n|$. The present work uses this same strategy to analyze the results of the wPPC and compares them with results obtained previously (Montanha et al., 2019).

The analysis of the errors considers four metrics applied to the three datasets of errors, minimum, maximum, mean, and standard deviation (Tables 1 and 2), and a fifth metric for analyzing global errors called the Effective Variability of the Errors (Table 2).

Table 1 presents an evaluation of the error values considering all experiments for each geometric model and numerical method. These values explain that some geometric models produce results with errors equivalent to those produced by numerical methods. Errors committed by PPC are equivalent to those committed by numerical methods (WLSm, NRm, and LSm). We can observe that errors may be larger or smaller depending on the quality of the acquired data, but in the general context, geometric models present better results than numerical methods.

The minimum error values presented in Table 1 create a hypothetical case of the lowest possible error in the evaluated dataset. In other words, depending on the available data, this operation sets up a case in which the data are accurate. As can be seen, even considering this hypothetical case that includes the most adequate data values, traditional methods (NRm, LSm, and WLSm) and geometric methods (MAI and TLI) propagate more significant errors when the data are of high quality. wPPC, among these minimum errors, has an average of 0.4. The CHC and PLI average 0.3. That is, when the data are good, wPPC produces a response as accurate as CHC and PLI.

Similarly, the maximum error values presented in Table 1 create the case for the greatest possible error in the evaluated dataset. For this case, traditional methods produce error averages between ~13 and ~20. Among geometries, PPC and PLI average ~15, and wPPC and CHC average ~10. MAI and TLI average ~8.

In the case of moderate errors, contemplating the occurrence of the most expected situation in the real world, wPPC has the lowest average error among all other methods.

With these analyses, Table 1 shows that, when there is high accuracy in the data, wPPC produces results with acceptable precision. When the data are bad or have moderate errors, the wPPC response is more accurate than other methods.

When considering the results of all experimental cases, Table 2 shows the variability of the errors committed (for each evaluating metric) by the methods in function of the errors in the data.

The Effective Variability of the Errors (Table 2) allows one to analyze how sensitive a method is to variation in data quality. In other words, this value is a metric that defines how well a method can approach an exact solution when it operates on data with errors. The lower this value is, the less sensitive the method is to errors in data; the method can therefore produce more accurate results. A simple analysis of the data in Table 2 shows that the proposed geometric models, compared with the traditional WLSm, NRm, and LSm methods, are more robust when they operate on data with errors. Among the geometric methods, the TLI, MAI, and wPPC have a greater capacity to process data with errors.

Table 2
Standard deviation of the errors.

Methods	Standard Deviation of the Errors			Effective Variability of the Errors
	x-axis	*y*-axis	distance	
wPPC	3.2	1.5	3.3	2.7
PPC[a]	4.1	3.8	4.5	4.1
CHC[a]	3.1	2.1	3.4	2.9
PLI[a]	3.3	4.1	4.9	4.1
MAI[a]	2.5	1.6	2.6	2.2
TLI[a]	2.3	1.0	2.3	1.9
NRm[a]	4.0	4.0	4.9	4.3
LSm[a]	4.3	6.7	7.4	6.1
WLSm[a]	4.2	4.3	5.5	4.7

[a] Available in (Montanha et al., 2019).

5. Conclusion

This work proposed the wPPC method as an extension of the PPC method, without increasing the computational cost $O(m^2)$ and without increasing the minimum number of nodes ($m \geq 2$) in the composition of the location network.

The ability of the PPC method to produce an exact solution has been formalized in Section 2.1.1. The results produced by wPPC are more accurate when processing data with errors (significant or not). This work helps to cope with the problem of applying 2D point location in a geometric relationship by reducing the number of arithmetic operations needed by the current conventional methods in use and the inherent error propagation in the acquired data. Therefore, this method can benefit wireless interaction among mobile phones for proximity contact tracing by improving the estimation accuracy of signal locations. The computational cost $O(m^2)$ of the geometric methods contrasts significantly with the cost $O(m^3)$ of the numerical and optimization methods. This fact allows for the development of localization applications for devices (such as cell phones) that have a low processing capacity. Such an application can run in the background and process signal data (Wi-Fi, Bluetooth, ultrasound, etc.) for location estimation. Each device can have the capacity to compute the locations of other devices in its vicinity, in either outdoor or indoor public areas (street, parks, supermarkets, public transport, etc.), offering support for the measuring and tracing of proximity relative to another device. The proposed wPPC method has the following limitations: (1) it is a 2D solution, and (2) it requires that the device be located inside the coverage area of the node network. Future work will include a 3D solution. When the device to be located is outside the region covered by the location network nodes, complex numbers are generated in the coordinates of the polar points. For this reason, in order to apply geometric methods, there is a need for

the device to be surrounded by the nodes of the location network. We should investigate, in future work, a better interpretation of the meaning of polar point coordinates given by complex numbers in the context of signal location using geometric methods.

Author contributions

A.M. Conceptualization, Data Curation, Formal Analysis, Investigation, Methodology, Project Administration, Resources, Software, Visualization, Writing – original draft. A.P. Conceptualization, Formal Analysis, Investigation, Methodology, Supervision, Validation, Writing – original draft. M.R Formal Analysis, Investigation, Methodology, Supervision, Validation, Writing – review & editing.

Declaration of competing interest

The authors declare that they have no known competing financial interests or personal relationships that could have appeared to influence the work reported in this paper.

Acknowledgments

Special thanks to the Universidad de Sevilla (Spain) and the State University of Maringá (Brazil).

Appendix A. Experimental Data

Tables A1, A2, and A3 present the data of the 12 experimental cases provided in (Montanha et al., 2019). Table A1 presents the coordinates of each node, in an arbitrary coordinate system (as shown in Fig. 7 and in the following). Each of these figures, including all figures presented in Appendix B, uses this same coordinate system and the same network nodes. Table 1 also presents the calibration parameter of the signal reference for each node (at 1 m in dBm). Table A2 presents the signal strength data acquired by each node in these 12 experimental cases. Table A3 presents the preprocessed data for generating the radial range of each node for each experimental case and presents the actual coordinates of the device that generated these signal data.

Table A1
Node positions and their respective calibration parameters.

Node k	Node Position (in meters) $C_k(x_k, y_k)$		Signal Reference (at 1 m in dBm) ρ_0^k
	x_k	y_k	
1	17.53	3.45	42.83
2	9.60	−2.84	38.17
3	0.00	0.00	43.50
4	0.68	9.81	42.33
5	10.33	10.34	44.67

Table A2
Measured signal strength from each node in each experimental case.

Experimental Case n	Measured Signal Strength ρ_k (in dBm)node k				
	1	2	3	4	5
1	70	63	51	55	68
2	71	60	63	59	71
3	70	56	60	66	69
4	62	57	71	68	67
5	48	67	75	69	60
6	52	60	71	68	68
7	60	59	74	67	68
8	63	56	70	62	62
9	65	71	71	66	49
10	62	59	69	63	50
11	62	67	66	62	59
12	61	61	66	66	63

Table A3
Experimental cases and the respective actual device positions and the signal range measured in each node.

Experimental Case n	Actual Device Position (in meters) $P_n(x_n, y_n)$		Radial Ranges r_k (in meters) node k				
	x_n	y_n	1	2	3	4	5
1	0.00	2.00	17.2	13.5	2.2	3.8	11.5
2	0.00	4.00	19.1	9.8	7.7	5.7	15.7
3	0.00	6.00	17.2	6.5	5.6	11.9	12.8
4	0.00	8.00	7.4	7.2	17.8	14.7	10.4
5	15.53	3.41	1.7	20.4	27.0	16.3	5.0
6	13.53	3.41	12.6	9.8	17.8	14.7	11.5

(continued on next page)

Table A3 (*continued*)

Experimental Case n	Actual Device Position (in meters) $P_n(x_n, y_n)$		Radial Ranges r_k (in meters) node k				
	x_n	y_n	1	2	3	4	5
7	11.53	3.41	6.0	8.9	24.3	13.2	11.5
8	9.53	3.41	8.3	6.5	16.0	7.8	6.1
9	10.33	8.34	10.2	31.1	17.8	11.9	1.6
10	10.33	6.34	7.4	8.9	14.4	8.7	1.7
11	10.33	4.34	7.4	20.4	10.5	7.8	4.5
12	10.33	2.34	6.7	10.9	10.5	11.9	6.8

Appendix B

26. Figs. 8 and 9 show the final results of the four experiments (2, 4, 5, and 12) shown in Table A3. The others eight results are presented by the figures in Appendix B. All these figures are referenced, in the respective caption, with a code (X – #). The nomenclature of these codes is as follows: X indicates that experimental data were used, and # is a number that indicates the experimental data, registered in Tables A2 and A3, corresponding to the result shown in the respective figure.

References

Acharya, R., 2014. Understanding Satellite Navigation, ISBN 9780128001899.

Ahvar, E., Daneshgar-Moghaddam, N., Ortiz, A.M., MyoungLeed, G., Crespi, N., December 2016. On analyzing user location discovery methods in smart homes: a taxonomy and survey. J. Netw. Comput. Appl. 76, 75–86. https://doi.org/10.1016/j.jnca.2016.09.012.

Apple and Google partner on COVID-19 contact tracing technology (accessed on May 11, 2020). https://www.apple.com/newsroom/2020/04/apple-and-google-partner-on-covid-19-contact-tracing-technology/.

Cho, H., Ippolito, D., Yu, Y.W., 2020. Contact Tracing Mobile Apps for COVID-19: Privacy Considerations and Related Trade-Offs.

eHealth Network Mobile Applications to Support Contact Tracing in the EU's Fight against COVID-19, 2020, p. 44.

Eubank, S., Eckstrand, I., Lewis, B., Venkatramanan, S., Marathe, M., Barrett, C.L., 2020. Commentary on Ferguson, et al., "Impact of Non-pharmaceutical Interventions (NPIs) to Reduce COVID-19 Mortality and Healthcare Demand. Bull. Math. Biol. https://doi.org/10.1007/s11538-020-00726-x.

Gandotra, P., Jhaa, R.K., Jain, S., January 2017. A survey on device-to-device (D2D) communication: architecture and security issues. J. Netw. Comput. Appl. 7815, 9–29. https://doi.org/10.1016/j.jnca.2016.11.002.

Gibson, C.G., 2004. Elementary Euclidean Geometry.

Hassan, N.U., Naeem, A., Pasha, M.A., Jadoon, T., Yuen, C., 2015. Indoor positioning using visible LED lights: a survey. ACM Comput. Surv. 48 (2), 1–32. https://doi.org/10.1145/2835376.

Ilyas, M., Mahgoub, I. (Eds.), 2005. 13. Beutel, J. Handbook of Sensors Networks: Compact Wireless and Wired Sensing Systems. CRC Press.

Klonowska, K., Analyst, A., Advisor, S., 2020. The COVID-19 pandemic : two waves of technological responses in the European Union Klaudia Klonowska. Assistant Analyst 1–15.

Lam, L.D.M., Tang, A., Grundy, J., 2016. Heuristics-based indoor positioning systems: a systematic literature review. J. Locat. Based Serv. 10, 178–211.

Lau, B.P.L., Marakkalage, S.H., Zhou, Y., Hassan, N.U., Yuen, C., Zhang, M., Tan, U.X., 2019. A survey of data fusion in smart city applications. Inf. Fusion 52, 357–374. https://doi.org/10.1016/j.inffus.2019.05.004.

Luo, M., Chen, X., Cao, S., Zhang, X., 2018. Two new shrinking-circle methods for source localization based on TDoA measurements. Sensors. https://doi.org/10.3390/s18041274.

Montanha, A., Polidorio, A.M., Dominguez-Mayo, F.J., Escalona, M.J., 2019. 2d triangulation of signals source by pole-polar geometric models. Sensors. https://doi.org/10.3390/s19051020.

Ng, Y., Li, Z., Chua, Y.X., Chaw, W.L., Zhao, Z., Er, B., Pung, R., Chiew, C.J., Lye, D.C., Heng, D., et al., 2020. Evaluation of the effectiveness of surveillance and containment measures for the first 100 patients with COVID-19 in Singapore - january 2-February 29, 2020. Morb. Mortal. Wkly. Rep. https://doi.org/10.15585/MMWR.MM6911E1.

WHO Considerations in the investigation of cases and clusters of COVID-19. Who2020 1–4, 2020.

PEPP-PT Pan-European Privacy-Preserving Proximity Tracing.

Pal, A., 2010. Localization algorithms in wireless sensor networks: current approaches and future challenges. Netw. Protoc. Algorithm. 2, 45–73. https://doi.org/10.5296/npa.v2i1.279.

Pedhadiya, M.K., Jha, R.K., Bhatt, H.G., March 2019. Device to device communication: a survey. J. Netw. Comput. Appl. 1291, 71–89. https://doi.org/10.1016/j.jnca.2018.10.012.

Rapid Audit of Contact Tracing for Covid-19 in New Zealand, 2020.

S, F., Atkinson, K.E., 1990. An introduction to numerical analysis. Math. Comput. https://doi.org/10.2307/2008519.

Sahoo, P.K., Hwang, I.S., 2011. Collaborative localization algorithms forwireless sensor networks with reduced localization error. Sensors 11, 9989–10009. https://doi.org/10.3390/s111009989.

Schneider, C., Zutz, S., Rehrl, K., Brunauer, R., Gröchenig, S., 2016. Evaluating GPS sampling rates for pedestrian assistant systems. J. Locat. Based Serv. 10, 212–239. https://doi.org/10.1080/17489725.2016.1259509.

Tarrío, P., Bernardos, A.M., Casar, J.R., 2011. Weighted least squares techniques for improved received signal strength based localization. Sensors. https://doi.org/10.3390/s110908569.

Wang, Y., Li, L., 2009. Localization in wireless sensor networks. RFID Sens. Networks Archit. Protoc. Secur. Integr. 2009, 275–296. https://doi.org/10.1201/9780429286841-13.

Wang, C., Liu, L., Hao, X., Guo, H., Wang, Q., Huang, J., He, N., Yu, H., Lin, X., Pan, A., et al., 2020. Evolving epidemiology and impact of non-pharmaceutical interventions on the outbreak of coronavirus disease 2019 in wuhan, China. medRxiv. https://doi.org/10.1101/2020.03.03.20030593.

Woburn collegiate institute's WCIPEG – programming enrichment group. http://wcipeg.com/wiki/Computational_geometry, accessed on Feb 13, 2018.

Wyk, C.J. Van, O'Rourke, J., 1995. Computational geometry in C. Math. Comput. 64, 894. https://doi.org/10.2307/2153463.

A. Yassin et al., "Recent advances in indoor localization: a survey on theoretical approaches and applications," in IEEE Communications Surveys & Tutorials, vol. 19, no. 2, pp. 1327-1346, Secondquarter 2017, doi: 10.1109/COMST.2016.2632427.

Aleksandro MONTANHA is PhD student in the Programa Doctorado Ingeniería Informática of the Universidad de Sevilla (Spain) and degree in data processing technology, two specializations and a master's degree in computer science from the State University of Maringá (Brazil).He works with signal processing and has extensive experience in academic, scientific and business projects.He is currently a member of Intel's Internet of Things Council, Chairman of the ABINC (Brazilian Association of Internet of Things) Smart Cities Committee.

Airton M. POLIDORIO is an adjunct professor at the State University of Maringá (UEM). He has degree in Chemical Engineering from the State University of Maringá (UEM), master in Electrical Engineering and Industrial Informatics by Federal Technological University of Paraná (UTFPR), and doctorate in Cartography by State University Paulista Júlio de Mesquita Filho (UNESP-Presidente Prudente Campus).He has extensive experience in Pattern Recognition, Computer Vision, and Image Processing.

María del Carmen ROMERO-TERNERO is an associate professor (lecturer and researcher) at the Universidad de Sevilla (Spain) with a PhD. in Computer Science Engineering and an MBA.She is a member of the Tecnología Electrónica e Informática Industrial research group of the Universidad de Sevilla. She has been working in data networks and artificial intelligence since 1999. Her main research interest is solving multidisciplinary problems applying system modelling and artificial intelligence techniques. She has participated in many research projects funded by regional, national or European programs and research contracts and collaboration agreements with several enterprises. As a result of her research, she is co-author of more than 50 scientific papers published in international journals and conferences.She is IEEE, ACM and AEPIA member.More information at http://personal.us.es/mcromerot.

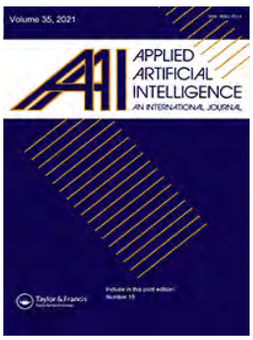

Applied Artificial Intelligence
An International Journal

ISSN: (Print) (Online) Journal homepage: https://www.tandfonline.com/loi/uaai20

A Context-Aware Artificial Intelligence-based System to Support Street Crossings For Pedestrians with Visual Impairments

Aleksandro Montanha, Andreea M. Oprescu & MCarmen Romero-Ternero

To cite this article: Aleksandro Montanha, Andreea M. Oprescu & MCarmen Romero-Ternero (2022): A Context-Aware Artificial Intelligence-based System to Support Street Crossings For Pedestrians with Visual Impairments, Applied Artificial Intelligence, DOI: 10.1080/08839514.2022.2062818

To link to this article: https://doi.org/10.1080/08839514.2022.2062818

Published online: 12 Apr 2022.

APPLIED ARTIFICIAL INTELLIGENCE
https://doi.org/10.1080/08839514.2022.2062818

Taylor & Francis
Taylor & Francis Group

A Context-Aware Artificial Intelligence-based System to Support Street Crossings For Pedestrians with Visual Impairments

Aleksandro Montanha [a], Andreea M. Oprescu [b], and MCarmen Romero-Ternero [b]

[a]Programa Doctorado Ingeniería Informática, Escuela Técnica Superior de Ingeniería Informática, Universidad de Sevilla, Seville, Spain; [b]Departamento de Tecnología Electrónica, Universidad de Sevilla, Seville, Spain

ABSTRACT

Artificial intelligence has the potential to support and improve the quality of life of people with disabilities. Mobility is a potentially dangerous activity for people with impaired ability. This article presents an assistive technology solution to assist visually impaired pedestrians in safely crossing the street. We use a signal trilateration technique and deep learning (DL) for image processing to segment visually impaired pedestrians from the rest of pedestrians. The system receives information about the presence of a potential user through WiFi signals from a mobile application installed on the user's phone. The software runs on an intelligent semaphore originally designed and installed to improve urban mobility in a smart city context. This solution can communicate with users, interpret the traffic situation, and make the necessary adjustments (with the semaphore's capabilities) to ensure a safe street crossing. The proposed system has been implemented in Maringá, Brazil, for a one-year period. Trial tests carried out with visually impaired pedestrians confirm its feasibility and practicality in a real-life environment.

ARTICLE HISTORY
Received 7 February 2022
Revised 30 March 2022
Accepted 1 April 2022

Introduction

Information and communication technology (ICT) interventions have an undeniable potential to help people with disabilities live their lives more independently and improve their quality of life (Lancioni et al. 2020). Artificial intelligence (AI) and mobile technologies have been shown to support people with disabilities by increasing their participation in society, helping them communicate, learn, shop, travel, move around town, among many others (Baumgatner, Rohrbach, and Schönhagen 2021), (Molina-Cantero et al. 2019), (Balasuriya et al. 2017), (Mahmud et al. 2020).

Specifically, assistive technologies using AI can improve the quality of life of people with visual disabilities. According to the World Health Organization, 2.2 billion people live with near or far-reaching vision impairment throughout

CONTACT Aleksandro Montanha mcromerot@us.es Programa Doctorado Ingeniería Informática, Escuela Técnica Superior de Ingeniería Informática, Universidad de Sevilla, Avda. Reina Mercedes S/n, 41012 Seville, Spain

the world (World Health Organization 2021). A challenging everyday activity for people with blindness or visual disabilities is mobility and, more specifically, street crossing (Hakobyan et al. 2013). Recently, more cities have already implemented accessibility features for street crossings, mainly in the form of sound alerts emitted by traffic lights. This alert can guide pedestrians by emitting a sound when the traffic light is green.

However, in cities where noise pollution is an issue, this type of solution may not be sufficient to provide the accessibility that people with visual disabilities need. In addition, cases where intersections are close to each other can also create confusion for visually impaired pedestrians. If there are multiple traffic lights that emit sound alerts at a single intersection, it can be confusing and time consuming for visually impaired pedestrians to recognize when it is safe to cross. Therefore, the sound alert system presents many deficiencies in terms of its ability to transcribe the environment. With solutions that can transcribe the environment and act on the traffic situation if necessary, besides potentially providing a safer option, could be empowering and improve the interaction of visually impaired users with the urban environment.

Currently, with the advent of the Internet of Things (IoT), which combines ubiquitous computing, sensing technologies, Internet communication protocols, and embedded devices (Suzuki 2017), a scenario with numerous solutions for smart city environments has emerged. Smartphones, as an important part of this paradigm, are widely available today to the general public. More importantly, in this context, visually impaired people use smartphones extensively as assistive technology (Khan & Khusro, 2020), (Retorta and Cristovão 2017).

We introduce a context-sensitive system that guides visually impaired people at street crossings by automatically detecting pedestrians and vehicles in traffic. The hardware installation at an intersection consists of smart traffic lights (Seebot Agent)[1] paired with cameras and WiFi antennas. Communication between the system and the visually impaired pedestrian is achieved through a mobile application installed on the user's smartphone. This method uses a signal trilateration technique and a computer vision pre-trained model to compute the user's location and the traffic situation.

Throughout the design and development process of this solution, potential users with visual impairment participated. Furthermore, field tests have been carried out with visually impaired users to test the application, which yielded positive results. The innovation of this work lies in 1) the solution has been built on existing hardware, an intelligent semaphore that was initially installed in Brazilian cities for smart city solutions related to traffic management; 2) the ability to transcribe the traffic situation to the user and to act on the situation to ensure user safety, since the semaphore can alter its behavior when a visually impaired pedestrian is crossing, if needed.

Related Work

Mobility solutions for visually impaired users have been widely addressed in the literature.

Advances in pedestrian detection and tracking using computer vision and machine learning techniques are discussed in (Brunetti et al. 2018). The authors call for more architectures to be implemented and tested. Additionally, one solution they point toward includes the use of RGB cameras paired with a DL strategy. (Chinchole and Patel 2017) developed a stick solution using an Arduino Nano microcontroller, two ultrasonic sensors, and an accelerometer. The authors also used a smartphone to obtain images of the user's surroundings. After processing with artificial intelligence techniques, these images provided information about the user's environment. A path hole detection system has been developed by (Islam and Sadi 2018) to assist visually impaired pedestrians using convolution neural networks (CNN). The authors achieved positive accuracy results in the experiments performed. A stick prototype for staircase and ground detection using a camera and an ultrasonic sensor has been proposed by (Habib et al. 2019). They used a pre-trained CNN model for training the system.

In addition, there is no doubt that crossing the streets is a major challenge for visually impaired pedestrians.

In this sense, an important number of solutions have been proposed in the literature. Some efforts have been devoted to developing an intelligent solution that includes traffic lights (through a connected device) in the cloud (Amazon Web Services-based system) and then alerts visually impaired users when approaching an intersection (Ihejimba and Wenkstern 2020). This work presents some limitations given the rough precision provided by GPS at ground level, especially at an intersection with several crossing directions. Other authors evaluated the feasibility of machine learning algorithms to identify traffic lights and track their status so that the visually impaired user can cross the road safely (Ghilardi et al. 2018). Furthermore, custom hardware implementations that apply image processing and machine learning to identify and track traffic lights have been reported in (Li et al. 2019). Information and feedback are provided to the visually impaired user through a voice synthesizer. Another similar version is based on a mobile phone device that must be held horizontally when crossing the street (Yu, Lee, and Kim 2019). The user is provided with guidance from the vibrations and sounds of the device. (Cheng et al. 2017) presented an assistive solution for crosswalk detection, consisting of an adaptive extraction and consistency analysis algorithm and a wearable navigation system (Intoer) for people with visual impairments. To achieve a more robust proposal, the authors considered several crosswalk situations that users can encounter: crosswalks at far distances from the user, crosswalks at close distances from the user, and crosswalks in front of the user. In addition, field tests were performed considering different variables,

such as time of day and weather. (Cheng et al. 2018) proposed a real-time Pedestrian Crossing Lights (PCL) detection algorithm using machine learning. The novelty of this work is based on its high precision and recall, robustness, and low complexity. Additionally, the authors applied a temporal-spatial analysis to track the detected PCL in order to improve the system's results in challenging scenarios. Communication between the user and the device, consisting of an Intel RealSense R200 camera, a pair of bone-conduction earphones and a portable PC, is achieved through voice instructions. (Tian et al. 2021) described an assistive solution to understand crosswalk scenes and provide users with key information and directions to cross the street. The device consists of a head-mounted mobile equipped with an Intel RealSense camera and a mobile phone. In their solution, the authors carried out field tests on crosswalk detection, pedestrian traffic light recognition, and distance measurement, and proved their practical usability. One of their main contributions is the SensingAI dataset with more than 11,700 images for the recognition of pedestrian traffic lights, key objects on the crossroads, and the crosswalk. (Yang et al. 2018) described a real-world framework using a wearable device to help visually impaired pedestrians with navigation tasks. Specifically, they study the context situation at an intersection by detecting the crosswalk, traffic light, pedestrian and vehicle. The authors carried out comprehensive experiments as part of their framework, comparing their own approach with other algorithms against several datasets.

The difficulties of visually impaired people experience using mobile applications have been studied (Qureshi and Wong 2019). The application of the user-centered design (UCD) philosophy is especially important for "not mainstream" user groups, and the resulting products have high acceptance rates (Krajnc, Feiner, and Schmidt 2010). Accessibility makes user interfaces perceivable, operable and understandable by people with a wide range of abilities and people in a wide range of circumstances, environments, and conditions. Therefore, accessibility also benefits people with disabilities and organizations that develop accessible products (Henry 2007).

In the literature, an increasing number of crosswalk assistive solutions for visually impaired pedestrians have been reported. Most of these advances are possible due to the increasingly higher processing power of devices, computer vision techniques, and different wearable devices and smartphones. Our solution also benefits from this aspect; however, in our case, the user only needs a smartphone. To our knowledge, this work is the first to report an ecosystem in which traffic alterations can be performed in favor of visually impaired pedestrians.

This work adds to our previous work in which the signal trilateration technique is proposed (Montanha et al. 2016). Compared to our previous work, the current proposed system incorporates the ability to segment visually impaired pedestrians automatically and in real time. In the previous version, they could not be distinguished from the rest of the pedestrians, so personalized

guidance could not be provided to cross the street. The previous version of the system could detect the presence of users and inform users carrying the smartphone application about the color of the traffic light. This work incorporates the visually impaired pedestrian segmentation technique, which allows the system to guide and assist them when crossing the street for the entire duration of the process. The app was designed and developed following the UCD approach.

Pedestrian Tracking Proposal

In this section, a proposal to detect and track pedestrians will be explored. The method implements a heuristic to estimate the pedestrian's location using a signal trilateration process and a deep learning model.

Signal Location Method to Support Pedestrian Tracking

The system establishes a communication canal between the smart traffic lights and the application installed on the smartphone of the visually impaired user. This is a wireless communication achieved via WiFi signals between the two parts. At least three WiFi antennas are placed at an intersection, as can be seen in Figure 1.

Figure 1. Proposal of camera and smart traffic lights installation in an intersection.

The smart traffic lights continuously monitor intersections using IP cameras. When a visually impaired pedestrian (with the mobile application opened) is detected to be within the WiFi range of at least one of the antennas, the localization process is requested. The system starts to compute a signal trilateration technique to identify in which quadrant the user is located (Montanha, Polidorio, and Romero-Ternero 2021). We explain this technique in detail in one of our previous works (Montanha, Polidorio, and Romero-Ternero 2021). The process continues when the user is located (the system detects in which quadrant they are). We will refer to this quadrant as the monitoring area. A processing thread is started for each pedestrian (visually impaired or not) that is located within the range of the monitoring areas, as they are being monitored by the cameras at the traffic light. The images captured from the monitoring area are further submitted to a pre-trained model whose function is to search for traces that identify pedestrians. This technique will be explained in more detail in the next section.

Neural Network Pre-trained Model to Support Pedestrian Tracking

The proposed system uses a pre-trained deep neural network model from the open-source toolkit OpenVINO[2] (Open Visual Inference and Neural Network Optimization), offered by Intel. The OpenVINO toolkit allows one to quickly develop and deploy a wide range of computer vision applications. The pre-trained model used, *person-detection-retail-0013*, is part of the Object Detection Models group of Intel's Pre-Trained Models. This model is based on the MobileNetV2-like backbone that includes depth-wise convolutions to reduce the amount of computation for the 3×3 convolution block. The single SSD head from 1/16 scale feature map has 12 clustered prior boxes. The model has an area under the precision/recall curve of 88.62%. The system implementing the neural network is capable of performing inference at a rate of one frame per second using the pre-trained model. The dimensions of the image are 640×480 pixels, and the color is RGB using codec H.265. The image format is MJPEG.

In the proposed solution, the information detailed below is collected by the pre-trained algorithms at a once-per-second acquisition rate: image data, the position relative to the image, date and time of the event, dimensions of the segmented pedestrian, and predominant colors. The image data is stored using the Base64 encoding algorithm, which is commonly used to embed the image data within other formats, JSON in our case.

Data Fusion for Signal Location and Image Processing Techniques

Data obtained by signal trilateration and image processing techniques are combined to improve pedestrian segmentation precision.

In each processing thread, a statistical data correlation process is performed between the position of the detected pedestrian in the spatial plane calculated by the signal trilateration technique (x_{tri}, y_{tri}) and the relative position of the pedestrian in the image, obtained from the image processing algorithm (x_{img}, y_{img}). Both pairs of coordinates refer to the pedestrian's location. If a correlation is established, the system then starts to look for the reidentification of the individual in the next frame to confirm the segmentation.

The Pearson correlation coefficient is used because it measures the strength of the linear relationship between two variables. Correlation analysis is calculated in the R programming language and the *pacman* package. As input, the script receives a .csv file generated by the algorithm. The following variables are stored in the .csv: date and time, trilateration ID, trilateration coordinates (x_{tri}, y_{tri}), pedestrian ID, pedestrian pixel coordinates in the image (x_{img}, y_{img}), predominant color of the pedestrian image, height and width of the pedestrian.

The system relies on the computation of the Pearson coefficient to guide the pedestrian through the street crossing process. Under certain circumstances (excess noise in the data, low visibility), it may occur that during the computation process a correlation is not found or is below the threshold of 90%. This implies that identification and tracking of the blind pedestrian are not possible, since we cannot merge information from cameras and signals. Since this is a possible event, an alternative procedure must be defined to allow the pedestrian to cross the street safely. The system prepares a contingency assistive procedure. This assistive procedure informs the visually impaired pedestrian about the status (color) of the traffic light.

System Design and Architecture

This section addresses the main components of the design and architecture of the system.

There are three main hardware components in the proposed system: smartphone, smart traffic lights, and WiFi antennas. The smart traffic lights monitor intersections using IP cameras and computing the signal trilateration and image processing algorithms. Meanwhile, the WiFi antennas installed at the intersections are responsible for the exchange of the WiFi signal with the smartphone. An overview of the system is shown in Figure 2.

There are two main software components: the computations running on the smart traffic light (signal trilateration technique, neural network-based image processing algorithm, data correlation process), and the mobile application.

The transmission of information between the mobile application and the smart traffic light is carried out using high-speed cellular network technology such as 3 G or 4 G. WiFi signals are used solely for localization purposes.

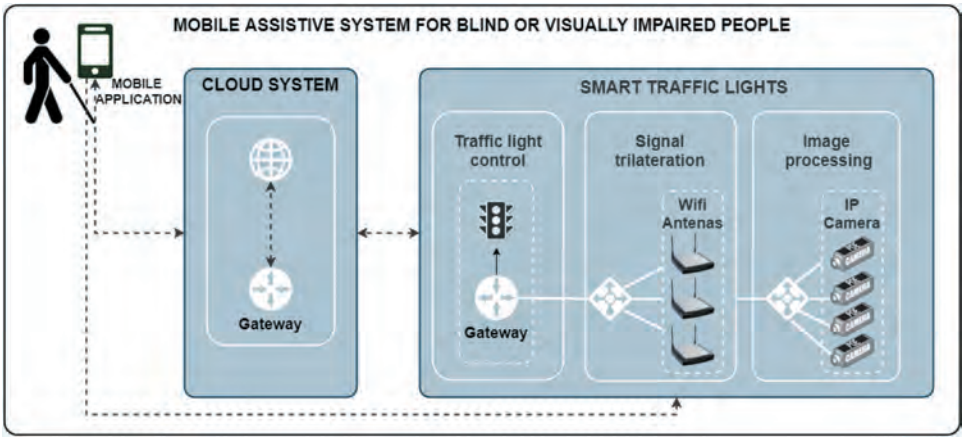

Figure 2. Overview of the system design for the proposed mobile assistive system.

As explained previously, the target user localization is first estimated in one of the quadrants (monitoring area) using our signal trilateration technique. Then, the image processing technique is added to the localization system, to segment the target user from the rest of the pedestrians. The images captured by the IP cameras from the monitoring areas are submitted to the pre-trained model. For each segmented pedestrian, the system stores information in a buffer. Each buffer has a space for analysis of 100 frames. Once the buffer is filled, the system starts the data fusion method. Once a correlation is established, the system then starts to search for the reidentification of the individual in the next frames to confirm the segmentation of the visually impaired pedestrian. OpenCV version 4.5.2 and Python 3 have been used to capture and process the images on a Debian 10 Linux distribution (Buster version).

The data resulting from the correlation process between the signal trilateration data and the image processing data need to exceed the selected threshold of 90% to start the assistance process. In addition, information from the traffic situation is checked, adding the following conditions to be met before initiating safe crossing: 1) the traffic light is closed for vehicles on the lane; 2) there are no vehicles on the lane, or, if there are, the first line of vehicles are stopped, waiting for the traffic light to turn green. If the traffic light is red for vehicles but there are vehicles moving in the lane, at high or low speeds, the system inspects the area closest to the crosswalk. If there is no line of stopped vehicles in front of the crosswalk, the system does not send instructions for crossing (we need to assume that a car could not stop at a red light).

Information is sent to the mobile application, alerting about the status of the traffic lights and the presence of vehicles in motion. The interaction between the mobile application interface and the user is explained in more detail in Section 4.2. In addition, smart traffic lights can increase the duration of the

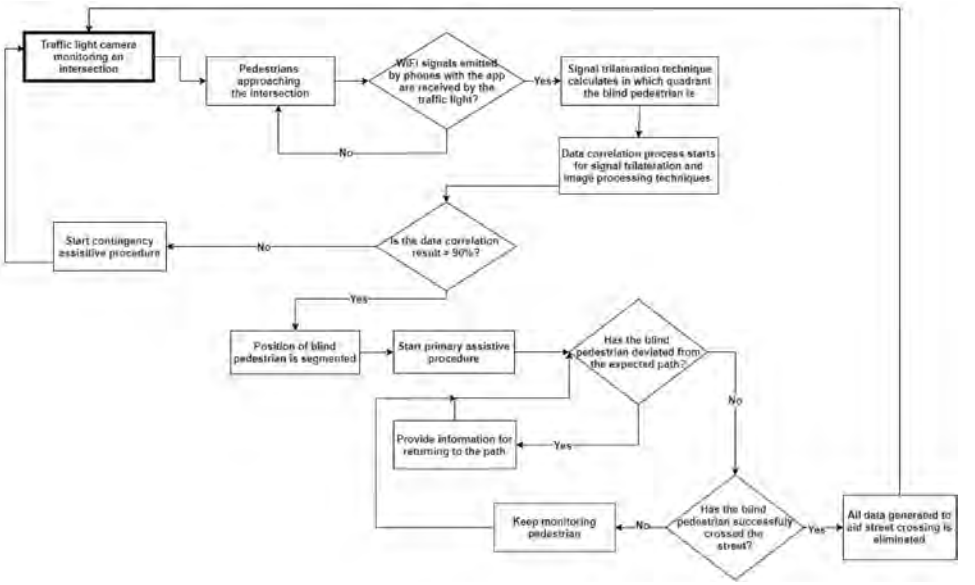

Figure 3. Process flow diagram of the mobile assistive system for blind or visually impaired people.

green light cycle when a visually impaired pedestrian has been detected. This change in the duration of the traffic light cycle must be made according to local traffic regulation laws.

If the user takes a deviation from the street crossing (gets out of the monitoring area), the system dynamically prepares a set of instructions to amend the trajectory. Once the system detects that the user has finished crossing the street and the light cycle ends, the algorithm terminates the instance and removes the data collected for the crossing, according to and complying with the local data protection regulation (Brazilian General Data Protection Law, in this case).

As mentioned above, if the system does not consolidate the data, the contingency system is activated, informing pedestrians about the status of the traffic light and about the inability to guide them during the crossing process. A flow diagram of the system operation process is presented in Figure 3. The system can assist more than one user at a time, since mobile devices are uniquely identified via the MAC address.

The Smart Traffic Light

The traffic light used in the proposed system is an Agent Seebot Smart Traffic Light.[3] This device incorporates an Intel I5 7th generation processor with a high-resolution LED display interface. This device has an Axis HD IP camera with image capture and a transmission rate greater than 30 fps. The connection protocols are Ethernet, Bluetooth, and WiFi. The device also incorporates an inclinometer, an accelerometer, and a motorized camera angle adjustment

Figure 4. Image of a pedestrian crossing retrieved from a Seebot agent installed at an intersection.

system, capable of tilting 80 on the Y-axis (vertical). The images captured by the smart traffic lights are at least 5.5 meters high, and the distance in relation to the area destined for the crossing is dynamic and can change according to the characteristics of the place. An image recovered from an installed semaphore can be seen in Figure 4. The crossing area is detected and marked in light green, the pedestrian is marked in fluorescent green, and the car lane is marked in red.

Generally, the area intended for pedestrian crossing is marked with a horizontal painting; however, in many places, they do not have constant maintenance and therefore may have a discrete appearance or even not exist. Therefore, it is necessary to inform the system of the location in the space plan where there is an area for pedestrians to cross. This feature allows drawing a polygon that serves as a pedestrian segmentation parameter. The system uses a camera with infrared lighting and, in some environments, has additional infrared lighting for places with low lighting during the night period. Each traffic light has the computational capacity to evaluate at least two crossing points in real time in both directions. Due to electronic control of the vertical angle of the camera installed on the device, the camera can be directed both at the viewing angle ahead, below, and even after crossing the lanes. This allows the traffic light to be installed in different intersection scenarios. Image capture is continuous, 24 hours a day.

The Mobile Application Interface

An Android-based mobile app to help urban mobility for visually impaired people has been developed. An Android-based smartphone device was chosen because of its popularity. The hardware and software needed for the solution are already available on the device (GPS, WiFi, Bluetooth, voice system, etc.). Additionally, many visually impaired people are familiar with these devices, so we decided to introduce this technology proposal to a group of target users. They

provided valuable insight and knowledge that we used to develop this mobile app interface. The group had experience with smartphones and was able to move autonomously in the urban environment. We were interested in understanding how they interact with signals, other individuals, obstacles, and more importantly technology. The group oriented us on how to establish an appropriate communication channel between a visually impaired user and the application, using speech recognition features, vibration, sounds, and voice messages. This application follows the set of accessibility compliance testing (ACT) rules recommended by the World Wide Web Consortium (W3C) (World Wide Web Consortium" 2008), and the international standards for the Web.

Several screenshots of the application are shown in Figure 5 (main screen for the initialization of the location of the pedestrian, an aerial view of the smart intelligent traffic lights installed on a street and their status, and an example of an alert created for a user to wait for the traffic light to open).

When a user approaches a street crossing, the application starts providing information by voice to the user on what to do next. Users are instructed to point the mobile device toward the direction where they wish to cross parallel to the ground, and once that has been done, the application instructs the user to confirm their direction by tapping twice on the screen. The application informs the user about the selected path (street name) and asks the user to confirm by sliding the finger over the screen. The application notifies the user of the confirmed path and informs the user of the state (color) of the traffic light. On the other hand, the traffic light is notified of the presence and desired direction of a visually impaired user. If the color is red, the system starts a countdown for the color to change to green. Finally, when the traffic light is

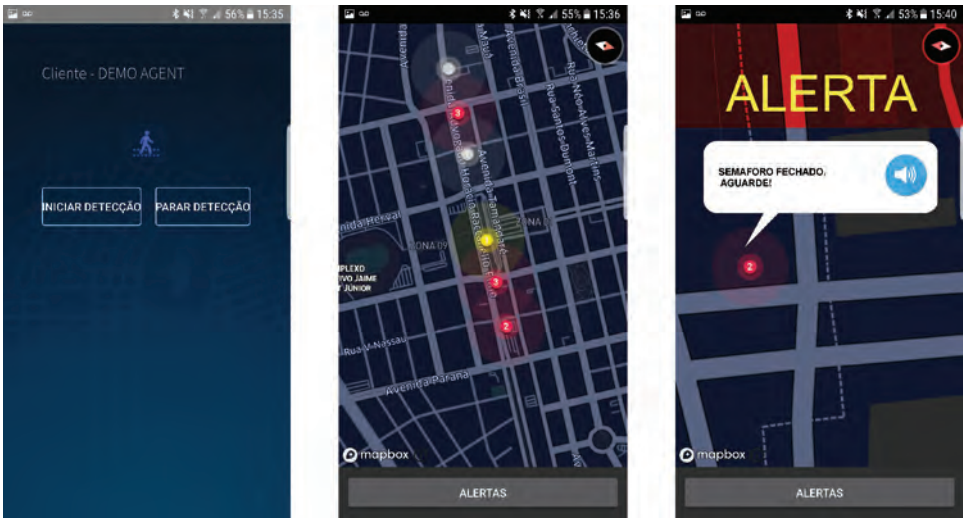

(a) App's main screen to initiate or stop localization process

(b) Aerial view of the intelligent semaphores on a street

(c) Alert to hold (closed semaphore, hold on)

Figure 5. Mobile application for street crossing assistance screenshots.

green, the user is informed that there are no vehicles on the street and that the light is green. Therefore, traffic light communication with the mobile application includes information about the conditions of the local environment (if there are vehicles, if vehicles are moving, or if the traffic light is opened or closed). Even if the visually impaired user has already started crossing the street without interacting with the application, guidance and information about the state of the road and traffic light are provided. If the user leaves the correct and safe route, a route error warning message is sent with instructions on how to correct the error.

Installation Process

To physically install the solution, we faced several challenges, as smart traffic lights were already installed. This represented our biggest operational challenge, since we wanted to interfere as little as possible with vehicle flow. A logistical operation was established in the city to divert traffic. We installed the WiFi antennas and adjusted the IP cameras so that they have enough aperture to capture both vehicles on the roads and waiting pedestrians (not only in the crossing, but also in the crosswalk area). Additionally, an uninterruptible supply system with a capacity of 4 hours of operation was installed at the intersection to guarantee autonomy in the event of a momentary power failure, common on stormy days.

Once the system was running, our next challenge was to integrate the proposed solution with existing semaphore software. As part of this adaptation, the main task was to calibrate the WiFi signal at each point. During the operation, a drone was used to measure the signal of each WiFi antenna in the waiting areas of the crosswalks.

The assistive system was in operation for tests for 30 days. After 30 days, the system was made available for testing so visually impaired users could validate the application.

Results

In this work, we will present some preliminary results collected from the installation in Maringá, Brazil.

The proposal to develop this feature raised the need to understand how blind people interact with mobile devices. We invited a group of visually impaired users to help us develop the app (applying UCD methodology). We observe the essential features that a mobile application interface must present to work with locomotion guidance in an urban environment. In this way, we carefully elaborated the messages and information the system offers as audio indications: indicating to the users their position in relation to the intersection, indicating the name of the streets at the intersection, and asking

which street the user would like to cross. An appropriate way to capture the user's response is by sliding on the screen in the horizontal direction for one choice or vertically for another choice. We found a practical way to notify users when approaching the intersection using smartphone vibrations and asking if they would like to access the assistant to cross the intersection. When the user responds affirmatively, they receive audible information (literal transcription) on the status of the traffic light, the presence of vehicles, and the assistance process for crossing.

In Table 1 the dynamic of the operation of the system over a period of 3 months can be observed (number of connections to the app, number of crossing assistance triggered, and number of segmentations). During the first month (07/2019), the app was made available to a user who made 7 connections to the application. Of the 7 connections, the system activated safe crossing assistance 6 times (when the data fusion result was above the 90% threshold). In the second month, the number of users who use the app increased due to the advertisement of the application in a social networking group. The number of connections also increased, and, in all cases, safe crossing assistance was successfully activated. During the third month, we experienced a high volume of app usage, as the group was motivated to try the solution. A significant number of cross-requests achieved good segmentation (96.5%). Safe crossing assistance was completed successfully in 80.8% of the total of app connections. The remaining 19.2% did not cross or crossed with human assistance and did not inform the platform.

The hardware on which the system is deployed is very potent, based on an Intel i5 7° Generation processor. It is an already existing and installed software (a Seebot agent). As it has been explained before, there are two main processes running in the system: the signal trilateration process and the image processing process. From our observations, as for the computational power needed for the signal trilateration technique, the usage is very low in comparison to the device's capabilities, it consumes 1–3% of one of the five cores and 10–20MB of memory with a time processing of 0.1 seconds. On the other hand, the image processing process (which includes frame capture, frame processing, pedestrians detection and reidentification) consumes 10–30% of two cores and 50–80MB of memory with 32 frames per second. In this scenario, there is a user detected in the signal trilateration system and there is a constant segmentation process of a visually impaired individual using the system. The detection of more than one user in the environment increases the processing consumption around 3–5% and the

Table 1. Number of app connections, assistance for safe crossings, and successful data fusion of the system operating over a 3 month period.

Period	App connections	Crossing assistance completed	Segmentation (trilateration and image processing)
07/2019	7	6	6
08/2019	14	14	14
09/2019	115	93	111

memory consumption around 10 MB. As we indicate before, considering this configuration and the availability of resources for the application in the traffic light, the system is able to handle up to 5 simultaneous individuals.

For a qualitative analysis, the mobile application was made available to 11 visually impaired user volunteers. We have interviewed users using a qualitative interview about their experience, usability, and user experience with the app. 27% of this population had reduced mobility. 83% of volunteers are familiar with the use of the app (50% always uses mobile apps to get information and navigate the city and 36.3% uses it routinely), while 8.3% rarely and 8.3% never. 100% of the users thought that the app was not complex to use and that the app does not need technical support for its use. Most people with visual impairments would learn to use the app quickly, and they felt safe and confident using the crossing system provided by the app. 58.3% did not need to learn anything else before using the app. 100% did not find it too complicated to use the app, thought that everything was well integrated and easy to use. All of them felt safe to cross while using the app. 66,6% were not instructed by other people to follow the crossing, even using the app.

Regarding the usability of the app, 33.3% ranked it with 10 out of 10, 33.3% with 9, 16.6% with 8 and 16.6% with 7.

Volunteers were asked what they would suggest to improve the app, and those who responded said: "That a campaign be made so that in more traffic lights the same was installed.," "Extending your range to other traffic lights and natural enhancements.," "It is great," "That there was a policy to have more of these traffic lights in the city.," "The app is just perfect and regarding something like that, it is hard to give any kind of suggestions.," "The app is excellent, but it should have other ways to use it without having to use the cell phone." and "No suggestions."

Discussion

One of the key aspects of the proposed system is its ability to translate and adapt the environment to user capabilities, which is a crucial feature when developing solutions for disabled individuals. When creating this solution, we have followed the principles of user-centered design by interacting with users throughout the design and development process. It was especially important to understand how these specific users interact with the urban environment and how they use mobile application interfaces to design and implement a solution that would be useful and easy to use.

This system is aware of the presence and location of visually impaired people. It not only describes the traffic situation, but can also inform the user about the crossing situation in real time, offering a personalized set of instructions. The system can adapt the environment to user needs by prolonging the duration of the interval to cross the street (the traffic light will remain green longer for

pedestrians). The real-world pilot study has shown great results; however, we are aware that our research presents several limitations. There is room to improve the accuracy of the system in more extreme circumstances, such as low visibility due to weather conditions or nighttime. Second, the performance and usage data could have been collected over a longer period to develop statistical information. Another drawback of the proposal could be that the system is highly dependent on the hardware installation. However, we consider this to be beneficial for the user who only needs to carry a smartphone. A usability problem was detected in situations where there is noise pollution due to heavy traffic or construction near the site. It can be difficult for the user to hear the instructions in this situation, so we are continuing to investigate alternative methods. Lastly, an analysis of different variants of the approach could have been beneficial to the study.

Although there are more solutions to include people with visual impairments in the urban environment, there are still obstacles to overcome. Specifically, for urban environments that aim to become inclusive smart cities. We believe that there is a need to design and implement technological solutions that are safe and useful to users, widely available, and economically viable.

This system was built into the existing computational platform of the intelligent traffic lights in use. These traffic lights already perform the task of segmenting vehicles and reading license plates. At each intersection, these tasks typically consume 70% of the available processing power. To avoid saturating the processor and therefore offering some level of slowness, there is an additional processing limit that can be used by additional resources to the primary tasks of the smart semaphore. For this reason, it is not possible to carry out more than three simultaneous processes of segmentation of people with visual impairments at the same intersection, and a fourth request would enter the process queue. If this happens, the system activates the emergency system and puts plan B into practice, notifying the user who cannot perform the assisted crossing.

Conclusion

In the context of AI-based technology, this work contributes to the development of assistive technology for the mobility of visually impaired pedestrians, specifically for street crossings. To our knowledge, this is the first study designed to aid visually impaired pedestrian street crossings that combines the use of smart traffic lights as an element to detect traffic and pedestrian situation through sensors, image processing, AI techniques, and mobile devices.

This solution is based on the paradigms of Smart Cities and Internet of Things, seeking the fusion of data and the use of intelligent infrastructure. The functionality of the existing smart traffic light has been extended by adding WiFi antennas and developing segmentation software. This system as a whole can carry out a great number of tasks: acquire and transmit real-time images of their coverage locations to a traffic control center, communicate with pedestrians in

possession of mobile devices or devices installed in vehicles via WiFi and/or Bluetooth signals, assistive crossing for visually impaired pedestrians, among many other traffic regulation tasks. Furthermore, the data collection performed by this device contributes to the creation of a training database.

We can conclude that the proposed solution adds as an innovating factor the use of existing infrastructure to deploy assistive technology for visually impaired pedestrians. Often, solutions to assist visually impaired people on a street crossing require the use of a portable device (in the form of glasses or a stick). We can see that there are benefits to a solution that limits the use of a smartphone on the user's end and relies more heavily on a common infrastructure facilitated by a smart city context. Furthermore, communication between assistive software and traffic regulation software can be beneficial for visually impaired users, as the traffic light can adapt to the traffic situation to ensure safe crossing.

Future Work

Further research is required to improve the functionality of the system at night. Without adequate light, most of the time the system is unable to segment the visually impaired pedestrian, and the emergency assistive system has to be applied.

Our results are encouraging, so further development of techniques and algorithms to improve accuracy can be carried out within the scientific community. As a continuation of this work, open-source code can be released, making it available on GitHub, so researchers around the world can contribute to the code and implement the system in their cities.

Notes

1. https://seebot.com.br/es/agent.html
2. https://docs.openvinotoolkit.org
3. https://seebot.com.br/es/agent.html

Disclosure Statement

No potential conflict of interest was reported by the author(s).

ORCID

Aleksandro Montanha http://orcid.org/0000-0002-6288-2753
Andreea M. Oprescu http://orcid.org/0000-0003-3308-4688
MCarmen Romero-Ternero http://orcid.org/0000-0001-6965-9485

References

Balasuriya, B. K., N. P. Lokuhettiarachchi, A. R. M. D. N. Ranasinghe, K. D. C. Shiwantha, and C. Jayawardena. 2017. Learning platform for visually impaired children through artificial intelligence and computer vision 2017 11th International Conference on Software, Knowledge, Information Management and Applications (SKIMA) (Manhattan, New York, U.S.: IEEE) Colombo, Sri Lanka 1–7 doi:10.1109/SKIMA.2017.8294106.

Baumgatner, A., T. Rohrbach, and P. Schönhagen. 2021. 'if the phone were broken, i'd be screwed': Media use of people with disabilities in the digital era. *Disability and Society* 1–25. doi:10.1080/09687599.2021.1916884.

Brunetti, A., D. Buongiorno, G. F. Trotta, and V. Bevilacqua. 2018. Computer vision and deep learning techniques for pedestrian detection and tracking: A survey. *Neurocomputing* 300:17–33. Retrieved from https://www.sciencedirect.com/science/article/pii/S092523121830290X

Cheng, R., K. Wang, K. Yang, N. Long, J. Bai, and D. Liu. August 2018. Real-time pedes- trian crossing lights detection algorithm for the visually impaired. *Multimedia Tools and Applications* 77(16):20651–71. doi: 10.1007/s11042-017-5472-5.

Cheng, R., K. Wang, K. Yang, N. Long, and H. Weijian. October 2017. Crosswalk navigation for people with visual impairments on a wearable device. *Journal of Electronic Imaging* 26:1.

Chinchole, S., and S. Patel. 2017. Artificial intelligence and sensors based assistive system for the visually impaired people. 2017 International Conference on Intelligent Sustainable Systems (ICISS) SCAD Institute of Technology, Palladam, India . 16–19 doi:10.1109/ISS1.2017.8389401.

Ghilardi, M. C., G. Simões, J. Wehrmann, I. H. Manssour, and R. C. Barros. 2018 Real-Time Detection of Pedestrian Traffic Lights for Visually-Impaired People 2018 International Joint Conference on Neural Networks (IJCNN) Rio de Janeiro, Brazil. 1–8 doi:10.1109/IJCNN.2018.8489516.

Habib, A., M. Islam, M. Kabir, M. Mredul, and M. Hasan. 2019, November. Staircase detection to guide visually impaired people: A hybrid approach. (Retrieved from) *Revued'Intelligence Artificielle* 33 (5):327–34. doi: 10.18280/ria.330501.

Hakobyan, L., J. Lumsden, D. O'Sullivan, and H. Bartlett. September 2013. Mobile assistive technologies for the visually impaired. *Survey of Ophthalmology* 58(6):513–28. doi: 10.1016/j.survophthal.2012.10.004.

Henry, S. (2007). *Just ask: Integrating accessibility throughout design*. Lulu.com. Retrieved from https://books.google.es/books?id=hRnpXbFB06cC

Ihejimba, C., and R. Z. Wenkstern. 2020. Detectsignal: Acloud-based traffic signal notification system for the blind and visually impaired, 2020 IEEE International Smart Cities Conference (ISC2) , 1–6 doi:10.1109/ISC251055.2020.9239004.

Islam, M. M., and M. S. Sadi. 2018. Path Hole Detection to Assist the Visually Impaired People in Navigation 2018 4th International Conference on Electrical Engineering and Information & Communication Technology (iCEEiCT) Bangladesh (Manhattan, New York, U.S.: IEEE) 268–73 doi:10.1109/CEEICT.2018.8628134.

Khan, A., S. Khusro, and J. D. Camba. 2020. An insight into smartphone-based assistive solutions for visually impaired and blind people: Issues, challenges and opportunities. *Universal Access in the Information Society* 1–34. doi:10.1007/s10209-020-00776-x.

Krajnc, E., J. Feiner, and S. Schmidt. 2010. User centered interaction design for mobile applications focused on visually impaired and blind people. In Leitner, G., Hitz, M., Holzinger, A. (eds) HCI in Work and Learning, Life and Leisure. USAB 2010. Lecture Notes in Computer Science. 195–202. Berlin, Heidelberg: Springer-Verlag. doi:10.1007/978-3-642-16607-5_12

Lancioni, G. E., N. N. Singh, M. F. O'Reilly, J. Sigafoos, G. Alberti, V. Chiariello, and L. Carrella. 2020. Everyday technology to support leisure and daily activities in people with intellectual and other disabilities. *Developmental Neurorehabilitation* PMID: 32118503. 23 (7):431–38. doi:10.1080/17518423.2020.1737590.

Li, X., H. Cui, J.-R. Rizzo, E. Wong, and Y. Fang. 2019. Cross-safe: Acomputer vision-based approach to make all intersection-related pedestrian signals accessible for the visually impaired , April. *Arai, K., Kapoor, S. (eds) Advances in Computer Vision. CVC 2019. Advances in Intelligent Systems and Computing* 944 . In (pp. 132146). 132146). Switzerland: Springer International Publishing 978-3-030-17798-0. doi:10.1007/978-3-030-17798-0_13

Mahmud, S., R. Haque Sourave, M. Islam, X. Lin, and J.-H. Kim. 2020. A vision based voice controlled indoor assistant robot for visually impaired people. 2020 IEEE International IOT, Electronics and Mechatronics Conference (IEMTRONICS) (Manhattan, New York, U.S.) . 1–6 doi:10.1109/IEMTRONICS51293.2020.9216359.

Molina-Cantero, A. J., C. Lebrato-Vázquez, M. Merino-Monge, R. Quesada-Tabares, J. A. Castro- García, and I. M. Gómez-González. 2019. Communication technologies based on voluntary blinks: Assessment and design. *IEEE Access* 7:70770–98. doi:10.1109/ACCESS.2019.2919324.

Montanha, A., M. J. Escalona, F. J. Dominguez-Mayo, and A. M. Polidorio. 2016. A technological innovation to safely aid in the spatial orientation of blind people in a complex urban environment 2016 International Conference on Image, Vision and Computing (ICIVC) . August. Manhattan, New York, U.S.: IEEE 102–107. doi:10.1109/ICIVC.2016.7571281.

Montanha, A., A. M. Polidorio, and M. Romero-Ternero April 2021. New signal location method based on signal-range data for proximity tracing tools. *Journal of Network and Computer Applications* 180:103006. doi: 10.1016/j.jnca.2021.103006.

Qureshi, H. H., and D. H.-T. Wong. 2019. A systematic literature review on user-centered design (UCD) interface of mobile application for visually impaired people, HCI International 2019 – Late Breaking Posters . (pp. 168175). Springer International Publishing, 168–175. doi:10.1007/978-3-030-30712-7_23.

Retorta, M., and V. Cristovão. July 2017. Visually-impaired Brazilian students learning English with smartphones: Overcoming limitations. *Languages* 2(3):12. doi: 10.3390/languages2030012.

Suzuki, L. R. 2017. Smart cities IoT: Enablers and technology road map. In *Smart City Networks: Through the Internet of Things*, 167–90. ISBN: 978-3-319-61313-0. doi:10.1007/978-3-319-61313-0_10. Berlin: Springer International Publishing.

Tian, S., M. Zheng, W. Zou, X. Li, and L. Zhang. 2021. Dynamic crosswalk scene understanding for the visually impaired. *IEEE Transactions on Neural Systems and Rehabilitation Engineering* 29 (29):1478–86. doi:10.1109/TNSRE.2021.3096379.

World Health Organization. (2021, October). *Blindness and vision impairment*. Retrieved from https://www.who.int/news-room/fact-sheets/detail/blindness-and-visual-impairment

World Wide Web Consortium". (2008, December). *Web content accessibility guidelines 2.0*. Retrieved from https://www.w3.org/

Yang, K., R. Cheng, L. M. Bergasa, E. Romera, K. Wang, and N. Long. 2018. Intersection perception through real-time semantic segmentation to assist navigation of visually impaired pedestrians. In *2018 IEEE International Conference on Robotics and Biomimetics (ROBIO)* (Manhattan, New York, U.S.: IEEE), 1034–39 doi:10.1109/ROBIO.2018.8665211.

Yu, S., H. Lee, and J. Kim. 2019. Street Crossing Aid Using Light-Weight CNNs for the Visually Impaired IEEE/CVF International Conference on Computer Vision Workshop (ICCVW) 2019 , October. Manhattan, New York, U.S.: IEEE doi:10.1109/ICCVW.2019.00317.